The Hydrography and Heat fluxes between South Africa and Antarctica

Raymond Edward Roman

Submitted in fulfillment of the requirements of a M.Sc. degree

Department of Oceanography
UNIVERSITY OF CAPE TOWN

2002

Abstract

Hydrographic sections between Africa and Antarctica; the A12, SR02 and SR02 sections conducted in 1990, 1990 and 1993 are presented here in comparison with the AJAX section of 1984. The numbered sections were undertaken as part of WOCE to better understand the ocean and the role it plays in the distribution of heat, salt, oxygen and nutrients south of Africa. In this study the focus was put on the SR02 section done in 1993 by South African scientists. The three sections also provided for a fresh look at the spatial and temporal variability of the hydrographic environment along the Greenwich Meridian.

The freshwater transport across the SR02 section was found to be $139 \pm 2 \times 10^9$ kg s^{-1}. This compared well with the $139 \pm 3.1 \times 10^9$ kg s^{-1} crossing the A12 section. The heat transport between Africa and Antarctica across the SR02 section was 0.815 ± 0.15 PW. This value was slightly higher compared to the 0.675 ± 0.15 PW calculated for the A12 section of 1990. The increase in transport can be attributed to seasonal temperature variations. The transport of salt and oxygen along the SR02 section of 1993 was $4800 \pm 69 \times 10^6$ kg s^{-1} and $29.2 \pm 0.51 \times 10^3$ kmol s^{-1} respectively.

Significant variability with respect to the strength of the fronts was found only along the Subantarctic Front and Subtropical Convergence. Four fronts were distinguishable along the three respective sections. These fronts were the Southern Front (Weddell Front), Antarctic Polar Front (APF), Subantarctic Front (SAF) and the Subtropical Convergence (STC). The STC had the most intense thermal signal of all the fronts and showed significant shifts in its latitudinal position. These shifts were linked to the position of the Agulhas Retroflection Region. In terms of transport however the SAF was the most prominent of the fronts with geostrophic velocities reaching 35.8 cm s^{-1} at the surface. This observation was however not consistent between all the sections.

Water masses along the WOCE sections indicate both spatial and temporal variability. Most of these differences are attributed to the presence of the Agulhas Retroflection Region in the SR02 sections. Along the SR02 sections typical Subtropical Surface Water (SSW) is observed as only a patch between Agulhas Rings shed at the retroflection region. Surface water of these two rings consists of a mixture of South Indian Surface Water and Tropical Surface Water resulting in a saline, high temperature water type with a oxygen minimum relative to typical Subtropical Surface Water. As a result SSW display a induced oxygen maximum compared to the surface water of the Agulhas Rings. In the section not crossing the Agulhas Retroflection Region SSW cover the whole area north of the STC. The Agulhas Rings also influence Antarctic Intermediate Water (AAIW) through Red Sea water that the two Rings carry at the same density level as AAIW. This mixing of Red Sea Water and AAIW results in increased salinities with respect to AAIW. In addition to the spatial variability, temporal variability was observed in Antarctic Surface Water (AASW). Summer sections displayed an intense temperature minimum layer, Winter Water and a decrease in salinities whilst along the winter section the intense temperature minimum was absent and surface salinities were generally higher. Subantarctic Mode Water (SAMW) consistent with findings in the Drake Passage had a salinity maximum and two separate oxygen minimums associated with it. Salinity values of SAMW were however 0.3-0.4 higher along the Greenwich Meridian.

Contents

List of Figures iv

List of Tables.....vii

List of acronyms used in the text.....ix

Abstract.....i

Chapter 1

Water masses and circulation of the Southern Ocean.....1

Chapter 2

Background.....4

Chapter 3

Objectives.....28

Chapter 4

Data and Methods.....29

Chapter 5

Results.....39

Chapter 6

Conclusion.....104

Chapter 7

Bibliography 110

List of Figures

Chapter 1

Figure 1.1: Map showing the WOCE SR02 section 2
Figure 1.2: WOCE Hydrographic Program One-time survey map of Atlantic ocean.....3

Chapter 2

Figure 2.4: Frontal patterns between 0° and 170°E.....19

Chapter 4

Figure 4.1: Distribution of XBT stations along the SR02 section.....30

Chapter 5

Figure 5a: Bathymetry of the Southern Ocean south of Africa.....39
Figure 5b: SR02a hydrographic section.....40
Figure 5c: SR02b hydrographic section.....40
Figure 5d: A12 hydrographic section.....40
Figure 5.3.2a: Vertical salinity and oxygen profiles in the SAZ of the SR02a section....53
Figure 5.3.2b: Vertical salinity and oxygen profiles in the SAZ of the A12 section.....54
Figure 5.3.2c: Vertical salinity and oxygen profiles in the SAZ of the SR02b section....54
Figure 5.3.3a: Salinity distribution across the Weddell Gyre for the SR02a section.....56
Figure 5.3.3b: Salinity distribution across the Weddell Gyre for the A12 section.....56
Figure 5.3.3c: Nitrate distribution across the Weddell Gyre for the A12 section.....57
Figure 5.3.3d: Phosphate distribution across the Weddell Gyre for the A12 section.....57
Figure 5.3.4: Salinity profile showing the influence of Agulhas rings on AAIW.....59
Figure 5.3.5a: Vertical distribution of oxygen, nitrate and phosphate for the A12 section.....61
Figure 5.3.5b: Vertical distribution of nitrates and oxygen for the SR02b section.....61
Figure 5.4.1a: Q-S relationship for Greenwich Meridian stations (SR02a) in the ACC and Weddell Gyre and the Drake Passage north of the APF.....64
Figure 5.4.1b: Q-S relationship for Greenwich Meridian stations (A12) in the ACC and Weddell Gyre and the Drake Passage north of the APF.....64

Figure 5.4.2: Erosion of the oxygen minimum across the ACC and Weddell Gyre shown as density versus oxygen for the A12 section.....66
Figure 5.1a: Potential Temperature section for the SR02a section.....68
Figure 5.1b: Potential Temperature section for the A12 section.....69
Figure 5.1c: Potential Temperature section for the SR02b section.....70
Figure 5.2a: Salinity section for the SR02a section 71
Figure 5.2b: Salinity section for the A12 section.....72
Figure 5.2c: Salinity section for the SR02b section.....73
Figure 5.3a: Potential Temperature section for the SR02a section (upper 1000m).....74
Figure 5.3b: Potential Temperature section for the A12 section (upper 1000m).....75
Figure 5.3c: Potential Temperature section for the SR02b section (upper 1000m).....76
Figure 5.4a: Salinity section for the SR02a section (upper 1000m).....77
Figure 5.4b: Salinity section for the A12 section (upper 1000m).....78
Figure 5.4c: Salinity section for the SR02b section (upper 1000m).....79
Figure 5.5a: Oxygen section for the SR02a section 80
Figure 5.5b: Oxygen section for the A12 section.....81
Figure 5.5c: Oxygen section for the SR02b section 82
Figure 5.6a: Nitrate section for the A12 section.....83
Figure 5.6b: Nitrate section for the SR02b section.....84
Figure 5.7a: Phosphate section for the A12 section.....85
Figure 5.7b: Phosphate section for the SR02b section.....86
Figure 5.8a: Silicate section for the A12 section.....87
Figure 5.8b: Silicate section for the SR02b section.....88
Figure 5.9a(i): Potential Density section for SR02a section.....89
Figure 5.9a(ii): Potential Density section for SR02a section(2000m).....90
Figure 5.9b(i): Potential Density section for A12 section.....91
Figure 5.9b(ii): Potential Density section for A12 section(2000m).....92
Figure 5.9c(i): Potential Density section for SR02b section.....93
Figure 5.9c(ii): Potential Density section for SR02b section(2000m).....94
Figure 5.10a: Geostrophic velocities for SR02a section 95
Figure 5.10b: Geostrophic velocities for A12 section 96

Figure 5.10c: Geostrophic velocities for SR02b section 97
Figure 5.5.1: Map indicating the A21, A12, A11, SR02a and I6 WOCE sections.....98
Figure 5.5.1a: Vertical integrated mass transport for A21 section.....100
Figure 5.5.1b: Vertical integrated mass transport for SR02a section.....100
Figure 5.5.1c: Vertical integrated mass transport for A12 section.....101
Figure 5.5.1d: Vertical integrated Heat transport for A21 section.....101
Figure 5.5.1e: Vertical integrated Heat transport for SR02a section.....101
Figure 5.5.1f: Vertical integrated Heat transport for A12 section.....102
Figure 5.5.1g: Vertical integrated Salt transport for the SR02a and A12 sections.....102
Figure 5.5.1f: Vertical integrated Oxygen transport for the SR02a and A12 sections...103

List of tables

Chapter 2

Table 1.1: Comparison of temperature, salinity and oxygen values of the Mellville-75 and MV Marion Dufresne/RRS Charles Darwin-29 of SASW.....8

Table 1.2: Comparison of temperature, salinity and oxygen values of the Mellville-75 and MV Marion Dufresne/RRS Charles Darwin-29 of SAMW.....9

Table 1.3: Comparison of temperature, salinity and oxygen values of the Mellville-75 and MV Marion Dufresne/RRS Charles Darwin-29 of AAIW.....12

Table 1.4: Comparison of temperature, salinity and oxygen values of the Mellville-75 and MV Marion Dufresne/RRS Charles Darwin-29 of UCDW.....13

Table 1.5: Comparison of temperature, salinity and oxygen values of the Mellville-75 and MV Marion Dufresne/RRS Charles Darwin-29 of LCDW.....14

Chapter 4

Table 4.1: Volume calibrations of the of the apparatus used in oxygen analysis.....33

Table 4.2: Mean difference and STD of nutrient duplicates.....34

Table 4.3: Mean difference and STD between pairs of deep sea reversing thermometers 35

Table 4.4: Mean difference and STD between DSRT and CTD temperatures.....35

Table 4.5: Comparison of DSRT on the CTD station 29.....36

Table 4.6: Mean difference and STD between DSRT pressure and CTD pressure 36

Chapter 5

Table 5.1.1: Position of the APF for the SR02a, SR02b and A12 sections.....42

Table 5.1.2: Position of the SAF for the SR02a, SR02b and A12 sections.....44

Table 5.1.3: Position of the STC for the SR02a, SR02b and A12 sections.....45

Table 5.1.4: Position of the SF for the SR02a, SR02b and A12 sections.....46

Table 5.2.1: Geostrophic velocities associated with the APF for the SR02a, SR02b and A12 sections.....48

Table 5.2.2: Geostrophic velocities associated with the SAF for the SR02a, SR02b and A12 sections.....49

Table 5.2.3: Geostrophic velocities associated with the STC for the SR02a, SR02b and A12 sections.....50

Table 5.2.4: Geostrophic velocities associated with the Southern Front for the SR02a, SR02b and A12 sections.....50

List of acronyms used in the text

AABW: Antarctic Bottom Water

AAIW: Antarctic Intermediate Water

AASW: Antarctic Surface Water

AAZ: Antarctic Zone

ACC: Antarctic Circumpolar Current

APF: Antarctic Polar Front

ASF: Antarctic Slope Front

CDW: Circumpolar Deep Water

CTD: Conductivity, Temperature and Depth Profiler

CZ: Continental Zone

PFZ: Polar Font Zone

IOCW: Indian Ocean Central Water

ISOS: International Southern Ocean Studies

JGOFS: Joint Global Ocean Flux Study

LCDW: Lower Circumpolar Deep Water

NADW: North Atlantic Deep Water

SAF: Subantarctic Front

SAMW: Subantarctic Mode Water

SASW: Subantarctic Surface Water

SAZ: Subantarctic Zone

SST: Sea Surface Temperature

SSW: Subtropical Surface Water

STC: Subtropical Convergence

Sv: Sverdrup ($\times 10^6 m^3$)

UCDW: Upper Circumpolar Deep Water

WOCE: World Ocean Circulation Experiment

WHP: WOCE Hydrographic Program

WW: Winter Water

XBT: Expendable Bathythermograph

Chapter1

This chapter aims to introduce the subject and to lay a foundation for the motivation for this study of the ocean.

Introduction

In recent years "global warming" and its potential effects on world populations has become a factor of great concern. Climate change would have catastrophic implications for many areas on the globe. Sea level rise due mainly to thermal expansion of the ocean and the melting of glaciers and small ice caps would have a huge impact on coastal populations. It is expected that the sea level will rise between 30 to 110 cm between 1990 and 2100 (Eid and Hulsbergen, 1991). This could mean the inundation of coastal wetlands and other low lands, the retreat of beaches by a few hundred meters and the breaching of protective structures. Flooding would threaten lives, agriculture, livestock, buildings and infrastructure. The landward advancing of salt water into aquifers and up estuaries would threaten water supplies, ecosystems and agriculture in some areas. Changes in climatic conditions such as a change in rainfall patterns would have a devastating result on agriculture. Wheat and rice are the most important staple food around the world and any climatic change would have a profound effect on global food security. Rice is highly sensitive to temperature changes and an increase in temperature would result in a decrease in yield in low latitudes (Sinha, 1991). Changes in climate have also been linked to a change in marine ecosystems. It could result in the change of the taxonomic composition of plankton and the range of the major fish stocks as well as in the species composition.

The cause of global warming is still uncertain but the number of causal factors can be divided into internal and external factors. External factors are those that are either external to the planet or derived from sources external to the climate system for example the enhancement of greenhouse gasses by human activity. Internal factors are those within the climate system namely the atmosphere, the ocean and those parts of the cryosphere that respond on time-scales of up to centuries (Wigley and Raper, 1991). General circulation models for the atmosphere have recently been developed based on data that have been gathered over the past hundred years in some areas. For the ocean the World Ocean Circulation Experiment (WOCE) was initiated with the

view of improving estimates of the circulation of heat, water and chemicals around the world ocean (Woods, 1985). The ocean covers more than 70% of the surface of the earth and has a heat capacity a thousand times that of air (Kawasaki, 1991). Due to the unequal distribution of heat across the surface of the planet the ocean plays an important part in moving heat from the tropics to the poles. It also acts as a sink for CO_2, a greenhouse gas that causes global warming. A detailed study of the ocean was thus necessary to best predict climate change due to natural fluctuations, human perturbations, and their interaction (Baker, 1991). As part of South Africa's contribution to WOCE a hydrographic section was carried out in February 1993 from Antarctica to Africa (figure 1.1) aboard the MV. SA Agulhas. This was a WOCE repeat section called the SR02 section and will form the basis for this study.

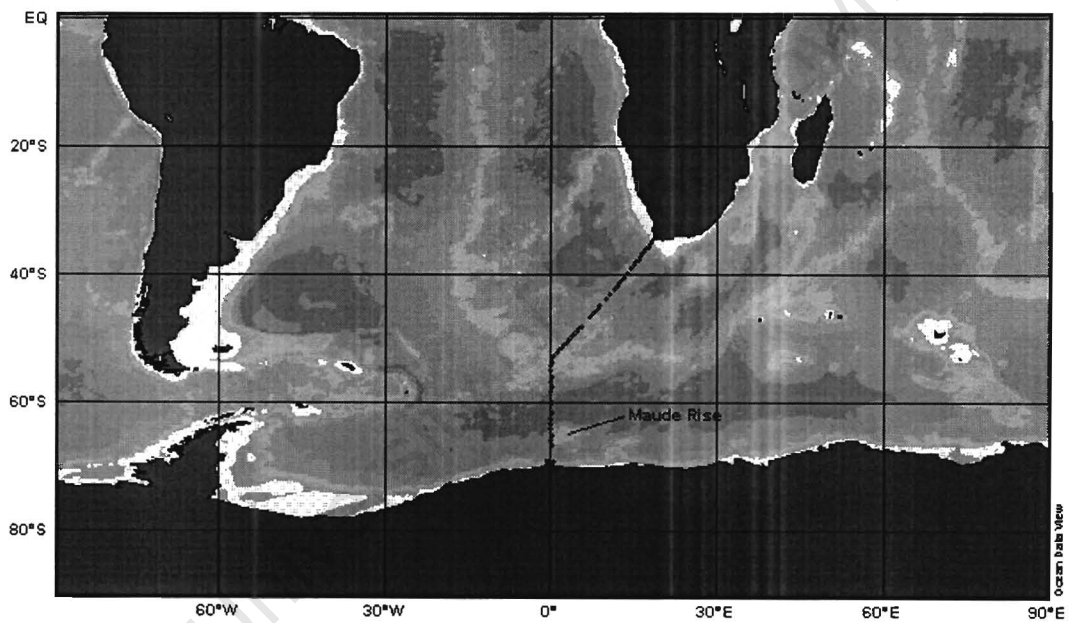

Fig. 1.1: Map showing the SR02 repeat section of February 1993

The section crosses the Southern Ocean as well as the South Atlantic, in particular the Agulhas Retroflection region. The initial planned WOCE cross sections of the South Atlantic Ocean are indicated in figure 1.2.

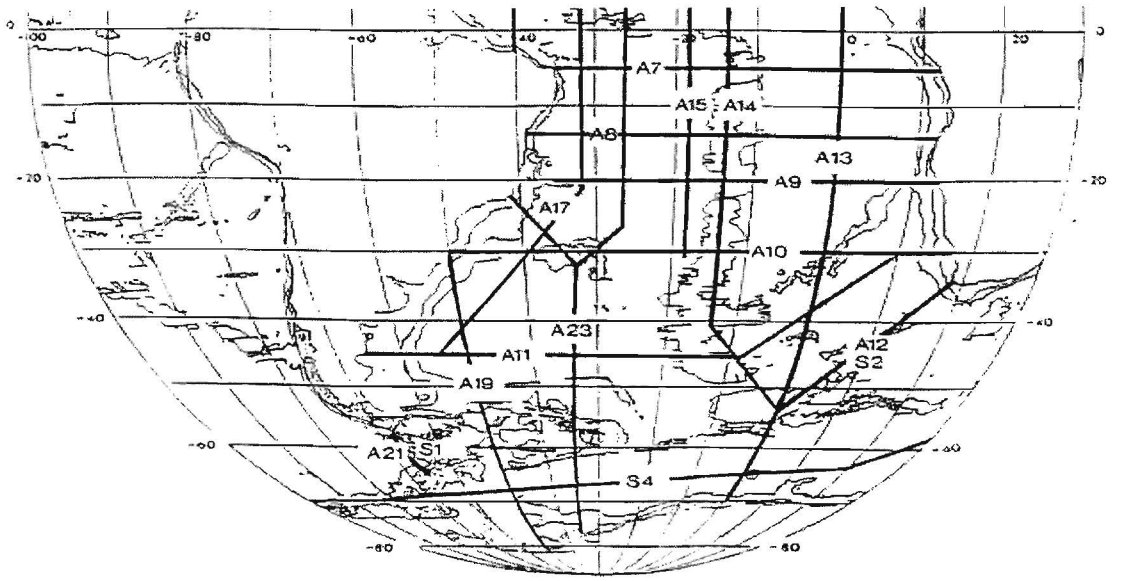

Fig.1.2: Map showing the sections of the WHP Survey of the South Atlantic Ocean

The Southern Ocean plays an important role in the dynamics of the world ocean. It has the world's strongest current system, namely the Antarctic Circumpolar Current (ACC), which flows around Antarctica uninterrupted and provides and efficient vehicle for heat and freshwater transport (Georgi and Toole, 1982). A vertical cross section of the Southern Ocean reveals regions of strong temperature and salinity gradients called fronts as well as a vertical layer structure. Each layer comprises a water mass. The fronts form the boundaries between the different water masses in the upper water column (Sievers and Nowlin, 1984). The hydrographic section shown in figure 1.2 also crosses the eastern section of the Weddell Gyre where 50-90% of all abyssal waters gain their characteristics (Fahrbach et al., 1994). In the next chapter I will give an in-depth look into the ACC, water masses, fronts, the Weddell Gyre and heat fluxes in the region of the section in order to establish what is known about this particular region.

Chapter 2

This chapter provides known information from the literature on the meso-scale oceanic features that were briefly mentioned in chapter one in relation to our area of study (figure 1.1). Temperatures unless otherwise specified will be potential temperatures.

Background

2.1 Antarctic Circumpolar Current (ACC)

The Southern Ocean plays an important role in determining the distribution of properties in the abyssal waters of the World Ocean. One reason for the importance of the Southern Ocean is its unique current system, the Antarctic Circumpolar Current, in which enormous amounts of water are being exchanged between ocean basins (Orsi et al., 1995; Gordon, 2001). Deacon (1937) pointed out the large-scale features of this circulation system over sixty years ago. The deep-reaching eastward flowing ACC is driven by the world's mightiest westerly winds that are found approximately between 45°-55 °S (Orsi et al., 1995). The path of the ACC is also firmly controlled by the major bottom ridges along its path (Gordon et al., 1978). Adjacent to Antarctica the flow is westward, driven by the prevailing easterly winds found south of about 65°S. At the transition between west and east winds isotherms and isohalines shoal, inducing clockwise flow under geostrophic balance. These cyclonic cells of re-circulating water develop south of the ACC of which the Weddell and Ross Gyres are the best known. Together with wind and buoyancy-driven westward flows these cyclonic circulations form the subpolar regime of the Southern Ocean (Orsi et al., 1995).

The ACC is associated with a steep rise of the isopycnals towards the south through the entire water column. Deacon (1937) noted that the poleward rise of the isopycnals and isohalines was not uniform, but occurred in a series of step-like patterns. Strong surface currents are associated with these bands of strong density gradients, which characterize the ACC fronts. The Subtropical Convergence forms the northern boundary of the Antarctic Circumpolar Current and until recently there was no well-defined boundary between the current and the subpolar regime (Orsi et al., 1995). The

two major fronts that have been shown to be continuous features of the ACC are the Subantarctic and Antarctic Polar Fronts. A third deep-reaching front is persistently observed as part of the ACC south of the Antarctic Polar Front called the Continental Water Boundary. This front is however only observed in the Drake Passage. The term Continental Water Boundary was initially used to delineate the northern boundary of the waters found to the south of the ACC, and not as a name for the frontal feature to the north of it. Since the southern most front is located such a distance from the Antarctic continent, Orsi et al. (1995) suggested that this term be abandoned.

Along the Greenwich Meridian Whitworth and Nowlin (1987) also found a third front that separates the Weddell Gyre from the ACC, which for mass balance reasons they included as part of the ACC. They stated that this front could be a downstream extension of the Scotia Front. Orsi et al. (1995) however found that as in the Drake Passage, at the Greenwich Meridian the southern most front in the ACC occurs where the Upper Circumpolar Deep Water has a temperature greater than 1.8°C. It was concluded that the front was continuous and was termed the southern ACC front. This front is the only front in the ACC that does not separate distinct surface water masses. The examination of transects indicate that the southern limit of Upper Circumpolar Deep Water characteristics are in good agreement with the observed change in geostrophic shear between the ACC and the subpolar regime. Suggestions are that this could be a useful definition of the southern boundary of the ACC (Orsi et al., 1995).

In later discussions the southern boundary of the ACC is referred to as the Weddell Front in the region south of Africa. Park et al. (2001) indicated that at the position of the Southern Front the salinity maximum changes abruptly from relatively saline (>34.72), warm (>1.5°C) ACC regime to fresh (~34.68) and cold (<0.4) Weddell regime. Schröder and Fahrbach (1999) used the S_{max} 34.72 and θ 1.5°C to distinguish the ACC from the Weddell Gyre. This definition will be adopted to identify the Weddell Front (Southern Front).

2.1.1 Transport

In the Drake Passage, the ACC does not consist of a broad, horizontally homogenous flow, but instead of bands of intense flow along three thermohaline fronts (the Polar Front, Subantarctic Front and Continental Water Boundary) with regions of weaker flow between these fronts (Sievers and Nowlin, 1988). In the Drake Passage, the geostrophic transports in these three fronts account for approximately 75% of the total baroclinic transport of the ACC relative to 2500 m (Nowlin and Clifford, 1982). The shear in these geostrophic flows extended all the way to the bottom (Sievers and Nowlin, 1988). Maximum velocities in the Atlantic and Pacific sectors occur at the Antarctic Polar Front and at the Subantarctic Front in the Indian Ocean. In the Southwest Atlantic Ocean North Atlantic Deep Water intrudes into the ACC, while south of Africa the Agulhas current transports warm saline water southwards into the ACC and creates a zone of enhanced baroclinicity, which extends into the ACC up to 70°E (Lutjeharms and Ansorge, 2001).

Previous estimates of the transport of the ACC lie within the range of a 130 to 140 Sv for the region south of Africa (Read and Pollard, 1993). Nowlin and Klinck (1986) reviewed the theoretical and observational progress in understanding the transport, structure and dynamics of the ACC over the decade of the ISOS program. They reported a mean transport through the Drake Passage of 134 Sv with an uncertainty of 10% and a estimated time variability of 20%. Most variability was seen in the barotropic field and not in the baroclinic shear. Whitworth and Nowlin (1987) estimated the transport of the ACC at the Greenwich Meridian to be 162 Sv, with the slightly higher value being attributed to the incorporation of North Atlantic Deep Water into the ACC in the South Atlantic. The net flow between Africa and Antarctica was estimated to be 142 Sv due to a flow of 19 Sv from the Indian Ocean to the Atlantic (Whitworth and Nowlin, 1987).

2.2 **Water Masses**

Oceanographers have been studying the vertical layer structure of the Southern Ocean since the beginning of the century. Recent studies have also focused on their importance in the regulation of the global climate. The waters that comprise these layers are all derived from surface waters from a particular area of the World Ocean. Conditioning of surface waters, result in them sinking to an equilibrium depth and spreading along appropriate density surfaces (Reid et al., 1977). Water masses are traditionally described by their core properties i.e. extremes of temperature, salinity, O_2 or nutrients. Continuous formation results in these water masses ventilating the World Ocean. As the water mass moves away from its source its characteristics are changed either through diffusion, mixing, biological processes or through interaction with the bottom sediments (Sievers and Nowlin, 1988)

Numerous publications have been written on water masses in the different regions of the World Ocean. Water masses present at the Drake Passage have been discussed by Sievers and Nowlin (1984) whilst those along the Greenwich meridian of the Southern Ocean have been dealt with by Whitworth and Nowlin (1987). Those of the Southwest-Indian Ocean sector have been discussed with by Jacobs and Georgi (1977). Along the Greenwich Meridian Whitworth and Nowlin (1987) found the following water masses to be present: Antarctic Surface Water, Sub-Antarctic Surface water, Circumpolar Deep Water, North Atlantic Deep Water, Antarctic Bottom Water and Subtropical Surface Water. Except for North Atlantic Deep Water all the other water masses have their origin in the Southern Ocean. Since the section under investigation is along the Greenwich meridian we will focus in on these water masses.

2.2.1 Subtropical Surface Water (SSW)

This water mass is found north of the Subtropical Convergence and is characterized by relatively high temperatures and salinities (>12°C, >35.1) and an oxygen minimum below 6ml/l (Park et al., 1993). Park et al. (1993) have found that in their study area there was no definite theta-S and theta-O_2 relationship but that these properties were spread over a wide range of values, with strong zonal anomalies.

2.2.2 Subantarctic Surface Water (SASW)

SASW is found in the Subantarctic zone (SAZ) between the Subtropical Convergence (STC) and the Subantarctic Front (SAF) from the surface to a depth of around 150 meters. SASW extend from the surface to the depth of the Antarctic Intermediate Water (AAIW) or Subantarctic Mode Water (SAMW) (Sievers and Nowlin, 1984).

Being the northernmost portion of the ACC, this water mass is strongly influenced by mixing with the adjacent subtropical gyres and air-sea interaction along its circumpolar path (Whitworth and Nowlin, 1987). At the Drake Passage the SASW is less saline than the waters of the Antarctic Polar Front zone, reflecting the relative fresh surface water of the South Pacific (Sievers and Nowlin, 1984). At the Greenwich Meridian, the surface water of the SAZ is about 0.3-0.4 more saline than that at the Drake Passage making it more saline than that at the PFZ (Whitworth and Nowlin, 1987). In the Drake Passage SASW is characterized as having a salinity minimum and a oxygen maximum compared with the underlying Subantarctic Mode Water (Sievers and Nowlin, 1984). Low salinities evident in the SAZ are due to a large excess of precipitation over evaporation rather than the injection of less saline water across the APF (McCartney, 1977). At the Greenwich meridian, Whitworth and Nowlin (1987) characterized it as having a subsurface salinity maximum and oxygen minimum due to the underlying AAIW. Table 1.1 gives some indication of the characteristic values associated with SASW.

Table 1.1: Comparison of temperature, salinity and oxygen values of the Melville-75 (1975) and MV Marion Dufresne/RRS Charles Darwin-29 (1991) of SASW

	Temperature	Salinity	Oxygen
Melville 75	<7 in summer	<34.1	----
MV M Dufresne/ RRS Charles Darwin	<9°C	<34	>7ml/l

2.2.3 Subantarctic Mode Water (SAMW)

SAMW lies mainly in the SAZ and is a relatively homogenous layer up to 700 m thick, beneath the SASW and above the AAIW. A weak salinity and O_2 maximum characterize this water mass (Sievers and Nowlin, 1984). This water mass is formed by vertical convective overturning at the end of winter. Cooling at the surface during the autumn and winter erases the seasonal thermocline allowing this deep convection (McCartney, 1977; Hanawa and Talley, 2001). McCartney (1977) has suggested that this water mass plays a role in the formation of AAIW in the South Atlantic. He claims that the waters being cooled and overturned to form AAIW are the coldest, freshest types of SAMW advecting in from the west along the SAF. Traditionally AAIW was considered to be formed by cross Polar frontal mixing of the low salinity Antarctic Surface Water and SASW (Sverdrup et al., 1942). Table 1.2 gives some indication of the characteristic values associated with SAMW.

Table 1.2: Comparison of temperature, salinity and oxygen values of the Melville-75 (1975) and MV Marion Dufresne/RRS Charles Darwin-29 (1991) of SAMW

	Temp	Salinity	Oxygen
Melville 75	4-6°C	34-34.2	----
MV M Dufresne/ RRS Charles Darwin	$11<\theta<14$°C	35-35.4	5.2-5.7ml/l

2.2.4 Transition zone between AASW and SASW

The transition between AASW and SASW occurs in the Antarctic Polar Front zone (PFZ), which lies between the SAF and the Antarctic Polar Front (APF). Moving from north to south, the transition is characterized by a sharp drop in surface temperature and salinity and a increase in O_2 concentrations. On entering the PFZ from the north, one crosses the SAF, which is characterized by a dramatic increase in the surface NO_3 and PO_4 concentrations. Surface characteristics within the PFZ are nearly constant until the abrupt changes in gradients associated with the Antarctic Polar Front are encountered (Whitworth and Nowlin, 1987).

2.2.5 Antarctic Surface Water (AASW)

AASW lies in the upper 250 m of the water column south of the APF (Sievers and Nowlin, 1984). These waters are cold, fresh, high in dissolved O_2 and high in nutrients relative to the SASW but lower in nutrients than the underlying water (Whitworth and Nowlin, 1987). The AASW differs from winter to summer. In winter it is a nearly homogenous water mass that extends down to the level of the summer temperature minimum (Sievers and Nowlin, 1984). However in summer AASW is characterized as having a intense temperature minimum at 200 m (commonly known as Winter Water) that marks the base of the winter mixed layer (Whitworth and Nowlin, 1987). This temperature minimum layer frequently contains patches of cold water separated by regions of warm water (Sievers and Nowlin, 1984). Seasonal variability was also observed in the salinity of AASW with the greatest salinities observed in winter (Deacon, 1937). The decrease in summer is mainly as a result of ice melting. AASW increases in temperature, from –1.9°C at the ice edge to 1°C or 3.5° C in summer at the APF, while the salinity drops from 34.6 to 33.8 at the ice edge (Deacon, 1937). At the Drake Passage a large variability was seen in the oxygen concentrations of this water mass. The main oxygen maximum had a oxygen concentration greater than 8 ml/l (Sievers and Nowlin, 1984). Park et al. (1993) found that in the South West Indian Ocean this water mass had a temperature less than 5°C and an oxygen maximum of greater than 7 ml/l.

2.2.6 Antarctic Intermediate Water (AAIW)

AAIW is a fresh, highly oxygenated water mass that sinks toward the north from the SAF at potential density values between 27.1 and 27.2 kg.m (Whitworth and Nowlin, 1987). Its core lies near the sea surface north of the Antarctic Polar Front Zone and deepens northwards to more than 1000 m in the mid-latitudes (Piola and Georgi, 1982). Initially two opposed theories were put forward for the formation of AAIW; one school attributed AAIW to wind-driven convergence (Sverdrup, 1940); the other attributed it to the thermohaline-driven circulation (Wüst, 1935; Deacon, 1933, 1937). The traditional idea that AAIW is derived in part from the northward movement and mixing of AASW is evidenced in the extension of the AASW temperature minimum into the AAIW. Recent proposed mechanisms include mixing across the Antarctic Polar Front by small-scale processes in the Scotia Sea and the

Drake Passage and divergence of geostrophic transport in the South Pacific (Gordon et al., 1977a; Joyce et al., 1978; Molinelli, 1981).

McCartney (1977, 1982) in contrast suggested that deep winter convection in the Subantarctic zone of the southeast Pacific plays a major role in the formation of AAIW. Subantarctic Mode Water (SAMW) due to convective overturning was shown to have properties similar to the winter outcrop and minimum values of potential vorticity. It has however been pointed out that there is striking differences between the salinity minimum values of the southwestern regions of the three southern hemisphere oceans (Jacobs and Georgi, 1977). This difference in AAIW varieties of the South Pacific and South Atlantic indicates that an Antarctic water mass component is required, because the required cooling and freshening of SAMW along its path through the Drake Passage is far too large to be explained solely by the heat and freshwater fluxes through the sea surface (Georgi, 1979; Piola and Georgi, 1982; Piola and Gordon, 1989). In the Drake Passage, the salinity minimum layer associated with the AAIW can be traced from the north, southwards across the PFZ to the APF (Sievers and Nowlin, 1984). However, in the Greenwich section this salinity minimum observed in the SAZ, surfaces at the SAF (Whitworth and Nowlin, 1987). Whitworth and Nowlin (1987) noted that although the connection between AAIW and AASW was not as clear as in the Drake Passage the lowest surface salinities were found immediately south of the Antarctic Polar Front.

AAIW terminates at about 10°S in the Pacific Ocean and about 5°S in the Indian Ocean (Wyrtki, 1971). No northward-flowing western boundary current of low salinity water is observed in the Indian Ocean. AAIW of the Indian Ocean is thus relatively salty and poorly ventilated (Piola and Gordon, 1989). The intermediate water of the South Pacific is mainly of Subantarctic origin. Piola and Gordon (1989) indicated that although intermediate water of Antarctic origin can be found in the southeast Pacific south of the Antarctic Polar Front, it is advected into the South Atlantic. Table 1.3 gives some indication of the characteristic values associated with AAIW.

Table 1.3: Comparison of temperature, salinity and oxygen values of the Melville-75 (1975) and MV Marion Dufresne/RRS Charles Darwin-29 (1991) of AAIW

	Temp	Salinity	Oxygen
Melville 75	-----	-----	6-7ml/l
MV M Dufresne/ RRS Charles Darwin	4.36°C	34.35	4.82ml/l

2.2.7 Circumpolar Deep Water (CDW)

CDW is the most extensive water mass in the ACC. Upon leaving the Drake Passage the ACC is influenced by water in the Weddell Sea to the south and by NADW to the north. The water mass that is most influenced between these two points is the CDW. CDW trapped in the Weddell Gyre has its characteristics eroded away and lost to the surface waters (Whitworth and Nowlin, 1987). It is common to distinguish CDW between its upper and lower layers namely, Upper Circumpolar Deep Water (UCDW) and Lower Circumpolar Deep Water (LCDW) based on properties acquired from different source regions (Gordon, 1967). An O_2 minimum and a nutrient maximum characterize UCDW whose source regions are in the Indian and Pacific Oceans (Callahan, 1972). UCDW also has a relative temperature maximum induced by the overlying AAIW and WW south of the SAF. LCDW has a salinity maximum and nutrient minimum, which derive from North Atlantic Deep Water (NADW). Near the source region of LCDW in the southwest Atlantic distinctions among UCDW, LCDW and NADW are not so clear because of mixing taking place (Whitworth and Nowlin, 1987).

It is the relatively warm, salty, oxygen rich and nutrient poor NADW that splits the CDW in two by penetrating it just below the oxygen minimum with the upper part characterized by a O_2 minimum layer advected through the Drake Passage. The lower branch also has a O_2 minimum induced by the overlying NADW and underlying Antarctic Bottom Water. This O_2 minimum feature is only found in the southwest Atlantic where the NADW first encounters the ACC. At the Greenwich meridian the O_2 minimum has been eroded away from the UCDW minimum to the bottom (Whitworth and Nowlin, 1987).

UCDW

In this water mass the oxygen minimum lies slightly below the maxima in the phosphate and nitrate. Mixing with NADW causes the differences between UCDW found at the Drake Passage and that at the Greenwich meridian. If one compares NADW with CDW, NADW is relatively warmer, more saline, high in oxygen and low in phosphate and nitrate. At the Drake Passage there is a increase in the O_2 concentrations in the minimum from the Subantarctic zone to the Antarctic zone. This trend reversed downstream due to the influx of NADW at the northern edge of the ACC. Interaction between NADW and UCDW also results in the erosion of the phosphate maximum, found at the Drake Passage. In the Drake Passage UCDW had a mean phosphate concentration of 2.42 µmol/l whilst that of nitrate was 35.4 µmol/l (Whitworth and Nowlin, 1987). At the Greenwich meridian the average phosphate concentration is reduced to 2.36 µmol/l. However, south of the Polar front where little mixing between NADW and UCDW has occurred, the phosphate maximum has the same value as in the Drake Passage (Whitworth and Nowlin, 1987).

Nitrate concentrations north of the Subantarctic Front along the AJAX section were less than those in the Drake Passage (34.8 µmol/l). However, nitrate values as high as 36.8 µmol/l were found near the Antarctic Polar Front. The highest concentrations found in the Drake Passage were 1 µmol/l lower (Whitworth and Nowlin, 1987). Table 1.4 gives some indication of the characteristic values associated with UCDW.

Table 1.4: Comparison of temperature, salinity and oxygen values of the Melville-75 (1975), MV Marion Dufresne/RRS Charles Darwin-29 (1991) and AJAX cruise of UCDW

	Temp	Salinity	Oxygen
Melville 75	-------	------	3.7-4.1ml/l
MV M Dufresne/ RRS Charles Darwin	-------	------	4.15ml/l
AJAX	-------	------	4.1-4.2ml/l

LCDW

This water mass is characterized by a salinity maximum and a phosphate and nitrate minimum which is derived from interaction with NADW. At the Drake Passage, which is the furthest from the NADW renewal source, the lowest CDW salinity maximum is observed in the entire Southern Ocean. The mean salinity maximum in the Drake Passage is 34.729. Between the Drake Passage and the Greenwich Meridian the salinity value increases to salinities greater than 34.73 due to mixing with NADW. Mixing between the CDW and the NADW to form LCDW occurs over both the SAF and the APF. Phosphate (nitrate) concentrations at the Drake Passage average 2.25(32.5) µmol/l. Mixing with NADW reduced this value to 1.98(29.9) µmol/l north of the APF on the AJAX section (Whitworth and Nowlin, 1987). Table 1.5 gives some indication of the characteristic values associated with LCDW.

Table 1.5: Comparison of temperature, salinity and oxygen values of the Melville-75 (1975) and MV Marion Dufresne/RRS Charles Darwin-29 of LCDW

	Temp	Salinity	Oxygen
Melville 75	------	34.729(max)	------
MV M Dufresne/ RRS Charles Darwin	------	34.73-34.76	4.2-4.3ml/l at salinity maximum

2.2.8 Antarctic Bottom water (AABW)

Antarctic Bottom Water occupies a large proportion of the deepest part of the ocean (Gill, 1973). Antarctic Bottom Water forms as a result of two processes within the Western Weddell Sea. Warm Deep Water at the shelf break mixes with the more saline Western shelf water to form Modified Warm Deep water. The modified water mass then mixes with Winter Water, which is less saline as a result of the stirring action of the shelf waves, to form AABW. Secondly, the super-cooling of Western shelf water beneath the ice shelf before it spills over the sill to mix with Warm Deep Water is also a mechanism of AABW formation. Trace measurements were found to be consistent with this input theory. Both processes require high salinity shelf water. Eastern Shelf Water in contrast to Western Shelf Water has salinities lower than the

Winter Water, which prevents the generation of a water mass dense enough to form Bottom Water. The formation of AABW is thus restricted to the southwestern Weddell Gyre (Fahrbach et al., 1994).

The Weddell Gyre is however, not the only source of AABW. Near bottom data over the Antarctic continental rise and slope have revealed that significant bottom water sources exist outside the Weddell Sea (Jacobs and Georgi, 1977). Other sources include the Ross Sea and Adelie Land (Gill, 1973; Rintoul, 1998). Antarctic Bottom Water has a bottom potential temperature minimum, salinity minimum and oxygen maximum. Along the Conrad-17 stations AABW had a temperature minimum of θ = -0.75°C, salinities below 34.660 and an oxygen maximum of 6.10 ml/l (Jacobs and Georgi, 1977). In the Crozet Basin near the Crozet-Kerguelen gap, the AABW had a salinity value of 34.667, temperature of –0.33°C and a oxygen maximum of 5.36ml/l whilst west of Amsterdam it had a temperature of 0.81°C, a oxygen concentration of 4.61ml/l and a salinity value of 34.709 (Park et. al, 1993).

2.3 Weddell Gyre

A Greenwich Meridian section crosses both the northern and southern limb of the Weddell Gyre. The southward flowing eastern boundary of the Weddell Gyre is located between 20° and 30°E. Its eastern position is perhaps related to the gap in the mid-ocean ridge. However, it may vary in its location depending on the strength of the eastward flowing Antarctic Circumpolar current. Near the Antarctic continent there is a westward flow of Circumpolar Deep Water from the ACC round the eastern end of the Weddell Gyre. This water loses most of its characteristics in the Weddell Sea either through alteration by biochemical processes, or in the production of Bottom Water (Whitworth and Nowlin, 1987). Carmack and Forster (1975) have estimated the total outflow towards the east from the Weddell Sea to be 96.9 Sv within limits of ±10%, of which 68.7% is bottom water, 23.8% deep water and 4.4% near-surface water. It has been shown that Antarctic Bottom water is formed year round in the southwestern part of the Weddell Sea (Foster and Carmack, 1976).

2.3.1 Transport

The Weddell Gyre shows little baroclinicity and the surface speeds are generally less than 2 cm/s. Whitworth and Nowlin (1987) have found a transport of 17 Sv relative to the bottom. They, however, state that this value may be a considerable underestimate if there is a significant barotropic component, which was not included. Using geostrophic calculations adjusted to direct current measurements Carmack and Foster (1975) estimated a transport of 97 Sv. A wind-driven transport of 76 Sv was calculated by Gordon et al. (1981) for the western boundary current of the Gyre, with about 60-70 Sv crossing the Greenwich Meridian.

Water Masses in the Weddell Gyre

2.3.2 Antarctic Surface Water

This near-surface water mass of the Weddell Gyre has a strong summer temperature minimum layer around 100 m (Whitworth and Nowlin, 1987). This water mass is described in detail in section 2.2.5. Below this water mass there is a relatively warm, saline layer, below which the water characteristics generally change monotonically through the Deep and Bottom Waters. The northern extend of the warm salty layer was considered to be the eastern extend of the Weddell-Scotia Confluence (Gordon et al., 1977a). The confluence separates the waters of the Weddell Sea and the Scotia Sea in the western Weddell Sea. However at the Greenwich Meridian the remnant of the confluence lies about 200 km south of the front that separates the Weddell Gyre from the Antarctic Circumpolar current (Whitworth and Nowlin, 1987).

2.3.3 Intermediate waters

This temperature maximum layer was considered by Deacon (1933) to be part of the "Warm Deep Water" that is found at depths greater than 2000 m in the tropics and rises abruptly at the Antarctic convergence. The name, Antarctic Circumpolar Deep Water was later proposed for this water mass and is now in common use. Deacon's term is now restricted to water between 0° and –0.7°C, limiting its applicability to the Weddell Sea where "Warm Deep Water" is least descriptive (Whitworth and Nowlin, 1987). Whitworth and Nowlin (1987) indicate that most of the intermediate waters of the Weddell Gyre to be LCDW from the southern ACC. They also show that in the central part of the Gyre this water mass is altered by biochemical processes to form a

distinct water mass they called the intermediate water of the central Weddell Gyre or central intermediate water in short.

The LCDW forming part of the intermediate waters of the Weddell Gyre does however undergo small changes between the Drake Passage and the Greenwich meridian. Water warmer than 0.8°C was more saline due to the influence of NADW whilst water cooler than 0.8°C were fresher due to the influence of the fresher Weddell Gyre. From the temperature profile of the AJAX section it was clear that only the densest LCDW was found near the axis of the Weddell Gyre. The relatively warm, saline LCDW rounds the eastern end of the Weddell Gyre and meanders around the Maude Rise (figure 1.1) towards the west. The most warmest, most saline CDW enters the gyre between 300 to 600 m to the north of the Maude Rise whilst some part of this does return eastward to the south of the rise (Whitworth and Nowlin, 1987).

Outside the Weddell Gyre the UCDW is characterized by a oxygen minimum below which concentrations increase monotonically through the LCDW and bottom waters. In the northern limb of the Weddell Gyre, an oxygen minimum is induced on the LCDW by the overlying high-oxygen near-surface waters. Whitworth and Nowlin (1987) found that near the axis of the gyre this oxygen minimum within the LCDW is absent and there is a separate minimum near σ=37.13 kg m^{-3}. South of this the oxygen minimum was associated with a maximum in nutrients, which extended in weakened forms into the northern and southern limbs of the Weddell Gyre. In the southern limb this layer lies about 800 m deeper than the LCDW remnant near 200 m. Whitworth and Nowlin (1987) referred to this layer as the intermediate water of the central Weddell Gyre to distinguish it from its parent LCDW.

As stated central intermediate water has an oxygen minimum associated with a maximum in nutrients, which suggest that it may be formed by in situ oxygen consumption and nutrient regeneration through bacterial decomposition of organic matter. Below the central intermediate water is a silicate maximum layer. The source of this layer is speculated to be either the Indian Ocean sector of the Southern Ocean, where deep and bottom layers have high concentrations through contact with the

bottom sediments or of sinking particulate matter following complete regeneration of phosphate and nitrate in the overlying water. It was however not possible to specify the mechanism by which this layer is generated since not enough is known about the eastern portion of the Weddell Gyre (Whitworth and Nowlin, 1987).

2.3.4 Deep and Bottom Water

Weddell Sea Deep Water is probably more important than the other Weddell Sea water masses in terms of ocean circulation, since it is the Deep Water that escapes the boundaries of the Weddell Sea to become the main ingredient of Antarctic Bottom Water. Deep Water is essentially featureless within the Weddell Sea, consisting mainly of old Bottom Water that has been displaced upward by the production of new Bottom Water. A relative temperature, salinity and nutrient minimum and a relative maximum in dissolved oxygen characterize Bottom Water (Whitworth and Nowlin, 1987). Carmack and Foster (1975) term the coldest Bottom Water with potential temperatures below –0.7° C to be Weddell Sea Bottom Water. Whitworth and Nowlin (1987) found that the salinity and silicate extrema characteristics of the Deep and Bottom Water were skewed towards the northern edge of the Weddell basin. They stated that this might be due to the presence of a deep boundary current, but that an influx of anomalous characteristics at the southern margin could also be responsible.

2.4 Southern Ocean Fronts in the Atlantic and Indian Oceans

In describing the structure of the deep waters of the ACC between Australia and Antarctica, Deacon (1937) noted that the general upward slope of isotherms and isohalines towards the south was 'not steep and unbroken, but gradual and in a series of steps'. Since then numerous investigators have described the structure of these fronts of the Southern Ocean. Investigations include that by Gordon et al. (1977b) south of Australia, Nowlin et al. (1977) in the Drake Passage, Gordon et al. (1977b) in the Western Scotia Sea and Lutjeharms and Valentine (1984) south of Africa. They have shown that the Southern Ocean can be divided in four zones namely, the Subantarctic zone (SAZ), the Antarctic Polar Frontal Zone (PFZ), the Antarctic Zone (AAZ) and the Continental Zone (CZ). More recent publications on the circumpolar structure of the fronts associated with the ACC include Orsi et al. (1995) and Belkin and Gordon (1996) for the region between the Greenwich meridian and Tasmania.

Southern Ocean fronts encountered from north to south are the Subtropical Convergence (STC), the Subantarctic Front (SAF), the Antarctic Polar Front (APF) and the Southern Front/Weddell Front (figure 2.4) for the region south of Africa.

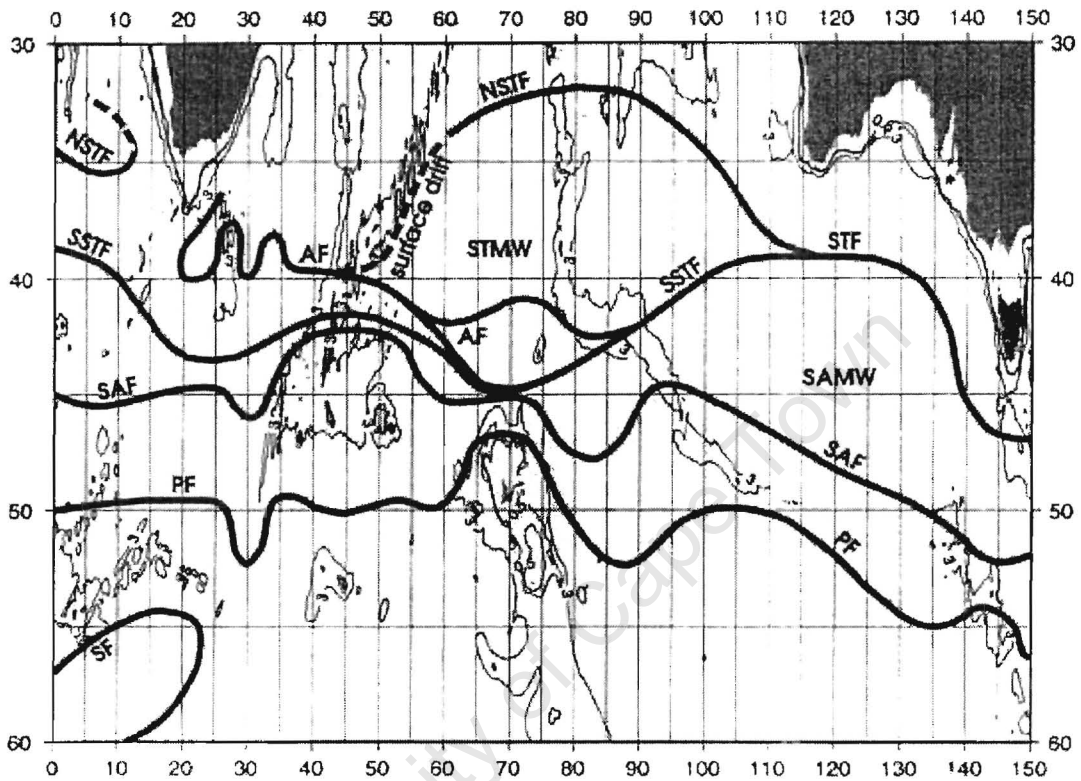

Fig 2.4: Frontal patterns from 0° to 150°E (from Belkin and Gordon, 1996).

Fronts associated with the ACC are easily identified as narrow regions of sharp horizontal gradients of water properties. They also mark the upper ocean boundaries of different water masses (Park et al., 1993). Because of this, fronts are most easily distinguished from one another in the upper water column, where they form boundaries between the different water masses (Whitworth and Nowlin, 1987). Park et al. (1993) suggest that these fronts are best marked at the sub-surface depth of 200 m in the South West Indian Ocean.

Definition of fronts (South of Africa and in the Southwest Indian Ocean)

Historically fronts have been defined as being located at fixed temperature or salinity values or at locations where specified changes in temperature or salinity values take place. These definitions usually have limited geographic applicability. Over the years many different definitions have been used in describing Oceanic fronts. Even the nomenclature used to describe the fronts has changed. It seems that the different definitions scientists have used for the fronts in the Southern Ocean has depended on the type and quality of data that was then available. This has particularly been the case in the data sparse regions away from the Drake Passage and where less than perfect historical data has been used (Nagata et al., 1988; Lutjeharms, 1985). In order to unambiguously place fronts we will look at different definitions pertaining to each of the fronts, but where possible the definitions as given by Whitworth and Nowlin (1987) will be used. It should be accepted that at times the circulation is 'messy' and that unambiguous definition of a single front is not possible.

2.4.1 Subtropical Convergence (STC)

The STC (also known as the Subtropical Front (STF)) is the northernmost front associated with the ACC and was first described by Deacon (1937). It occurs where the denser Subantarctic waters sink below the warmer and more saline Subtropical Waters. Recently the STC has been shown to have a double structure in the South Atlantic and the South Pacific consisting of a North and South STC (Belkin and Gordon, 1996). They describe the Southern STC as having a subsurface S_{max} south of the front as well as a sharp change of the surface salinity (S_0) across 35.0. It has a average surface temperature (T_0) range of 10.1-15.1°C and a salinity range of 34.30-35.18 at the surface in the African sector. The Northern STC is described as having a sharp change of S_0 across 35.5 combined with a sharp change of the surface temperature (T_0) across 20.0°C. For the Northern STC the average salinity and temperature ranges were 34.87-35.58 and 14.0-16.9°C at the surface (Belkin and Gordon, 1996). The location of the surface STC described by Whitworth and Nowlin (1987) actually corresponds with the SSTC as described by Belkin and Gordon (1996).

Whitworth and Nowlin (1987) noted that at the Greenwich Meridian the STC, unlike other Southern Ocean fronts, is not evident in all property distributions nor do the associated horizontal gradients persist below the surface layer. Lutjeharms and Valentine (1984) show that the average temperature change on crossing the front is approximately 7°C. The average sea surface temperature at its location was 14.2°C. Upon crossing the STC there is a clear decrease in the surface and subsurface salinities as one move from north to south. Surface salinities great than 34.8 are indicative of subtropical surface waters, north of the STC. At the STC the decrease in salinity is partially compensated for by the decrease in temperature (Whitworth and Nowlin, 1987). At the Greenwich meridian as observed by Whitworth and Nowlin (1987), the STC is a near surface feature and the geostrophic velocities associated with the front attenuate rapidly with depth. Along the AJAX section the STC had a maximum surface geostrophic velocity of 13 cm s^{-1} (Whitworth and Nowlin, 1987). In contrast results from a drifter study by Hoffman (1985) show a mean near-surface velocity of 26 cm s^{-1} for 35 observations in the STC.

2.4.2 Subantarctic Front (SAF)

First identified south of Australia and New Zealand the SAF lies in between the STC and the APF and separates the SAZ from the PFZ. The SAF is observed as the most prominent thermal feature between Australia and Antarctica, being much more easily recognizable in the sea surface temperature (SST) than either the STC or APF (Zillman, 1970). Emery (1977) also described this front between south of Australia and the Drake Passage and suggested the generic term, the Subantarctic Front. South of Africa Sievers and Emery (1978) and Lutjeharms and Valentine (1984) defined the SAF to be located where the most vertically orientated isotherm within a subsurface temperature gradient lying between the 3°C and 5°C isotherms occurred. Along the Greenwich Meridian, Whitworth and Nowlin (1987) defined the SAF to be located where the most rapid descent of the salinity minimum occurred. This definition is usually unambiguous but cannot be used with expendable bathythermograph (XBT) sections. Whitworth and Nowlin (1987) indicate that at the SAF there is a sharp change in the surface salinities, suggesting that the SAF may be defined as being at that location where a sharp drop in the surface salinity occurs in a range of 33.8 to 34.2. This drop in surface salinities was also, observed by Belkin and Gordon (1996) in their study of the African sector (0°-40°E) of the Southern Ocean. However

Allanson et al. (1981) cautions that this drop in salinity may not always be present in the Southern Ocean south of Africa. Surface definitions of the SAF may not be satisfactory since the location of the surface and subsurface expressions of the front do not always coincide (Lutjeharms and Valentine, 1984). The best definition for the SAF is therefore one based on subsurface salinity measurements, namely that of Whitworth and Nowlin (1987). The subsurface expression used by Nagata et al. (1988) placed the position of the SAF at the 7°C isotherm at a depth of 100 m. They claim that the results obtained broadly coincide with those of Lutjeharms and Valentine (1984) in the ocean south of Africa.

The intensity of the SAF varies distinctly with longitude. If neither continental boundaries nor zonal submarine ridges affect the ACC, the SAF is weak (Emery, 1977). At the Greenwich Meridian the SAF has a maximum geostrophic surface speed of 26 $cm.s^{-1}$ (Whitworth and Nowlin, 1987), while Hoffman's drifter results show mean surface speeds of 43 $cm\ s^{-1}$. This is in good agreement with the Drake Passage where the SAF has surface speeds of between 30 and 45 $cm\ s^{-1}$ and an average width of 50 km (Nowlin and Clifford, 1982). When the surface and subsurface expressions of the front are distinct, each front may be associated with a relative geostrophic velocity core each being weaker than when the two SAF indicators coincide. This has been found to true of the APF in the Drake Passage (Nowlin and Clifford, 1982).

2.4.3 Antarctic Polar Front

The APF separates the waters of the PFZ from the AAZ and has in some cases a separate surface and subsurface expression (Lutjeharms and Valentine, 1984). Many different definitions of the APF have been put forward and its consistency has been debated for decades. Belkin and Gordon (1996) used Botnikov's (1963) criterion in determining the position of the APF. They stated the reasons for this to be that the 2°C isotherm is a good approximation of the northern extent of the subsurface T_{min} almost everywhere in the Southern Ocean. Secondly, in winter the 2°C extends to the surface, providing a reliable indication of the APF location in the absence of the APF's cold core rings. The third motivation for this is that generally this definition is in conformance with the Gordon (1971) definition of the APF as the location of the rapid descent of the T_{min}, which reflects the baroclinic nature of the APF. Whitworth

and Nowlin (1987) in their discussion of the AJAX section indicated the APF to be located where the temperature minimum associated with AAIW begins its rapid descent. This definition would put the APF slightly northward compared to that of Belkin and Gordon (1996).

Previous definitions of the APF are;

a) the location where the temperature minimum dips below 200 m (Deacon, 1933)
b) the northernmost position of the 2°C isotherm in the 100-300 m layer (Botnikov, 1963)
c) the axis of the salinity minimum at the 200 m depth (Ostapoff, 1962)
d) the northern termination of the temperature minimum layer or where its depth changes abruptly (Gordon, 1967)
e) the location where the temperature minimum rapidly increases with depth (Gordon, 1971a)

Thus it seems that the SAF is best defined in terms of salinity, while the APF is best defined in terms of temperature. For the region south of Africa the average meridional location of the front was found to be 50° 47' S (Lutjeharms and Valentine, 1984). At the Greenwich meridian, Whitworth and Nowlin (1987) found the maximum geostrophic velocity associated with the velocity core of the APF to be 23 cm s^{-1}. This result was less than that found in Hoffman's drifter study in which the APF had a average velocity of 40 cm s^{-1} (Hoffman 1985). In cases where the surface and subsurface expressions of the APF are observed to be distinct, each front may be associated with a relative geostrophic velocity core, each being weaker than when the two APF indicators coincide (Sievers and Emery, 1978).

2.4.4 Agulhas Front

Belkin and Gordon (1996) describes this front as mainly a subsurface/intermediate front which is quite strong and deep beneath the upper 100-150 m. Previous definitions of the AF are;

a) the axial T_{200}=15°C (Gründlingh, 1983)
b) the T_{200} range=10-17°C (Gordon et al., 1987)

c) the axial T_{150}=18°C (Nagata et al., 1988)

d) 200 m axial values of 14°C and 35.3 (Park et al., 1993)

The criterion used by Belkin and Gordon (1996) for the AF was the depth range of the 10°C isotherm, namely Z_{10} =300-800 m as well as the existence of a thermostad on its warm side in the 150 to 300 m layer.

2.4.5 Southern Front/Weddell Front

Forming the southern boundary of the ACC, the circumpolar nature of Southern Front was first discussed by Orsi et al. (1995). South of the APF along the Greenwich meridian Whitworth and Nowlin (1987) indicated this front to be located immediately poleward of the mid-ocean ridge. The history of this front and definitions used in establishing this front were discussed as part of the ACC (section 2.1).

2.4.6 Movement of fronts

Fronts in the Southern Ocean are not static features. Substantial meridional movement of these fronts occurs. Observed meanders of the APF cause meridional shifts of up to 2 degrees of latitude in the course of a few weeks (Legeckis, 1977; Sievers and Emery, 1978; Sciremammano et al., 1980). These waves may develop into deep-reaching cold-core rings, with diameters of 60 - 100 km, which drift in the ACC or migrate northwards across the PFZ (Sievers and Emery, 1978; Joyce et al., 1981). Sievers and Emery (1978) observed the formation of such a cold-core ring in the Drake Passage which drifted northwards, eventually resulting in a double (surface and subsurface) expression of the SAF. Computations by De Szoeke and Levine (1981) seem to indicate that ring/ eddy formation provides an important contribution to meridional heat transport. Peterson et al. (1982) showed that near fronts the necessary conditions for both baroclinic and barotropic instability is met. Thus if warm rings can form to the south of each front and cold rings can form to the north of fronts, 6 types of rings are possible, all of which have been already observed (Joyce and Patterson, 1977; Joyce et al., 1981; Peterson et al., 1982; Hoffman and Whitworth, 1985; Gordon et al., 1977a and Nowlin and Zenk, 1988). Mesoscale eddy activity at the ACC fronts no doubt enhances cross-frontal exchange, as does the small-scale interleaving present at the fronts. Whitworth and Nowlin (1987) suggest that ACC

fronts cannot be considered to be barriers to meridional fluxes, and that their presence may even intensify this exchange.

2.5 **Heat fluxes**

The unequal distribution of the sun's energy over the globe has been known for a long time. The incoming short wave radiation from the sun is not locally compensated by outgoing long wave radiation. In the long term however the tropics are not heating up and the polar regions are not cooling down. The mechanisms for transporting heat from the tropics to the poles are primarily via the ocean and atmosphere (Hall and Bryden, 1982). In terms of heat fluxes the South Atlantic is of interest because of its geographical location linking the Pacific and the Indian Ocean. Water masses formed in the Indian, Pacific and North Atlantic enter the South Atlantic where they are modified and exported again. North Atlantic Deep Water passes through the South Atlantic where it is exported to the Indian and Pacific oceans (Boddem and Schlitzer, 1995).

The South Atlantic displays a curious feature in that there is a northward heat flux. The warmer upper waters move northward and are compensated by the southward moving, cooler deep water and ultimately warm the northern regions of the North Atlantic (Gordon et al., 1999). There has been some controversy as to the origin of this northward heat flux. It was suggested by Gordon (1986) that the northward return flow in the South Atlantic occurs mainly in the warm thermocline layer, which is derived primarily from Indian Ocean Central Water (IOCW) entering the South Atlantic by a branch of the Agulhas Current that does not complete the retroflection. Rintoul (1991) using hydrographic data and inverse calculations to derive heat and mass transports found that the net inflow of IOCW to be incompatible with the hydrographic data. The northward flow is suggested by Rintoul (1991) to be derived from waters entering the Drake Passage, equally split between the surface layers, intermediate and bottom waters. Using hydrographic and chloroflouromethane data Gordon et al. (1992) arrive at a circulation pattern different from that of Gordon (1986) and Rintoul (1991). The northward flow was suggested to have a large intermediate water component that enters through the Drake Passage and partly flow into the Indian Ocean before returning to the Atlantic. Gordon et al. (1992) also suggested that about 10 Sv of water warmer than 9°C from the Indian Ocean is fed

into the South Atlantic in addition to the intermediate water. Boddem and Schlitzer (1995) used a model approach to address the controversy on the possible flow patterns. As Rintoul (1991) their model showed that intermediate water made a large contribution to the northward component of the circulation in the South Atlantic. Consistent with Rintoul (1991) their model experiment showed a net transport of warm water from the South Atlantic into the Indian Ocean. In contrast to Gordon (1986) the model showed the northward component to be dominated by intermediate water for the upper layer northward flow, rather than northward flowing of mainly thermocline water. One of the experiments done by Boddem and Schlitzer (1995) indicate that water flowing across 30°S cannot be completely derived from warm inflowing IOCW and there has to be a local production within the South Atlantic by cold to warm water conversion.

As stated the model indicated a net transport from the Atlantic to the Indian Ocean that was in contrast to what Gordon et al. (1992) found. The model indicated a transport of between 3.6 and 6.9 Sv to the Indian Ocean whereas Gordon et al. (1992) found a net inflow of 4 Sv to the Atlantic. Boddem and Schlitzer (1995) enforced the 4 Sv flow across 30°E to test whether this net inflow of warm water from the Indian Ocean is consistent with temperature and salinity distributions in the South Atlantic. They found that the injection of warm IOWC into the Benguela Current rises from 2.5 to 5.9 Sv in results they obtained. The model however refused to continue the transport of the inflowing water across 30°S. The model reacts by creating a downwelling cell in the retroflection region where the water is incorporated into the intermediate water of the South Atlantic Current and transported back to the Indian Ocean.

Several methods exist for the calculation of ocean heat transport. The traditional method used is to examine air-sea exchanges of all type of energy. It was deduced that the net amount of energy lost to the atmosphere by the ocean poleward of a latitude circle must be imported from regions equatorward of that latitude by ocean currents. Satellites have also more recently become a promising tool for the monitoring of the global radiation balance (Hall and Bryden, 1982). I will however employ the direct method in obtaining the heat flux.

Direct estimates of the mass and heat fluxes are obtained by vertically integrating the meridional velocity and temperature fields derived from (mainly zonal) hydrographic sections spanning the oceans. Initially, simple geostrophy and some ingenious constraints were used to estimate heat flows from these hydrographic sections (Bryan, 1962; Bryden and Hall, 1980, de Soezke and Levine, 1981). Later the use of inverse methods allowed for more robust estimates (Roemmich, 1980; Wunsch, 1984; Rintoul, 1991). An advantage of this method is that it is a direct estimate that does not rely on the accuracy of estimates of other quantities such as air-sea exchange and atmospheric heat fluxes. Perhaps the greatest advantage of the method is that, being a direct in situ calculation, it allows some insight into the detail and mechanisms of these meridional heat fluxes in the ocean. However, a disadvantage of the method is that the data sets are sparse and exist only for limited time periods, thus making it difficult to infer long-term estimates of heat fluxes. The essential assumption of the method is that the large-scale flows are sufficiently steady so that single sections taken over a short period of time are representative of the time-averaged state. The documentation of the "Great salinity anomaly" by Dickson et al. (1988) highlights the extent of the error that may be introduced by the above "steady-state" assumption.

Most investigators divide the heat fluxes estimated from hydrographic sections into heat fluxes due to upper layer Ekman transports, fluxes due to geostrophic motions and eddy heat fluxes. The geostrophic heat fluxes can further be subdivided into baroclinic heat transports and barotropic heat transports. In general the Ekman heat transports dominate in the tropics, while in the mid-latitudes the geostrophic heat transports are dominant. Towards the poles it seems that eddy heat fluxes dominate (Bryden, 1979, Gordon, 1981). The accuracy of estimates of Ekman heat transports is dependant on errors in the specification of time-averaged wind stress fields. These errors are characteristically large especially in low latitudes where there are substantial seasonal fluctuations in the wind fields. Errors in the geostrophic heat flux estimates are dependant on the variable spatial resolution and time differences between hydrographic sections, while estimates of eddy fluxes are known to have large error bounds due to both spatial and temporal under sampling.

Chapter 3

In this chapter the key questions that will be addressed in this study are presented.

As stated in Chapter 1 the cruise was undertaken to support the goals of WOCE in obtaining ocean variables with the view in improving estimates of the circulation of heat, water and chemicals around the world ocean. Part of this study will thus be dedicated in achieving this goal. However from the literature of dedicated work along the Greenwich Meridian it is clear that except for the AJAX section described by Whitworth and Nowlin (1987) very little has been published on this area and its variability. Read et al. (2002) only describe the upper water column along the Greenwich meridian. The WOCE program provided for three cruises to be undertaken along the Greenwich meridian which allows to take fresh look at the oceanic environment between Africa and Antarctica and its variability.

Key Questions

a) What is the:

i) the zonal flux of heat,

ii) salt

iii) and nutrients fluxes between Africa and Antarctica along the SR02 section

b) What is the variability within the region with respect to:

i) geostrophic flow patterns and velocities,

ii) frontal structures and

iii) water mass properties with other observations in the Drake Passage and Greenwich Meridian.

Chapter 4

In this chapter the methodology followed in answering the key question stated in chapter 3 are presented.

4 Methods

The methods described in this chapter refer only to SR02 section done from January 16 to February 21, 1993 as part as South Africa's contribution to WOCE The section was occupied south to north. The data were not submitted to WOCE due to quality considerations. Data for the other sections, the A12 done in 1992 and the SR02 section done in 1990 were obtained from the WOCE hydrographic program website. The methods for obtaining fluxes however refer both to the SR02 section (1993) and the A12 section.

4.1 Cruise

The cruise track and stations positions are shown in Figure 1.2 with the solid circles denoting CTD stations. In total 62 CTD stations were completed along the WOCE line SR02. A twelve 8-litre bottle rosette fitted with a Neil Brown MK IIIB CTD underwater unit and a profiling fluorometer (Aquatracker) was used. A CTD station consisted of two casts and a Bongo or RMT trawl. At selected stations an additional CTD cast was undertaken for productivity measurements. In addition 36 XBT stations were deployed in the vicinity of the fronts to increase the resolution.

4.2 CTD Stations

The following water sample measurements were made at each CTD station: salinity, oxygen, silicate, nitrate, nitrite, and phosphate. Biological measurements were also taken as part of the JGOFS program. In order to get a 24 bottle resolution, two casts were required comprising a shallow and a deep cast. The shallow cast extended to 300m and the deep cast to 10m from the bottom. The depths sampled on the shallow casts were: 0, 10, 20, 30, 50, 75, 100, 125, 150, 200, 250, and 300 m and on the deep cast: 400, 500, 750, 1000, 1250, 1500, 1750, 2000, 2500, 3000, 4000, and 5000 m.

4.3 XBT Stations

Figure 4.1 shows the positions of the 36 XBT stations. Stations X01-X07 were deployed to establish the start of the WOCE line and the position of the ASF. Stations

X08-X19 was deployed to increase the resolution in the vicinity of the APF and stations X20-X36 to increase the hydrographic resolution at the SAF and the STC.

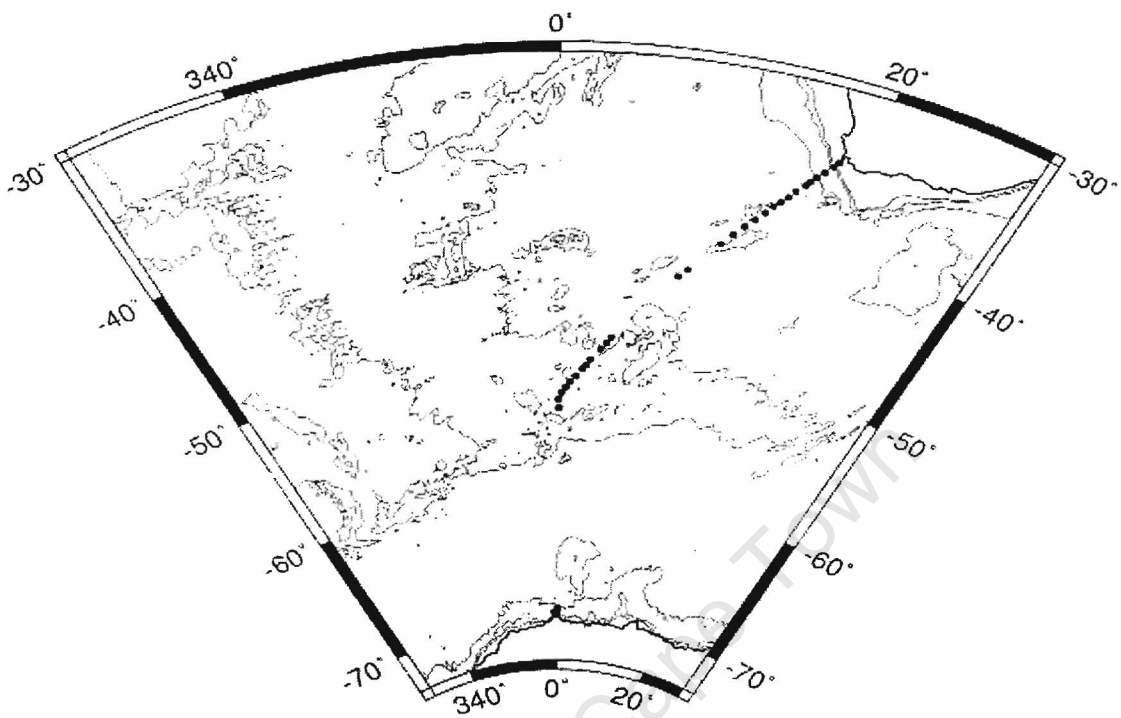

Fig. 4.1: Map indicating XBT stations along the SR02 section

4.4 **Major Problems**

Before the cruise the M.V. SA Agulhas had just undergone a major scientific refit and refurbishment. This being the first cruise since the refit a number of unexpected problems arose. The most serious was the hydrographic winch that had spooling problems. Deep stations required the bottom layers of the winch cable to be packed with a rope and fire hose, adding greatly to station times. On a number of occasions the rosette had to be removed and weights attached so that the cable could be completely re-spooled.

The ships bow thrusters failed from station 43, which caused problems at stations 46 and 47 where there was a big swell causing a big drift of the CTD when it was coming back up. There was also a seven-day gap between CTD stations 37 and 38 due to a medical evacuation of a member of the South African team on Gough Island. The ship

was required to steam to Gough Island to pick up the injured person to be transferred to a SA Navy vessel.

The Neil Brown CTD units also had some problems. A Neil Brown MK IIIC underwater unit purchased for this cruise was flooded during its first deployment on sea trials. Of the two remaining units, the first became in operational after the first CTD station where the fast response thermistor on the CTD got damaged. The second unit was used the rest of the cruise. It was however not fitted with a oxygen sensor. In addition this unit also experienced major problems with the communications boards within the unit intermittently throughout the cruise.

The Guildine Autosal Salinometer on board behaved erratically on an intermittent basis. At station 38 two channels on the Techicon II Autoanalyser (nitrate and nitrite) became inoperable and subsequent samples were frozen and analysed back on shore.

4.5 **Underway Measurements.**

4.5.1 **XBT**

The XBT's were launched from a Sippican hand launcher, usually from the rear corner of the afterdeck. The data for the first 21 stations were obtained with the Sippican MK12 data acquisition of the SA Agulhas. The motherboard of the data acquisition PC failed after station 21 and the rest of the stations were undertaken using a Sippican MK9 backup system. T7 XBT probes were used and sea surface temperatures were obtained using a Crawford bucket and from the DDS at each XBT station.

4.5.2 **Salinity Data**

Salinity samples were taken from the ships uncontaminated water supply at underway XBT stations. The inlet of this water supply is at a depth of approximately 5 m.

4.5.3 **Thermosalinograph**

Continuous underway measurements of the surface salinity and temperature were made with a shipboard mounted SEACAT 21 thermosalinograph. It has a resolution of 0.001C and 0.0001 S/m for temperature and conductivity. The seawater intake for this instrument is also approximately 5 m below the sea surface.

4.6 Hydrographic measurement techniques and calibrations

4.6.1 Salinity Measurements

4.6.1.1 Equipment and technique

Bottle salinities were taken in order to calibrate the CTD. The conductivity ratio was determined using a Guildline Autosal Model 8400A salinometer, and followed the methods described in the Guildline Autosal Operational manual. The conductivity was converted to salinity using the equations by UNESCO (1983).

4.6.1.2 Sampling procedure

Glass bottles were rinsed three times with the sample water and then filled up to the shoulder of the bottle. The bottle was then capped with a polyurethane cap that was rinsed in the sample and the neck of the bottle is then dried. Samples were analyzed as soon as they reached room temperature, which generally took between 8 to 36 hours.

4.6.1.3 Standardization of the salinometer

The salinometer was standardized with IAPSO Standard Seawater. Only 18 standardizations were performed throughout the cruise owing to the limited supply of standard seawater.

4.6.1.4 Duplicate analyses

Sixty-four duplicate samples were collected from the same Niskin bottle at different stations during the cruise. The mean difference in the salinity for these duplicates was 0.002 ± 0.003. Of the duplicates, 30 were less than 3000m giving a mean difference and STD of 0.001±0.002

4.6.2 Dissolved Oxygen measurements

4.6.2.1 Equipment and technique

The dissolved oxygen was determined by Carpenter (1965) modification of the Winkler (1888) titration method. A Metrohm Dosimat 650 was used to dispense the sodium thiosulphate solution in the titrations.

4.6.2.2 Sampling procedure

The oxygen flasks were rinsed three times with the sample water and then filled to overflowing to ensure minimal contamination with atmospheric oxygen. The two fixing reagents, $MnCl_2$ and NaOH/NaI, were added and the oxygen flask stoppered securely. These were inverted a few times to mix the reagents. The precipitate that formed was allowed to settle to about halfway to the bottom of the flask before the samples were shaken again. These were left in a cooler box for about 10 to 20 minutes or until the precipitate completely settled to the bottom of the flask. The samples were then acidified and titrated with sodium thiosulphate.

4.6.2.3 Standardization of thiosulphate solution

Carpenters (1965) method of standardization was modified to include the addition of 1ml of $MnCl_2$ before titration. Triplicates were done for each standardisation and 52 were performed during the cruise.

4.6.2.4 Volume Calibrations

The volume of the apparatus used (mainly pipettes and oxygen flasks) were individually weight calibrated. All weights were corrected for air buoyancy and weights converted to volumes (at 20°C) using WOCE equations (WOCE Operations Manual, 1991). The 10 ml glass pipette used to dispense the iodate standard up to and including station 17, due to a breakage this was replaced by an Eppendorf Varitip S from station 18 onwards. Both pipettes were weight calibrated. The results of the calibration are shown in table 4.1.

Table 4.1: Volume calibrations of the apparatus used in oxygen analysis

Volume	Dispenses	Number	Mean Vol
10 ml (glass)	iodate for standardization	14	10.035 ± 0.038
10 ml (Eppendorf)	iodate for standardization	16	10.008 ± 0.017
1 ml glass	iodate for blank determination	10	1.014 ± 0.010
1 ml	H_2SO_4	20	1.001 ± 0.001
1 ml	NaOH/NaI	-	
1 ml	$MnCl_2$	-	

The 125 ml oxygen flasks were also weight calibrated and these were then used in preference to manufacturers values. Duplicate calibrations of 18 oxygen sample flasks were done giving a mean difference and STD of 0.011 and 0.005 respectively.

4.6.2.5 Duplicate analyses

A total of 247 duplicates were sampled, generally there were 4 duplicates for each CTD cast. These were selected so that the entire range of observed oxygen concentrations were covered. The mean difference (absolute) in oxygen concentration (ml/l) for these duplicates was 0.010 ± 0.010. If necessary, the oxygen data can be converted from ml/l to µmol/kg using the following equation:

$$O_2\ (\mu mol/kg) = 44.660 \cdot O_2(ml/l)/q_{sw}$$

where q_{sw} is the density of seawater at the potential temperature of the water sample.

4.6.3 **Nutrient analysis**

4.6.3.1 Equipment and Techniques

Inorganic nitrate (NO_3), nitrite (NO_2), silicate (Si) and phosphate (PO_4) were measured using a Techicon II Autoanalyser, according to the standards and methods of Parsons et al. (1984).

4.6.3.2 Sampling Procedure

Samples for nutrients were taken about 10-20 minutes after the rosette was on deck. Samples taken from station 38 onwards were frozen due to the Cd column breaking on the autoanalyser. Samples were analyzed using an autoanalyser in the Sea Fisheries Research Institute.

4.6.3.3 Duplicate analyses

Duplicate samples were taken from the same Niskin bottle, mean difference between all the duplicates and standard deviation (STD) are shown for each nutrient in the table 4.2 and Fig 9. The % error is well out of the range specified by WOCE.

Table 4.2: Mean differences and STD of nutrient duplicates

Nutr-ient	Min Conc	Max Conc	First – second Mean diff ± STD	First - second Mean diff ± STD (absolute)	% Error of absolutes	No. Obs.
Si	0	148.5	-0.11 ± 1.93	0.76 ± 1.780	1.96 ± 3.69	1108
NO_3	0.11	6.74	0.00 ± 0.16	0.49 ± 0.740	3.41 ± 6.16	1125
NO_2	0	2.52	0.00 ± 0.54	0.03 ± 0.045	14.00 ± 18.00	1084
PO_4	0.24	62.6	-0.01 ± 0.89	0.09 ± 0.140	4.14 ± 5.66	1117

4.6.4 **Deep Sea Reversing Thermometers (DSRT)**

4.6.4.1 Equipment and techniques

Four of the rosette bottles were fitted with DSRT racks and Gohla Deep Sea Reversing Thermometers (DSRT). These were always attached to Niskin bottles 1, 3, 5 and 7 on the deep cast. Each DSRT rack held 2 protected (temperature) thermometers and 1 unprotected (pressure) thermometer. The thermometers were read about 1-2 hours after the rosette was brought back onto the deck. Two readings were taken for each thermometer. Corrections were applied to these readings to determine the temperature and pressure, using equations described by UNESCO (1983).

The performances of the thermometers were determined by comparing thermometer pairs and then comparing these with the corresponding CTD temperature. The results of the comparison of paired thermometers are shown in table 4.3.

Table 4.3: Mean difference and STD between pairs of deep sea reversing thermometers.

Rack No.	Station Numbers	Thermometers Unprotected	Thermometers Protected	Mean diff ± STD (°C)	No. Obs.
A	2 to 38	11518	11814, 11815	0.003 ± 0.004	43
B	4 to 38	11512	11811, 11810	-0.001 ± 0.009	38
C	1 to 38	11543	11812, 11642	-0.003 ± 0.006	41
D	1, 5 to 38	11510	11819, 11824	0.005 ± 0.006	40
A	39 to 61	11518	11811, 11814	0.004 ± 0.005	21
B	39 to 61	11512	11815, 11810	0.001 ± 0.006	22
C	39 to 61	11543	11462, 11819	-0.001 ± 0.005	22
D	39 to 61	11510	11824, 11812	0.008 ± 0.004	22

The preliminary results of the comparison with the uncorrected CTD temperatures are shown in table 4.4.

Table 4.4: Mean difference and STD between DSRT and CTD temperatures

Thermometer Number	DSRT-CTD (°C) Mean diff ± STD	No. Obs.
11462	0.003 ± 0.010	66
11810	0.002 ± 0.012	64
11811	0.007 ± 0.011	63
11812	0.002 ± 0.007	65
11814	0.005 ± 0.006	66
11815	0.001 ± 0.008	66
11819	0.004 ± 0.017	66
11824	0.003 ± 0.023	65

At station 29 all the Niskin bottles were triggered at the same depth, of 75m. Unfortunately this is the depth of the thermocline, so this must be taken into consideration when comparing thermometers. The results of the difference of temperature between the paired thermometers are in table 4.5.

Table 4.5: Comparison of DSRT on CTD station 29

Bottle No.	Rack No.	Therm No	Corrected Tp (°C)	DSRT1-DSRT2	Uncorr CTD T (°C)	DSRT - CTD
1	C	11812	3.0261	0.014	2.990	-0.036
1	C	11642	3.0399		2.990	-0.050
3	D	11819	3.0446	0.001		
3	D	11824	3.0457			
5	A	11814	3.0401	0.001	3.094	0.054
5	A	11815	3.0392		3.094	0.055
7	B	11810	3.0593	0.006	2.961	-0.098
7	B	11811	3.0533			

Similarly comparisons were made between CTD pressure and those calculated from the unprotected thermometers. These measurements were made over a considerable range of pressures.

Table 4.6: Mean differences and STD between DSRT pressure and CTD pressure

Thermometer Unprotected	Thermometer Protected	DSRT - CTD P (db) Mean diff ± STD	No. Obs.
11543	11462	8.4 ± 5.1	41
11543	11812	9.1 ± 6.2	19
11543	11819	7.6 ± 3.5	22
11510	11812	3.1 ± 4.2	21
11510	11824	3.6 ± 9.6	22

4.6.5 **CTD measurements**

4.6.5.1 Equipment, calibrations and standards

The CTD equipment used on this cruise was the property of Sea Fisheries Research Institute. The following equipment were deployed on the CTD/rosette:

1. Neil Brown MK IIIB underwater unit
2. Fluorometer (Aquatracker III)
3. 8-litre General Oceanics Niskin Bottle rosette

Calibration of the MK IIIB CTD temperature and pressure sensors were carried out at the SFRI calibration facility. No post-cruise calibrations were performed. Conductivity calibration was carried out at sea using water bottle samples.

4.6.5.2 CTD conductivity (salinity) calibration

The CTD salinity was monitored by comparison with water bottle salinities during the cruise.

4.6.5.3 CTD temperature calibration

Stability of temperature calibration during the cruise was monitored by comparison with reversing thermometers.

4.6.5.4 CTD pressure calibration

The CTD pressure was monitored by comparison with DSRT's during the cruise.

4.6.5.5 Equipment performance

The CTD hardware/software system performed adequately. The only real problem was the hard disk on the data acquisition system crashed during logging of data on the deep cast on station 59. This lead to the loss of data from station 58 which had not yet been backed up.

4.6.5.6 Limitations of the Dataset

Due to problems experienced by the Techicon II Autoanalyser no reliable nutrient values could be obtained. A major blow however is that due to the CTD communication problems salinity and temperature values could not be corrected to within WOCE data standards for up to half the stations.

4.7 **Fluxes**

The property fluxes were calculated using the inverse box method. The heat fluxes and salt fluxes were only calculated for the SR02 section (1993) done as part of the South African contribution to WOCE, the A12 section (1992) and not for the SR02 section done in 1990. No estimation of nutrient fluxes was possible due to problems with the instruments mentioned in chapter 4 for the SR02 section. The matlab programs used to calculate the fluxes were obtained from the website http://puddle.mit.edu/~ganacho/hydrosys.html where they were made available by Dr. A. Ganachaud. A full description of the various methods is given in Wunsch (1996) and Ganachaud (1999).

In order to conserve mass and other traces within individual layers bounded by neutral surfaces, a geostrophic circulation with a surface Ekman layer is required (McDougall 1987). The Ekman transport was obtained using the average winds stress over the

period January 1993 to December 2000 from NCEP reanalysis data. The Ekman transport was broken down into two components:

$$T=T_{ini}+\Delta T_{ek}$$

T_{ini} is the initial Ekman transport and is calculated from climatology and ΔT_{ek} is the correction required by the conservation equations. Because of the loss of most of the nutrient samples in the SR02 section done in 1993 the only conservation property that was considered was mass. The transport north across the A11 section (figure 4.5.1) was calculated by Ganachaud (1999) and found to be 0.92×10^9 kg s^{-1}. This was considered to be negligible compared to the 139×10^9 kg s^{-1} transported eastwards of the 140×10^9 kg s^{-1} entering the Drake Passage. Thus only the A21 and SR02 and A12 sections were considered for the box. Since only the mass flux was considered to be conserved the following boundary conditions were applied, namely the 140×10^9 kg s^{-1} entering the Drake Passage across the A21 section as calculated by Ganachaud (1999). All reference surfaces were taken at the bottom, as that is where the velocities were likely at their weakest. These boundary conditions were considered to be constant.

Chapter 5

In this chapter the hydrography of four different sections along the Greenwich Meridian will be compared to gain some understanding of the variability of this region. The sections are the AJAX section discussed by Whitworth and Nowlin (1987) and three other WOCE sections; namely the SR02 section carried out 1990 and repeated in 1993 as well as the A12 section (figure 5d) done in 1992. I will refer to SR02 line done 1993 as the SR02a section (figure 5b) and the section done in 1990 as the SR02b section (figure 5c) henceforth. In addition the fluxes along the SR02a and A12 sections will also be presented in this chapter.

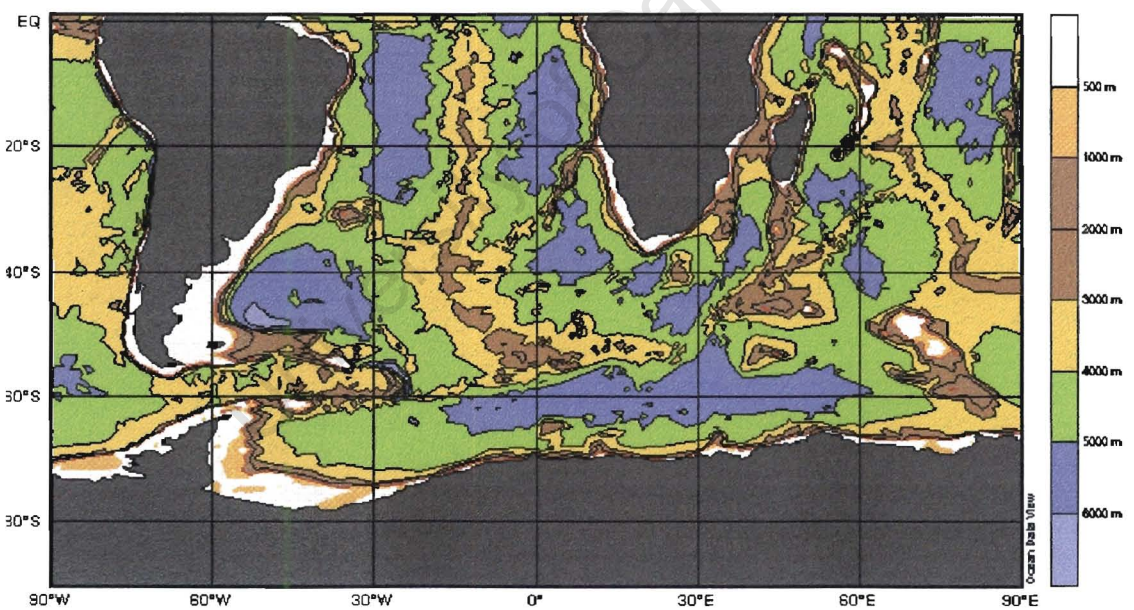

Figure 5a: Bathymetry of the Southern Ocean south of Africa

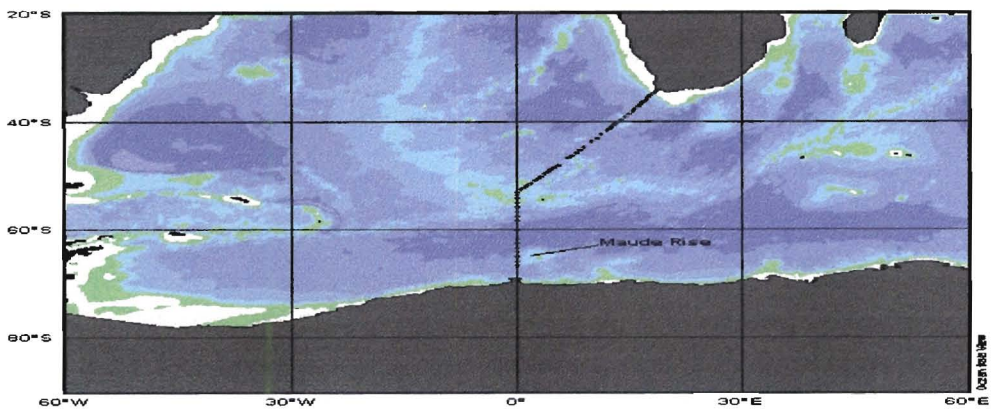

Figure 5b: Map showing the SR02a section

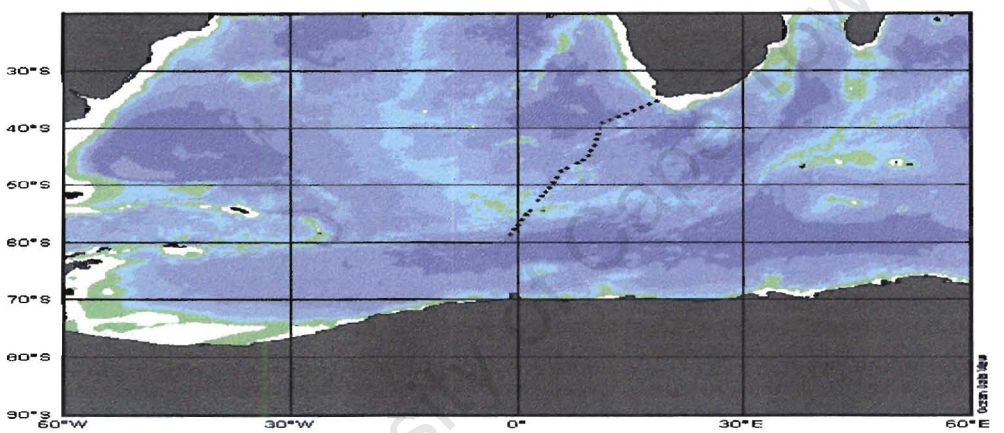

Figure 5c: Map showing the SR02b section

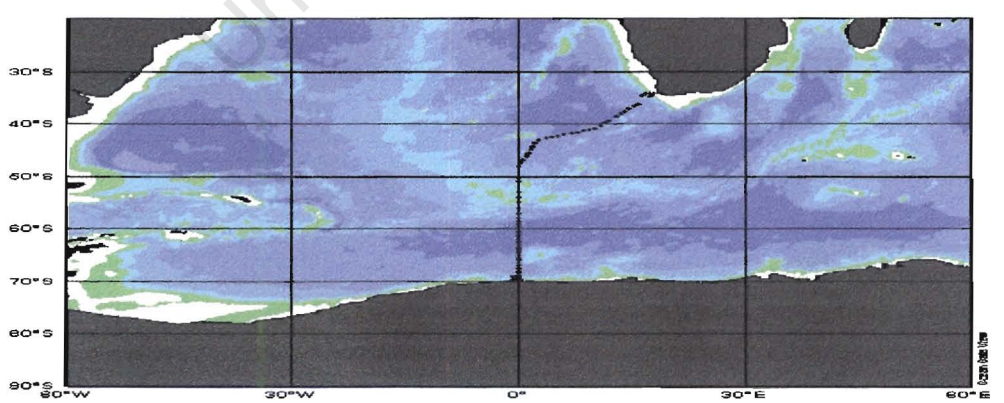

Figure 5d: Map showing the A12 section

5.1 Fronts south of Africa

Characteristic of the Southern Ocean, fronts are physical features that separate water masses from each other. As our objective is to look at variability, fronts along the A12 and SR02b sections will be looked at in relation to the SR02a section and ultimately to results found by Lutjeharms and Valentine (1984). When comparing the SR02 sections with that of the A12 section the longitudinal position needs to be considered since the fronts are not zonal south of Africa (Belkin and Gordon, 1996). According to Lutjeharms and Valentine (1984) the mean position of the APF is 50° 18'S, 46° 23'S for the SAF and around 41° 05'S for the STC. However although the frontal positions will be compared with that of Lutjeharms and Valentine (1984), the definition of the fronts will in most cases be based on that of Whitworth and Nowlin (1987). Frontal widths in most part, is dependant on station spacing. This needs to be considered when comparing the three sections with each other. For the SR02 sections the stations were around 30 nm apart whereas in the A12 section they were 40 nm apart.

5.1.1 Antarctic Polar Front (APF)

This front is prominent along all three sections under investigation. In their discussion Lutjeharms and Valentine (1984) indicate a separation in the surface and sub-surface expression of the front for the region south of Africa. The sub-surface expression was found to be north of the surface expression in most cases (Lutjeharms and Valentine 1984). The position of the APF was established as defined by Botnikov (1963). Positions as defined by Whitworth and Nowlin (1987), are also included. As the above two definitions are sub-surface expressions of the APF, the definition used by Lutjeharms and Valentine (1984) was used to establish the position of the surface expression. Their definition, indicate the surface expression APF to be where the maximum gradient of the sea surface temperature occurs between 2°C and 6°C.

The surface and sub-surface position of the front along the SR02a section (figure 5.3a) are indicated in table 5.1.1. In terms of variability in comparison with the A12 and SR02b sections (table 5.1.1) the subsurface expressions the front showed less movement when compared with the surface expression. The mean position of the APF at the surface for the three sections was 50° 24' S. This is only slightly to the south of the mean calculated by Lutjeharms and Valentine (1984) but inside their calculated range. Its mean sub-surface position also fell within this range. Using the definition of Whitworth and Nowlin (1987) the position of the front was found to be only slightly to the north of the range except in the case of the SR02b section (table 5.1.1). According to their definition the front had a mean position of 49°18'S. Although Botnikov's (1963) definition was used to indicate the position of the APF the strongest geostrophic velocities (figures 5.10a, b, c) was found to be associated with the position as defined by Whitworth and Nowlin (1987) for all three sections. Along the Greenwich Meridian this definition would thus seem to best define APF.

Along the SR02a section the APF had a frontal width of 117.5 km. The frontal width along the A12 and SR02b sections was 166 km and 144.7 km respectively and the mean width was 142.7 km for the three sections. This difference could be an artifact of station spacing since in the case of the A12 stations were further apart. The mean width was greater than the 126 km calculated by Lutjeharms and Valentine (1984).

Table 5.1.1: Position of APF for the SR02a, SR02b and A12 sections including the range given by Lutjeharms and Valentine (1984). Positions as defined by Whitworth and Nowlin (1987) are given in parentheses

Section	Surface	Sub-surface Botnikow (Whitworth and Nowlin)
SR02a	51°S	49° 48' (49 12') S
SR02b	51°S	50° 48'(49 42') S
A12	49° 12'S	49° 42'(49 12') S
Range	49° 39'-50° 47'S	

5.1.2 Subantarctic Front (SAF)

The position of the front was established using Whitworth and Nowlin's (1987) definition of the steepest descent of the salinity minimum at the subsurface (450 m). This position corresponded well with the fastest geostrophic velocities (figure 5.10a, b, c). It needs to be noted however that this definition was not used by Lutjeharms and Valentine (1984) in establishing their frontal position and mean range for the SAF. Their determination of frontal position was mainly based on the use of temperature profiles. They described the SAF as having a z-like structure. This is significant in that we will use the results of Lutjeharms and Valentine (1984) for the purpose of comparison.

The latitudinal position of the front for the SR02a section (figure 5.4a) is given in table 5.1.2. Variation in its position was less than 1 degree of latitude when compared with the A12 (figure 5.4b) and SR02b (figure 5.4c) sections (table 5.1.2). At the position of the SAF the two SR02 sections has diverged eastwards from the Greenwich meridian. This is significant in that east of the Greenwich meridian the SAF shifts slightly southward (Belkin and Gordon, 1996). This southward shift was however only observed in the case of the SR02a section. The mean position of the SAF for the three sections was 45° 24'S. Despite the difference in definition this mean latitudinal position for the SAF fell within the range calculated by Lutjeharms and Valentine (1984) using only temperature profiles (table 5.1.2). The mean position however was well north of the mean calculated by the abovementioned authors. The frontal width of the SAF for the SR02a section was 273 km. The front had widths of 193 km and 263.4 km respectively for the A12 and SR02b sections indicating substantial variation in the region of 70-80 km. This difference cannot simply be considered an artifact of station spacing, as the variability is far too great. In fact from the station spacing it would have been expected that the front would be the widest along the A12 section. The mean frontal width for the three sections was 243.2 km. This value compares well with the mean calculated by Lutjeharms and Valentine (1984).

Table 5.1.2: Latitudinal positions of the SAF and range given by Lutjeharms and Valentine (1984)

Section	Position
SR02a	45° 48'S
SR02b	45 ° 12'S
A12	45° 12'S
Range	45° 15'--46° 23'S

5.1.3 Subtropical Convergence (STC)

In the South Atlantic the STC consist of a Southern STC (SSTC) and a Northern STC. In the South African sector (10°-35°E) the Northern STC is not distinct (Belkin and Gordon, 1996). They suspected it either blends with the SSTC or the AF or both. Alternative suggestions include it bending northwards (Belkin and Gordon, 1996). Below I will look only at the SSTC and in most cases I will refer to it as simply the STC.

Separating the waters from the subtropics from that of the subantarctic the STC is prominent along all three sections (table 5.1.3). To establish the position of this front I used the 34.8 isohaline. Salinities greater than approximately 34.8 are normally associated with subtropical gyre (Whitworth and Nowlin 1987). Whitworth and Nowlin (1987) in their analysis of the AJAX section indicated an increase in temperature from about 10°C to 14°C across the front. Along the AJAX section, the STC was not present in all the property distributions and its horizontal gradients did not persist below the surface level (Whitworth and Nowlin 1987).

Across the front there was a temperature increase northwards from about 11°C to 17°C in the SR02a (figure 5.3a) section with a middle temperature of 14°C. The position of the front for this section is indicated in table 5.1.3. Comparing latitudinal positions with respect to the A12 and SR02b sections (figures 5.3b, 5.3c and table 5.1.3) we find that the

STC showed some degree of variability; greater that 1 degree of latitude and had a mean position of 40° 48'S. This mean position is within the range calculated by Lutjeharms and Valentine (1984). Sectional comparisons indicate a marked northward shift, outside this range in the case of the A12 section. This northward shift is also visible in the AJAX section where the front is north of 40°S. This difference is explained by the longitudinal position of the two SR02 sections with respect to that of the A12 and AJAX sections. Whilst the A12 and AJAX sections follow the Greenwich meridian the SR02 sections has diverged eastward. The southward shift east of the Greenwich meridian in the region Agulhas Retroflection is not uncommon and is clearly depicted in figure 2.4. It needs to be noted however that sections SR02a and SR02b do not actually cross the Agulhas Current or Return Current but are influenced by eddies shed at the Retroflection region. This is visible in the salinity and temperature sections of the two sections (figure 5.1a, c and 5.2a and c). Variability was also noticed with respect to the width of the front. In the SR02a section the STC was 212.9 km wide. In the A12 section it was 273 km wide whilst in the SR02b section it was a mere 115 km wide. As would be expected from the station spacing the front is the widest along the A12 section. The difference in the SR02 sections can however not be explained as such as in both sections the station spacing was around 30 nm. The mean width of the three sections was 200.3 km. This is slightly less than the 225.1 km calculated by Lutjeharms and Valentine (1984).

Table 5.1.3: Positions of the STC for the SR02a, SR02b and A12 section including the range given by Lutjeharms and Valentine (1984)

Section	Position
SR02a	41° 18'S
SR02b	41° 30'S
A12	39° 36'S
Range	40° 35'--42° 36'S

5.1.4 Southern Front (SF) or Weddell Front (WF)

Forming the southern boundary of the ACC this front is discussed in detail by Orsi et al. (1987). It is described as separating stratification typical of the Weddell Gyre from that of the ACC (Whitworth and Nowlin 1987). Lutjeharms and Valentine (1984) do not include this front in their discussion of Southern Ocean fronts. The position of the front will thus be discussed in relation to that found by Whitworth and Nowlin (1987) along the AJAX section. The frontal position of the SF for the SR02a section is indicated in table 5.1.4. Although so stated, Schröder and Fahrbach's (1999) definition was not used to determine the position of the Weddell Front, as it did not coincide with the position of the Weddell Front along the Greenwich meridian. Instead its position was in agreement with the definition given by Orsi et al. (1995) using the southern edge of the UCDW (figures 5.1a, b, c and 5.2a, b, c). This puts the position of the front around the S_{max} 34.70 and θ_{max} 1.5°C and not at the S_{max} 34.72 and θ_{max} 1.5°C as defined by Schröder and Fahrbach (1999). This position was also in agreement with the strongest geostrophic velocities associated with the Southern Front (Weddell Front). Compared to the other two sections namely the A12 and SR02b (table 5.1.4) the front showed little shift in its latitudinal position. The position of the front was just south of the mid-ocean ridge. The mean position of the front was established at around 55° 30'S. This position compares well to its position along the AJAX section where the front was situated around 55°S.

Table 5.1.4: Positions of the Southern Front for the SR02a, SR02b and A12 sections

Section	Position
SR02a	55° 24'S
SR02b	55° 36'S
A12	55° 30'S

5.2 Geostrophic Velocities

In the previous section we have looked at the variability in the structure and position of fronts along the sections under discussion. As stated most of the transport within the ACC occur along these fronts (Orsi et al. 1995). Therefore we will look at geostrophic velocities associated with each of the fronts for the SR02a section, comparing it with the other two WOCE sections and ultimately with that found along the AJAX section by Whitworth and Nowlin (1987). It needs to be noted that all geostrophic velocities presented in this section are calculated using the deepest common depth as a reference level. This was done because direct current measurements had shown that the current shear in the ACC extends to the bottom (Whitworth and Nowlin 1987).

5.2.1 Antarctic Polar Front (APF)

Associated with the ACC this front separate the PFZ from the SAZ (Orsi et. al 1995). It has separate surface and subsurface expressions and Whitworth and Nowlin (1987) in their discussion of the AJAX section found two separate geostrophic cores associated with the front. These coincided with the surface and subsurface expressions.

In the SR02a section (table 5.2.1, figure 5.10a) the APF had two separate velocity cores associated with it. From the results (table 5.2.1) it is clear that the northern core velocities are slightly higher than that of the southern core. In comparison with the other WOCE sections, the SR02b (table 5.2.1 and 5.10c) and the A12 (table 5.2.1 and 5.10b) sections, the geostrophic velocities for the two cores are slightly higher in the SR02a section. Consistent with the SR02a section though, is the fact that the southern core velocities are weaker than that of the northern core. The average geostrophic velocity for the northern and southern core of the APF for the three-abovementioned sections was 19.7 cm s^{-1} and 15.6 cm s^{-1} respectively. Compared with the AJAX as calculated by Whitworth and Nowlin (1987), results for the northern core along all three sections were lower. The southern core ranged from being similar in the case of the SR02b section to higher in the SR02a and A12 sections. Consistent with that of Whitworth and Nowlin (1987), the fastest geostrophic velocities were associated with the subsurface expression of the APF. Hoffman's (1985) surface drifter velocities are at least twice as fast as that found along

all the sections using geostrophy. This discrepancy could be ascribed to two possible factors. Firstly in choosing the bottom as the reference level we assume that the current velocity at this level is zero. This is however not always the case and can lead to an underestimation of the current speed. Secondly surface drifters, drift in the ekman layer. This layer is not well resolved by geostrophy (Wunsch 1996).

Table 5.2.1 Geostrophic velocities of the APF for the SR02a, SR02b and A12 sections

Section	Southern core	Northern core
SR02a	21 cm s^{-1}	18 cm s^{-1}
SR02b	18 cm s^{-1}	13 cm s^{-1}
A12	20 cm s^{-1}	16 cm s^{-1}
AJAX	23 cm s^{-1}	13 cm s^{-1}
Hoffman	40 cm s^{-1}	

5.2.2 Subantarctic Front (SAF)

The SAF is described as the most prominent feature of sea surface temperature decrease between Australia and Antarctica with horizontal gradients exceeding that of the APF and STC (Zillman 1970). Findings by Lutjeharms and Valentine (1984) indicate the opposite for the region south of Africa.

The geostrophic velocities associated with this front for the SR02a section are indicated in table 5.2.2. Velocities associated with the SAF are much greater than that of the APF for this section. This observation is also consistent with that found along the A12 section (table 5.2.2). Conversely this observation was not true along the SR02b section (table 5.2.2). The geostrophic velocity for the SAF along this section was less than half that found long the other two sections. The mean geostrophic velocity for the SAF was 27.3 cm s^{-1}. Compared with the AJAX this velocity (average velocity) is only slightly greater. In terms of the SR02a and A12 sections however we find that the geostrophic velocities is far greater and more comparable with that found in the Drake Passage where Nowlin and Clifford found surface geostrophic speeds between 30 to 45 cm s^{-1}. Results (table

5.2.2) were however still lower than that of Hoffman (1985). This discrepancy is discussed in section 5.2.1.

Table 5.2.2 Geostrophic velocities of the SAF for the SR02a, SR02b and A12 sections

Section	Geostrophic Speed (cm s^{-1})
SR02a	15 and 32
SR02b	14
A12	36 and 29
AJAX	26
Hoffman	43

5.2.3 Subtropical Convergence (STC)

The STC is the northern boundary of the ACC (Whitworth and Nowlin 1987). For the region south of Africa it has a thermal gradient second to only the AF (Lutjeharms and Valentine 1984).

The surface geostrophic velocity associated with the STC (table 5.2.3, figures 5.10a) for the SR02a section was slightly higher than that of the APF (table 5.2.1). Compared with the A12 section the surface geostrophic velocity of the STC was only slightly lower in the case of the A12 section. Along the SR02b section its speed drops dramatically in comparison with the other two WOCE sections (table 5.2.1). The mean surface geostrophic velocity for the WOCE sections was 19 cm s^{-1}. In comparison with the AJAX this mean value is much greater than the 13 cm s^{-1} found along AJAX section. Noted though is the fact that the surface geostrophic speed for the SR02b section was in line with that found along the AJAX section. Hoffman's (1985) surface drifter results were however still greater than that found or along any of the WOCE sections mentioned above. The reason for this is given above in section 5.2.1. Whitworth and Nowlin (1987), describe this front as a near surface feature. This observation is reinforced by the fast attenuation of the geostrophic velocities in the A12 section with depth (figure 5.10b). Conversely in the SR02a and SR02b sections geostrophic velocity attenuation with depth

is comparable with that of the SAF (figures 5.10a and 5.10c). This could be as a result of the Agulhas ring situated just north of the STC.

Table 5.2.3: Geostrophic velocities of the STC for the SR02a, SR02b and A12 sections

Section	Geostrophic velocity (cm s^{-1})
SR02a	23
SR02b	14
A12	20
AJAX	13
Hoffman	26

5.2.4 Southern Front (Weddell Front (WF))

Forming the southern boundary of the ACC this front is situated just south of the mid ocean ridge (Orsi et al. 1995). Smith (1989) described it as a downstream expression of the Scotia front. Orsi et al. (1995) however clearly displayed the circumpolar structure of this front. The surface geostrophic core of the front was found just south of the mid-ocean ridge for the SR02a section (figure 5.10a). The surface geostrophic velocity for this front (table 5.2.4) is relatively weak compared with the other fronts along the SR02a section (table 5.2.1, 5.2.2 and table 5.2.3). This observation is consistent for the A12 and SR02b sections (table 5.2.1, 5.2.2, 5.2.3 and table 5.2.4). The mean surface geostrophic speed, for the three WOCE sections were 7.45 cm s^{-1}. Compared with the AJAX as calculated by Whitworth and Nowlin (1987) this value is much lower. The Southern Front was not discussed in Hoffman (1985) in her drifter study and thus no comparison could be made.

Table 5.2.4: Geostrophic velocities the WF for the SR02a, SR02b and A12 sections

Section	Geostrophic velocity (cm s^{-1})
SR02a	9
SR02b	7
A12	7
AJAX	12

5.3 Water masses

As was the case in the above sections we will describe the below mentioned water masses with respect to the SR02a section where after these observations are compared to the other WOCE sections and ultimately to what is known, namely the AJAX section as described by Whitworth and Nowlin (1987).

5.3.1 Subtropical Surface Water (SSW)

If we take the characteristic description of Subtropical Surface Water, as a saline (>34.8) warm (>12C) water mass with a oxygen concentration greater than 5.4 ml/l, then Subtropical Surface Water is visible north of the STC in the SR02a section only as a patch at 39°S (figures 5.2a, 5.3a and 5.5a). Compared to the A12 section there is a marked difference. In this section (figure 5.2b, 5.3b and 5.5b) Subtropical Surface Water covers the whole area north of the STC. Oxygen, salinity and temperature sections of the SR02b section (figures 5.2c, 5.3c and 5.5c) show a situation similar to that seen in the SR02a section with the patch at 39°S. The difference compared with the A12 section is that for the SR02a and SR02b sections two rings shed at the Agulhas Retroflection Region are added features. The water of the Agulhas Current and the Agulhas Return Current is a mixture of Indian Tropical and Subtropical Surface Water resulting in a warm, saline water mass with oxygen values less than 5.4 ml/l (Lutjeharms and Ansorge 2001). Subtropical Surface Water is thus seen as only a patch between the two Agulhas rings. The depth to which this water mass reaches differs for the three different WOCE sections. For the SR02a and SR02b sections it nearly reaches 400 m whilst in the A12 section it only reaches to 220 m (figures 5.2a, b, c; 5.3a, b, c and 5.5a, b, c).

Compared with the AJAX section the A12 section shows similar characteristics with the whole area north of the STC covered with Atlantic Subtropical Surface Water. The SR02a and SR02b sections with respect to the AJAX section showed differences similar to above described differences with the A12 section.

5.3.2 Subantarctic Surface Water and Subantarctic Mode Water

Subantarctic Surface Water

Found in the Subantarctic Zone between the SAF and the STC Whitworth and Nowlin (1987) describes this water mass as having a monotonically decreasing temperature, an induced salinity maximum and oxygen minimum due to the underlying AAIW. Sievers and Nowlin (1984) in their description of this water mass refer to this water mass as having a salinity, phosphate and nitrate minimum and a weak oxygen maximum. Compared with descriptions of water masses in the Drake Passage as described by Sievers and Nowlin (1984), Whitworth and Nowlin's (1987) description for SASW closely resemble that of Subantarctic Mode Water in the Drake Passage. In this discussion I will revert back the description of Sievers and Nowlin (1984) for SASW for reasons that will become apparent.

In the SAZ of the SR02a section, we find that the upper water column (above 200 m) has a salinity minimum and a oxygen maximum compared with the underlying water (figures 5.2a, 5.4a, 5.3.2a). This layer extends to a depth of only 80 m and has summer maximum temperature above 7°C (figure 5.1a). Compared with the A12 and SR02b sections a similar picture is observed (figures 5.2b, 5.2c, 5.4b, 5.4c, 5.3.2b and 5.3.2c). The upper water column water mass has a salinity, phosphate and nitrate minimum and a weak oxygen maximum. These characteristics resemble SASW as described by Sievers and Nowlin (1984) in the Drake Passage. For this reason thus we reverted back to the description given by Sievers and Nowlin (1984). However compared with surface salinity values found in the Drake Passage by Sievers and Nowlin (1984), values along two of the three WOCE sections were much higher. Compared to values less than 34.1 in the Drake Passage, salinities along the two sections (the A12 and SR02b sections) were higher by approximately 0.1-0.4 (figures 5.3.2a, 5.3.2b, 5.3.2c).

It needs to be noted that whilst the above consistencies exist between the three sections small differences in the temperature characteristics can be observed. In the case of the winter section, the A12 the 7°C isotherm surfaces north of the SAF whereas in the other two sections it surfaces to the south. This was in agreement to findings in the Drake

Passage (Sievers and Nowlin 1984). This shift can probably be attributed to winter cooling. Compared with other surface water masses SASW is a very shallow water mass. As stated above it reaches a depth of 80 m in the SR02a section whilst in the A12 and SR02b sections its depth ranges from a 140 m to 60 m respectively.

Subantarctic Mode Water

Described as SASW along the AJAX section by Whitworth and Nowlin (1987) this water mass is distinguishable as having a salinity maximum (figures 5.3.2a) and an oxygen minimum in the SAZ of the SR02a just below the SASW. These characteristics are also observed in the SR02b and A12 sections below the SASW in the SAZ (figures 5.3.2b and 5.3.2c). Compared to the Drake Passage salinities associated with this water mass are more saline by 0.3-0.4 along the Greenwich Meridian. SAMW also has an induced oxygen minimum compared to the overlying SASW. In agreement with some sections done in the Drake Passage (Sievers and Nowlin 1984) a second separate oxygen minimum is found just above the AAIW (figures 5.3.2a, 5.3.2b and 5.3.2c).

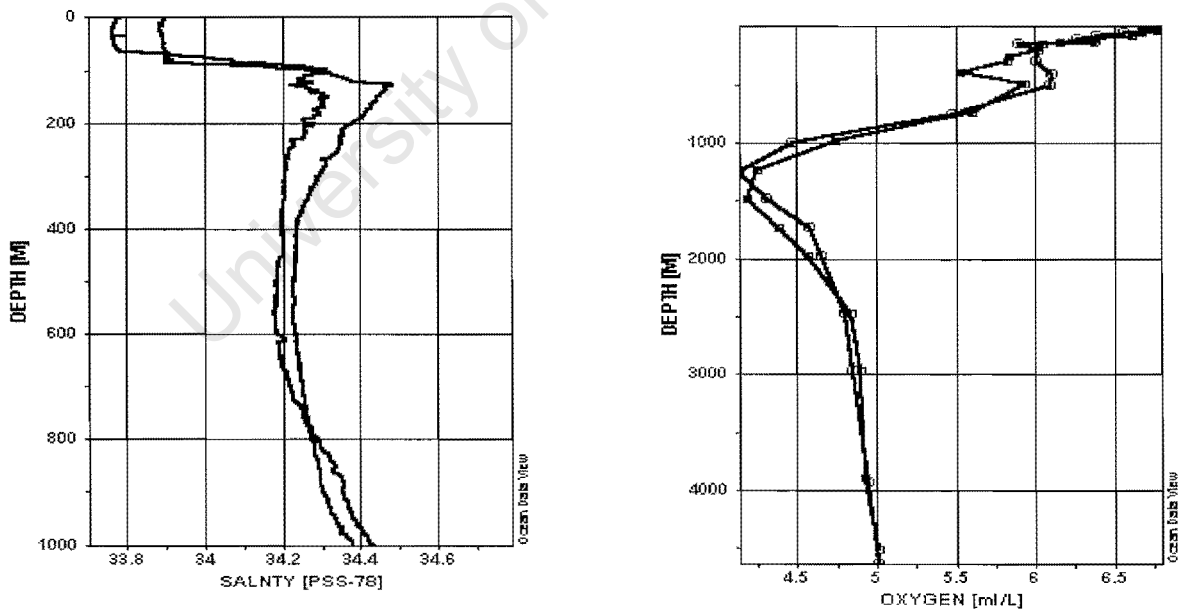

Figure 5.3.2a: Vertical salinity and oxygen profiles in the SAZ of the SR02a section

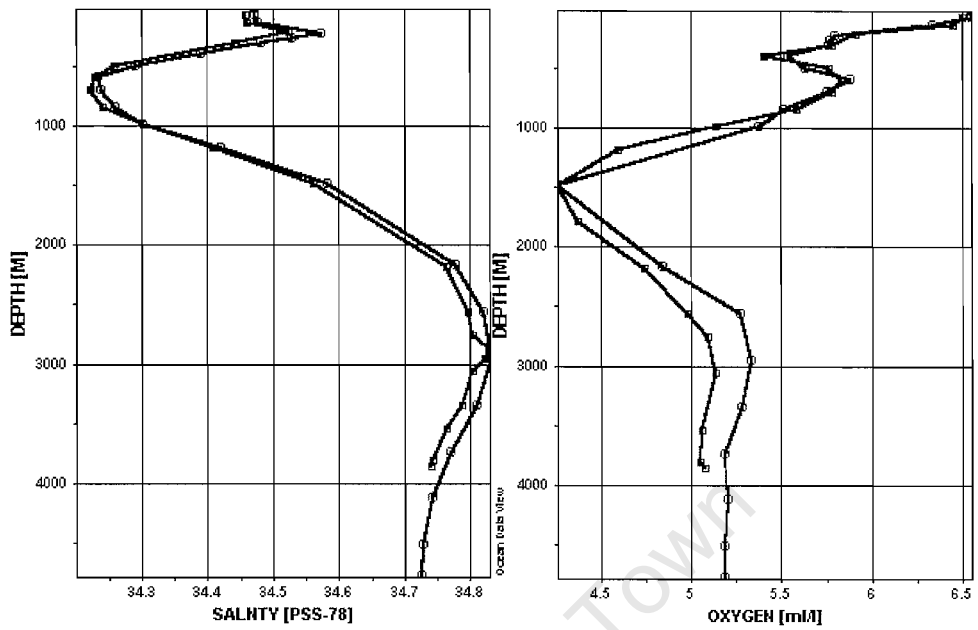

Figure 5.3.2b: Vertical salinity and oxygen profiles in the SAZ of the A12 section

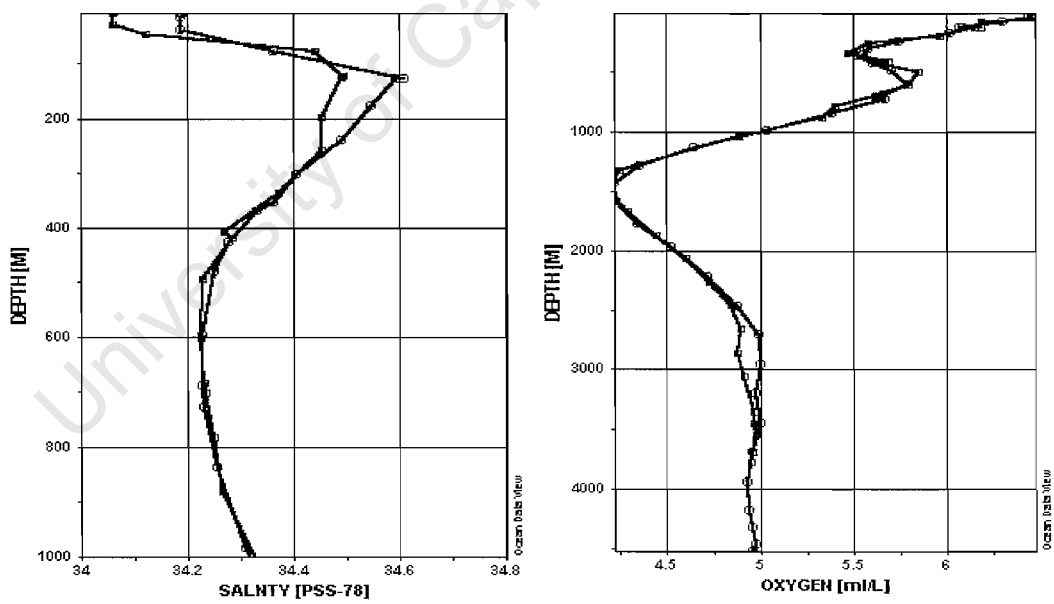

Figure 5.3.2c: Vertical salinity and oxygen profiles in the SAZ of the SR02b section

5.3.3) Antarctic Surface water

AASW is characterized as being a cold, fresh water mass with a high oxygen concentration. This water mass is found south of the APF in the SR02a section (fig 5.3a, fig 5.4a, fig 5.5a). In this section an intense temperature minimum is observed at 120 m (fig 5.3a). Commonly referred to as Winter Water the intense temperature minimum layer forms as a result of spring and summer heating of the upper layer (Sievers and Nowlin 1978). The layer in which the temperature minimum occurs is not a continuous layer but is observed as two cold patches surrounded by relatively warmer water (fig 5.3a). Other characteristics observed along the SR02a section include a slight salinity minimum and an oxygen maximum (figures 5.4a and 5.3.3a) near the axis of the Weddell Gyre.

Compared with the A12 section (fig 5.3c, fig 5.4c, fig 5.5c) there is some notable differences. Inconsistent with the SR02a section no temperature minimum and patches are observed within the AASW of the A12 section. The explanation for this can be found in the formation of this layer. As stated above this layer is formed as a result of spring and summer heating. The A12 section was done in June, during the southern hemisphere winter and thus the absence of this layer. Consistent with the SR02a section however is a slight salinity minimum that can be observed near the axis of the Weddell Gyre (figures 5.4b and 5.3.3b). South of the salinity minimum however, the water is much more saline compared to the SR02a section. This is indicated by the 34.3 isohaline surfacing in the A12 section, which is not the case in the SR02a section (figures 5.2a and 5.2b). In fact surface salinities across the whole Weddell Gyre were greater in the A12 section compared to the SR02a section (figures 5.3.3a and 5.3.3b). This difference can be attributed to seasonal freezing and melting. In winter the water freezes and releases its salt contents resulting in the higher salinity values in the A12 section. In summer the opposite occurs with a release of fresh water due to melting resulting in the lower salinities in the SR02a section. Nutrient values indicate lower nutrients near the axis of the Weddell Gyre along the A12 section with an increase to the north and south (figures 5.3.3 c, and d). Because of the loss of nutrient samples for the SR02a section no comparison could be made. Consistent with the SR02a section, AASW along the SR02b section has a characteristic temperature minimum layer at 100 m (fig 5.3c). The presence

or absence of patches could not be confirmed, as this section does not reach across the Weddell Gyre to the Antarctic continent. Comparisons with respect to the axis of the Gyre could also not be made.

Characteristics of AASW along the SR02a section was consistent with that found along the AJAX section as described by Whitworth and Nowlin (1987). It needs to be noted though that the consistency in terms of nutrients could not established for reason stated above. In terms of the A12 section the differences and similarities compared to the AJAX are similar to that of the A12 compared to the SR02a section. Nutrient comparisons of the near axis characteristics of the Weddell Gyre along the A12 section, showed similar characteristics to that of the AJAX section.

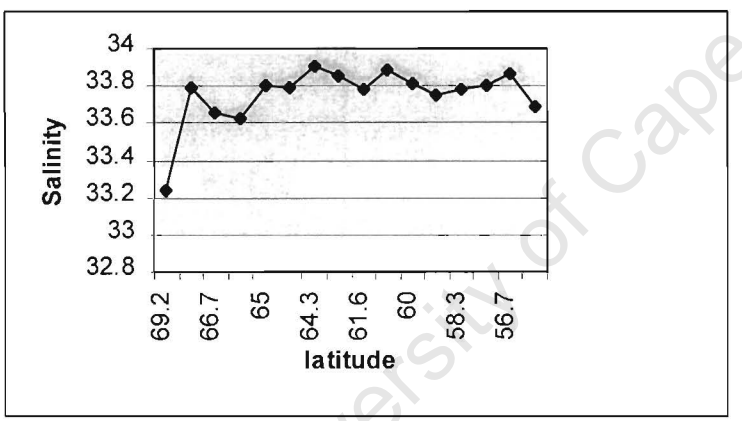

Figure 5.3.3a: Salinities across the Weddell Gyre for the SR02a section

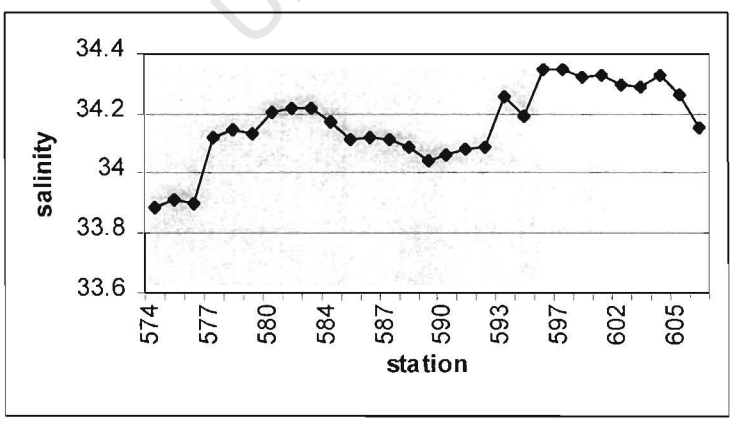

Figure 5.3.3b: Salinities across the Weddell Gyre for the A12 section

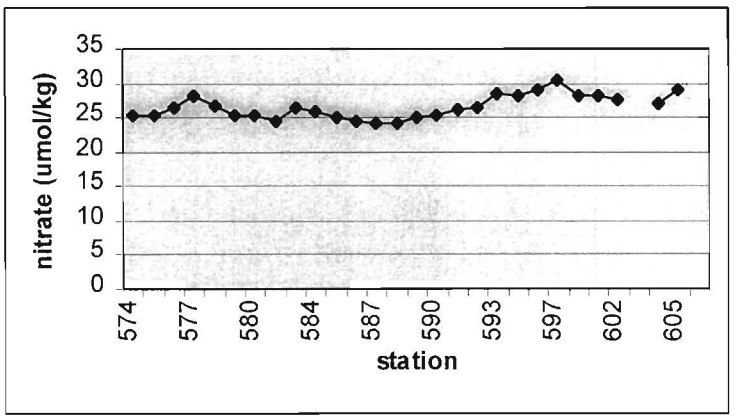

Figure 5.3.3c: Nitrate concentration across the Weddell Gyre for the A12 section

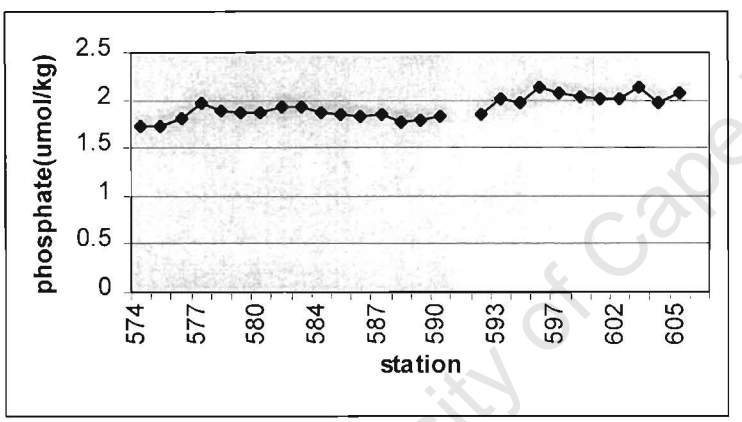

Figure 5.3.3d: Phosphate concentration across the Weddell Gyre for the A12 section

5.3.4 Antarctic Intermediate Water

AAIW characterized by its salinity minimum and oxygen maximum sinks below the SASW as relatively fresh water mass towards the north from the SAF. Along the SR02a (figure 5.3a, figure 5.5a) section AAIW sinks toward the north along density values between 27.1 and 27.2 kg/m3 (figures 5.9a(i)). The salinity minimum (34.2 to 34.25) associated with AAIW surfaces at the SAF and does not reach across the PFZ to the APF. This is in contrast to findings in the Drake Passage (Whitworth and Nowlin 1987). North of the STC this water mass seems to be influenced by Agulhas rings. This influence is seen as a low salinity patch at 38°S (figures 5.3a,c; 5.4a, c and 5.3.4), north and south of which there is a slight salinity maximum within the rings. Temperature and salinity

profiles of the two sections indicate the intrusion of warm, salty, low in oxygen water, associated with the Agulhas Current and Return Current (figures 5.1a,c and 5.2a and c). These characteristics are typical of Red Sea Water in the Agulhas Retroflection region (Lutjeharms and Ansorge 2001). This water mass is carried in the current along the same density level as AAIW. The mixing of the two water masses within the rings would thus result in higher salinities within the Agulhas rings and thus the patch at 38°S.

Except for the influence that the rings shed at the Agulhas Retroflection region have on the SR02a section, the A12 section (figures 5.3b, 5.5b and 5.11b) show similar characteristics to that of the SR02a section. This can be explained in the fact that the A12 section does not cross the Agulhas Retroflection region. The SR02b section (figures 5.3c, 5.5c and 5.11c) in contrast does cross this region and characteristics similar to that of the SR02a section are observed. The low salinity patch is observed at a similar position, 38°S between two Agulhas rings.

In the case of the A12 section the abovementioned observations of AAIW are consistent with observations found by Whitworth and Nowlin (1987) along the AJAX section. Thus as can be expected the SR02a and SR02b sections display one notable difference compared with the AJAX section, namely increased salinities in the AAIW within the Agulhas rings. In their discussion of the AJAX section, Whitworth and Nowlin (1987) found that although no clear connection could be made between AAIW and AASW they noted that the lowest surface salinities were found immediately south of the Polar Front. This observation was noted along all three respective sections (figures 5.4a, b and c).

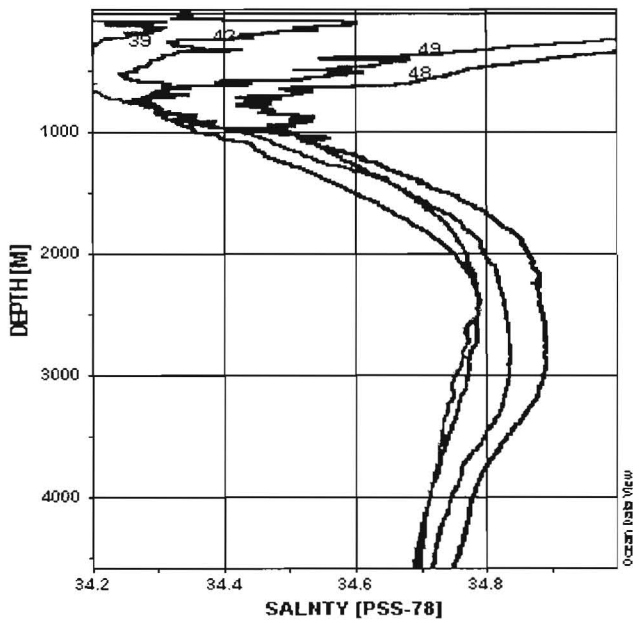

Figure 5.3.4: Salinity profile of the SR02a section showing the influence of Agulhas rings on AAIW (station 48 is in the ring; station 49 north of the ring and stations 39 and 42 is south of the ring)

5.3.5) Upper Circumpolar Deep Water

Found just below the AAIW the UCDW is characterized by its oxygen minimum and nutrient maximum. This water mass is clearly distinguished in the SR02a section by its oxygen signature (figure 5.5a). South of the APF this water mass has an induced temperature maximum by the overlying winter water (fig 5.1a). In comparison to the Drake Passage there is a reversal in the oxygen trend. In the Drake Passage the oxygen concentrations in the minimum increases from 3.7 ml/l in the Subantarctic Zone to 4.1ml/l in the Antarctic Zone. Along the SR02a section the minimum oxygen concentration of 4.2 ml/l in the Subantarctic Zone decreases to 4.1 ml/l in the Antarctic Zone. This reversal is due to the influence of NADW (Whitworth and Nowlin 1987). Findings along the A12 (figures 5.5b, 5.6b and 5.7a) and SR02b (figures 5.5c, 5.6c and 5.7b) sections are consistent with that along the SR02a section. In addition these two sections show the following nutrient trends. Nitrate concentrations for the A12 and SR02b north of the Subantarctic Front are slightly less than that in the Drake Passage. The highest nitrate value at the Antarctic Polar front for the A12 section was 35 μmol/L

(figure 5.6a). It needs to be noted that this maximum is well south of the Polar front. For the SR02b section the highest nitrate value at the APF was 36 μmol/L (figure 5.6b). It needs to be noted though that the highest average concentration of nitrates in the SR02b occurred south of the Subantarctic front whereas in the case in the A12 section the highest average concentration was found to be north of the Subantarctic front (figure 5.6a and 5.6b). Another trend that can be observed is the fact that the phosphate and nitrate maxima, lie slightly below oxygen minimum for the A12 (figures 5.5b, 5.6a, 5.7a and 5.3.5a) and SR02b sections (figures 5.5c, 5.6b, 5.7b and 5.3.5b).

The characteristics discussed above are in most cases consistent with observations found along the AJAX section as discussed by Whitworth and Nowlin (1987). Notable differences are however observed. Whitworth and Nowlin (1987) describe this water mass as having a relative temperature maximum due to the overlying AAIW and Winter Water. This was not the case along any of the three sections. The UCDW temperature maximum along these sections is induced only by the overlying Winter Water and not AAIW. Nutrient levels also show some deviation from observations along the AJAX section. Along the AJAX section values as high as 36.8 μmol/L was recorded near the Antarctic Polar front which was at least 1μmol/L higher than that found in the Drake Passage. Values along the A12 and SR02b sections were lower and nearly in line with that found in the Drake Passage. Consistent with the AJAX section the highest average concentration of nitrates occurred south of the Subantarctic front for the SR02b section (Whitworth and Nowlin 1987). This was not the case in the A12 section where the highest average concentration was found to be north of the Subantarctic front.

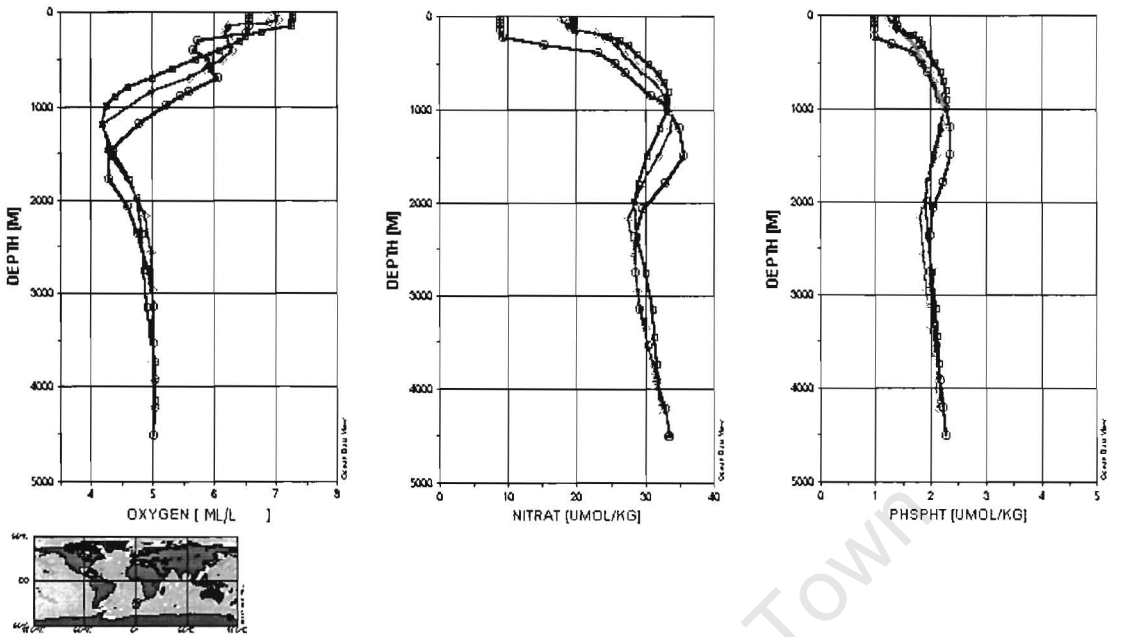

Figure 5.3.5a: Vertical distribution of oxygen, nitrate and phosphate for the A12 section

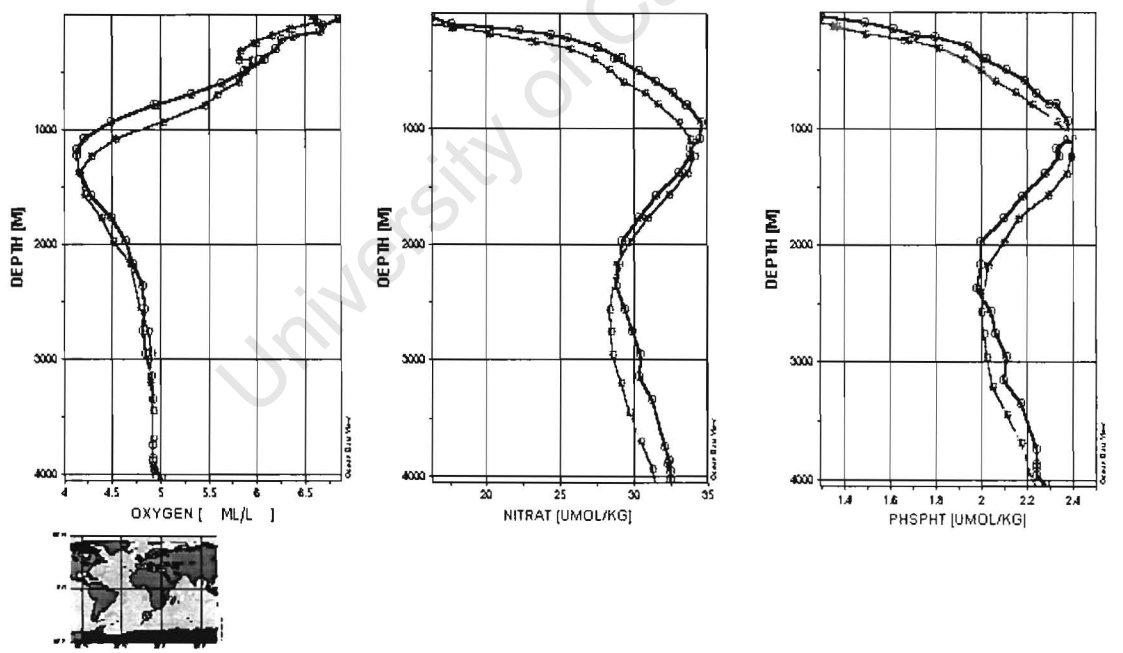

Figure 5.3.5b: Vertical distribution of oxygen, nitrates and phosphate for the SR02b section

5.3.6) Lower Circumpolar Deep Water

LCDW is characterized as having a salinity maximum and nutrient minimum. Due to the loss of the nutrient samples of the SR02a section LCDW can only be located using its salinity maximum characteristics (figure 5.2a). Whitworth and Nowlin (1987) indicated 34.729 to be the salinity maximum for CDW in the Drake Passage. Along SR02a section salinities greater than 34.75 cross both the SAF and APF and nearly the entire ACC (figure 5.2a). This salinity trend is observed in both the A12 (figure 5.2b) and SR02b (figure 5.2c) sections. Conversely nutrient values of phosphate (nitrate) along the A12 section (figures 5.6a and 5.7a) show a reduction in the minima compared to the Drake Passage from 2.25 (32.5) μmol/l to values less than 2 (29.9) μmol/L north of the Polar Front. This reduction is due to the influence of NADW (Whitworth and Nowlin 1987). The influence of NADW does however seem to differ between the SR02b and the A12 sections. The phosphate (nitrate) sections (figures 5.6a, b and 5.7a, b) for the SR02b and A12 sections indicate that interaction with NADW was much more extensive in the case of the A12 section with concentrations less than 2(30) μmol/L reaching across the Polar front. However in both the A12 and the SR02b sections an induced maximum in the nutrient concentrations can be observed in the densest CDW due to the penetration of low nutrient NADW across the ACC. This maximum is found at the bottom north of the mid-ocean ridge and at very shallow depths in the Weddell Gyre.

The abovementioned sections, the SR02a, A12 and SR02b show similar characteristics to that of the AJAX in terms of its salinities and nutrients trends. The only notable differences that can be observed are seen in the nutrient concentrations across the APF. The SR02b show similar trends to the AJAX in that phosphate (nitrate) concentrations do not drop below 2(30) μmol/l across the APF as was the case in the A12 section.

5.4 Weddell Gyre

Surface water of the Weddell Gyre consists of Antarctic Surface Water with its strong temperature minimum layer (section 5.3.3). Below this water mass there is a relatively warm, saline water mass in the SR02a section (figures 5.1a, 5.2a and 5.3a) and A12 section (figures 5.1b, 5.2b and 5.3b). This warm salty layer terminates around 58°S in the SR02a section. In addition, this water mass also displays a weakened oxygen minimum. Gordon and Huber (1984) suggested its termination point as being an eastward extension of the Weddell-Scotia Confluence. The confluence can be considered the northern boundary of the Weddell Gyre near the Scotia Sea. However in the AJAX section along the Greenwich Meridian it was found 200km south of the front that separated the Weddell Gyre from the ACC (Whitworth and Nowlin 1987). This was also found to be the case along the SR02a section. The above characteristics were not so clear along the A12 section. Although the relative oxygen minimum could be observed, the warm salty layer was continues across the whole Weddell Gyre (figures 5.1b, 5.2b and 5.5b).

5.4.1 Intermediate waters of the Weddell Gyre

Whitworth and Nowlin (1987) indicated the intermediate waters of the Weddell Gyre to be unmodified LCDW. They found that in the central part of the Weddell Gyre this water mass is biochemically altered resulting in a distinct water mass they called the intermediate water of the central Weddell Gyre.

Comparing the SR02a section with the A21 section (Drake Passage), reveal that changes have taken place in the LCDW between the Drake Passage and the Greenwich Meridian. Water warmer that 0.8°C just north of the APF along the SR02a section is saltier than that found in the Drake Passage (figure 5.4.1a). Whitworth and Nowlin (1987), attributes this increase in salinity to the introduction of NADW in the south west Atlantic. In comparison with the Drake Passage water cooler than 0.8°C was fresher and reflects the influence of the fresher Weddell Gyre. Within the Weddel Gyre salinities are 0.01-0.02 lower at the equivalent salinities in the Drake Passage (figure 5.4.1a).

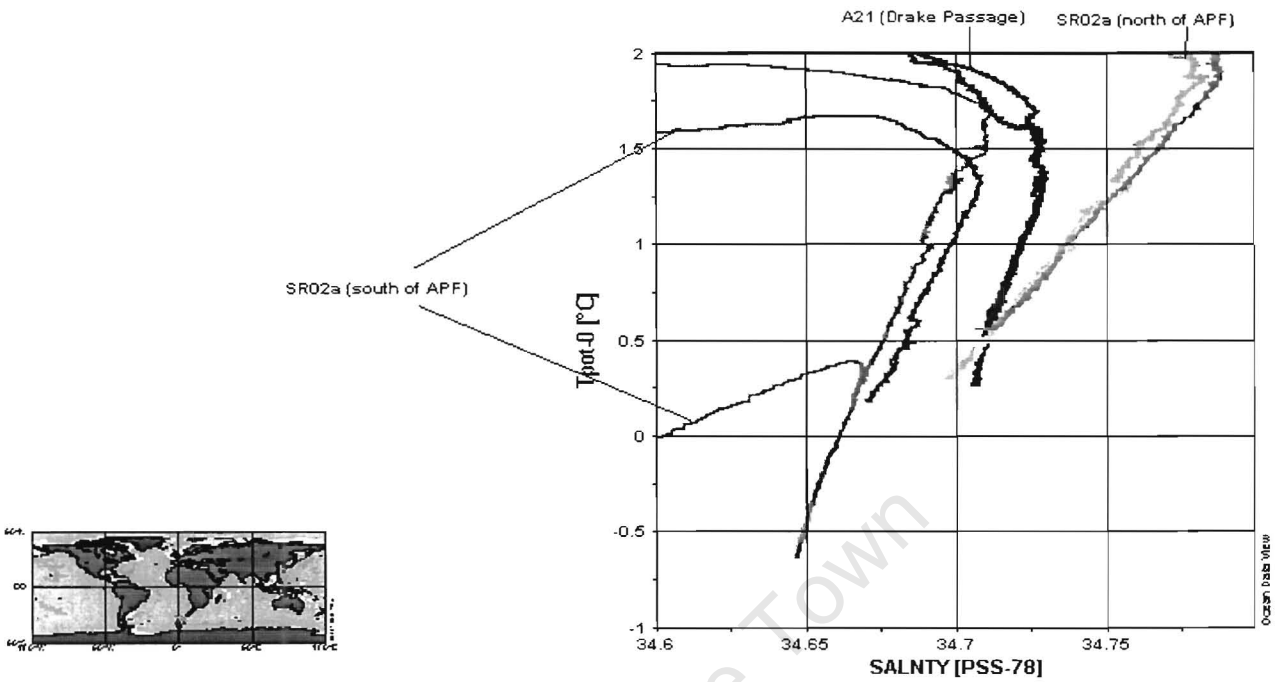

Figure 5.4.1a: Q-S relationship for Greenwich Meridian stations (SR02a) in the ACC and the Weddell Gyre and Drake Passage stations north of the APF

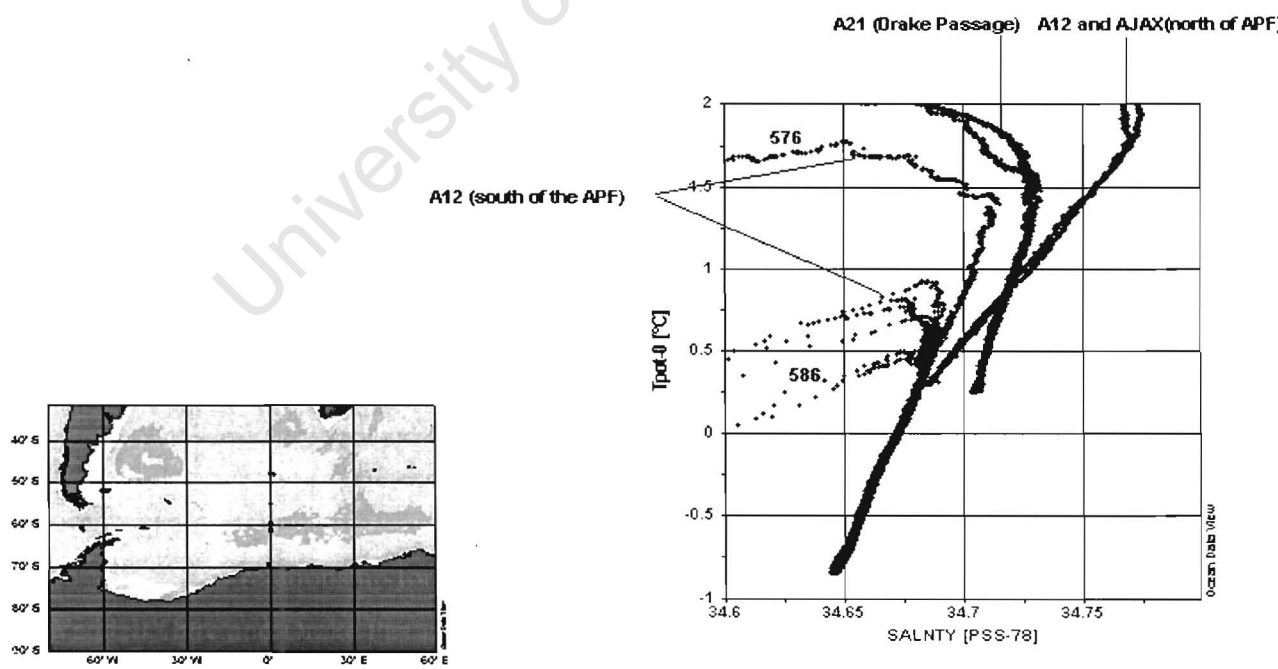

Figure 5.4.1b: Q-S relationship for Greenwich Meridian stations (A12) in the ACC and the Weddell Gyre and Drake Passage stations north of the APF

From the SR02a section it is clear that only the densest LCDW form part of the axis of the Weddell Gyre. This is shown in that LCDW found in the intermediate layer of the Weddell Gyre is found near the bottom north of the Mid Ocean Ridge (figure 5.9a(ii)). The southern limb of the Weddell Gyre with its relatively warm, saline LCDW can be clearly seen as it meanders around the Maude Rise in the SR02a section (figures 5.1a and 5.2a). The warmest, most saline water rounds the Rise to the north between 300 m and 600 m with some part returning eastward around the south (figures 5.1a and 5.3a). Its relative high temperature and relatively high salinity indicate it to be LCDW. Also seen in the southern limb is a relatively low oxygen layer around 300 m which is a remnant of somewhat less dense LCDW which form just above the salinity maximum layer (figures 5.2a and 5.5a). In the northern limb of the Weddell Gyre, an oxygen minimum is induced on the LCDW by the overlying high oxygen waters. A separate minimum at 60°S is visible at 500 m in the SR02a section (figure 5.5a). This feature extends in weakened form across the northern and southern limb of the Gyre.

Observations along the A12 section are consistent with that of the SR02a section. Similar to the SR02a section water warmer than 0.8°C are saltier that that of the Drake Passage whilst that cooler than 0.8°C are fresher reflecting the influence of NADW and the fresher Weddell Gyre (figure 5.4.1b). Also seen is the oxygen minimum layer in the southern limb of the Weddell Gyre of the A12 section at around 300 m (figure 5.5b). Although a little further south, the separate oxygen minimum near the axis of the Weddell Gyre can also be seen along the A12 section (figure 5.5b).

The AJAX section as described by Whitworth and Nowlin (1987), the SR02a section and the A12 section are comparably similar with respect to the characteristics discussed above. However it needs to be noted that unlike the AJAX and A12 sections no deepening in the oxygen layer occurs in the southern limb of the Weddell Gyre of the SR02a section.

5.4.2 Central intermediate water

This water mass is distinguished using its oxygen minimum and nutrient maximum. Whitworth and Nowlin (1987) describe its formation as dense LCDW that circulates the Weddell Gyre, eventually spiraling inward and upward to become intermediate water of the central Weddell Gyre. Ultimately it is eroded away from above through mixing with the winter mixed layer (Gordon et al. 1984). Because of the loss of nutrient samples in the SR02a section we will only look at this water mass with respect to the A12 section. Along the A12 section this water mass has it characteristic oxygen minimum (figures 5.5b and 5.4.2) and nutrient maximum (figure 5.8a). Also observed is the fact that the silicate maximum occurs just below the oxygen minimum (figures 5.5b and 5.8a). The silicate maximum for the A12 section was 128.1 μmol/l.

The above, described characteristics are similar to that found along the AJAX section. The only notable difference are observed on the maximum concentration of silicates in this water mass. Along the AJAX silicate levels exceeded 140 μmol/l whereas in the A12 section it did not exceed 128.1 μmol/l. Whitworth and Nowlin (1987) put forward the Indian Ocean as a possible source for this high silicates as well as the dissolution of sinking particulate matter following the complete regeneration of phosphate and nitrate in the overlying waters.

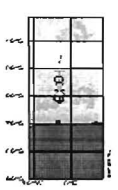

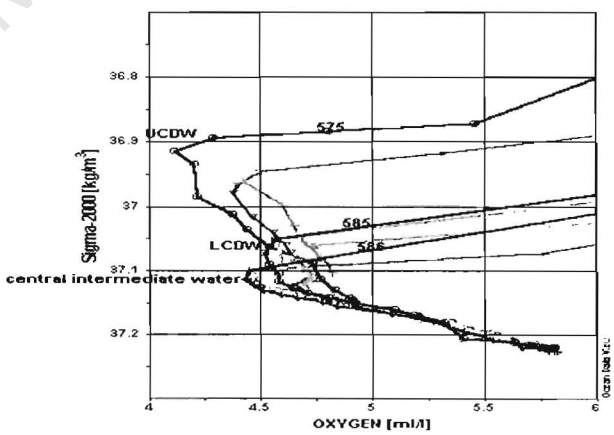

Figure 5.4.2: Erosion of the oxygen minimum across the ACC and Weddell Gyre, shown as density (2000m) versus O_2 for the A12 section

5.4.3 Deep and Bottom Waters

Weddell Sea Deep Water, as defined by Reid et al. (1977) lies between –0.7°C and 0°C. It is this water that escapes the boundaries of the Weddell Sea to become the main ingredient of Antarctic Bottom Water. Weddell Sea Bottom Water is characterized as having a potential temperature of below –0.7°C. It has a relative minimum in temperature, salinity and nutrients and a relative maximum in oxygen. Except for nutrients these characteristics are consistent with those found along the SR02a section (figures 5.1a, 5.2a and 5.5a). No nutrients were available for the SR02a section and therefore no comparison could be made. The extrema characteristics of the deep and bottom waters are observed as skewed towards the north in the SR02a section. Whitworth and Nowlin (1987) indicate that this might be due to the presence of a deep boundary current but that an influx of anomalous characteristic at the southern margin could also be responsible. The A12 section display similar characteristics compared to the SR02a section (figures 5.1b, 5.2b and 5.5b). Compared with the AJAX section abovementioned sections display no notable differences with respect to the abovementioned characteristics.

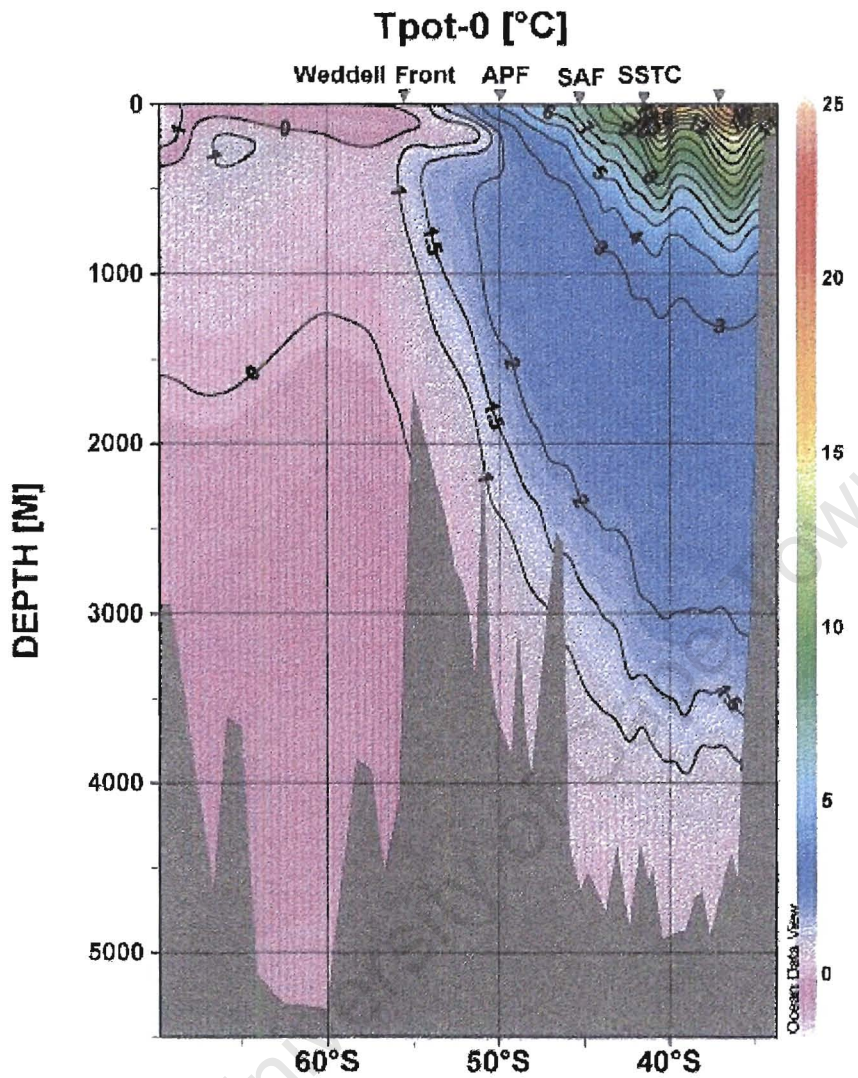

Fig 5.1a: Vertical Potential Temperature section of the SR02a section

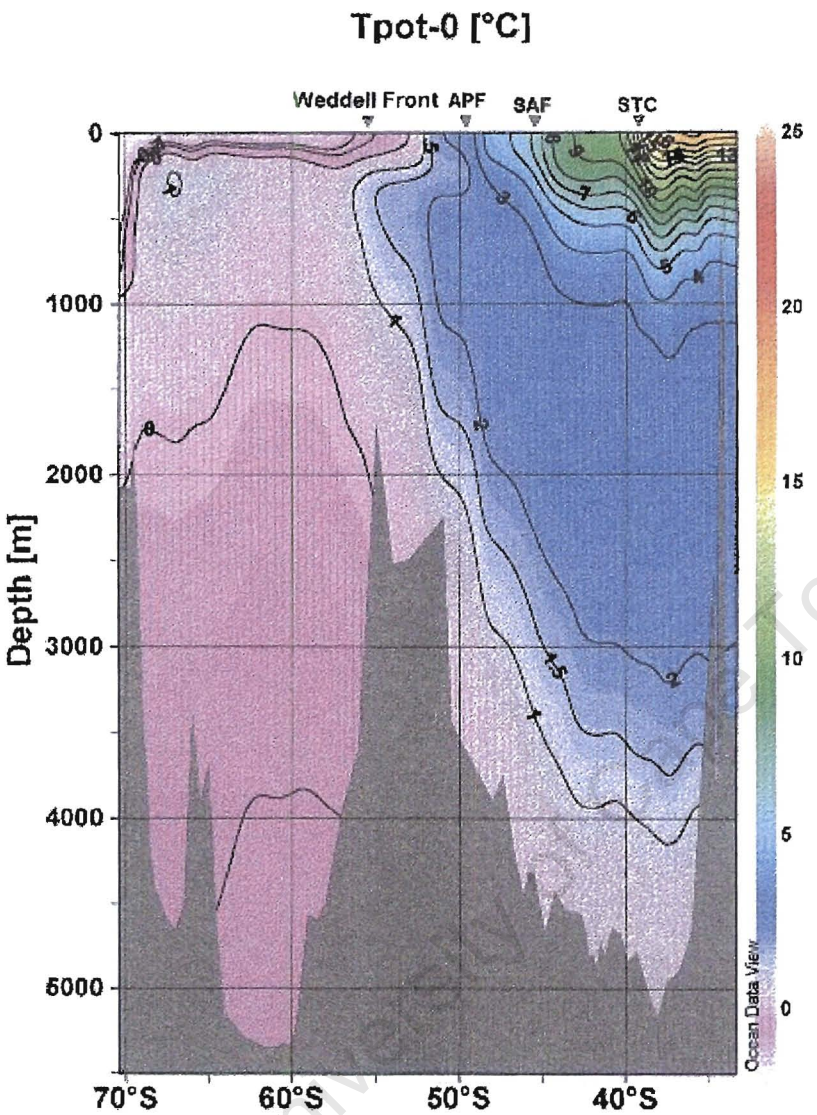

Fig 5.1b: Vertical Potential Temperature section for the A12 section

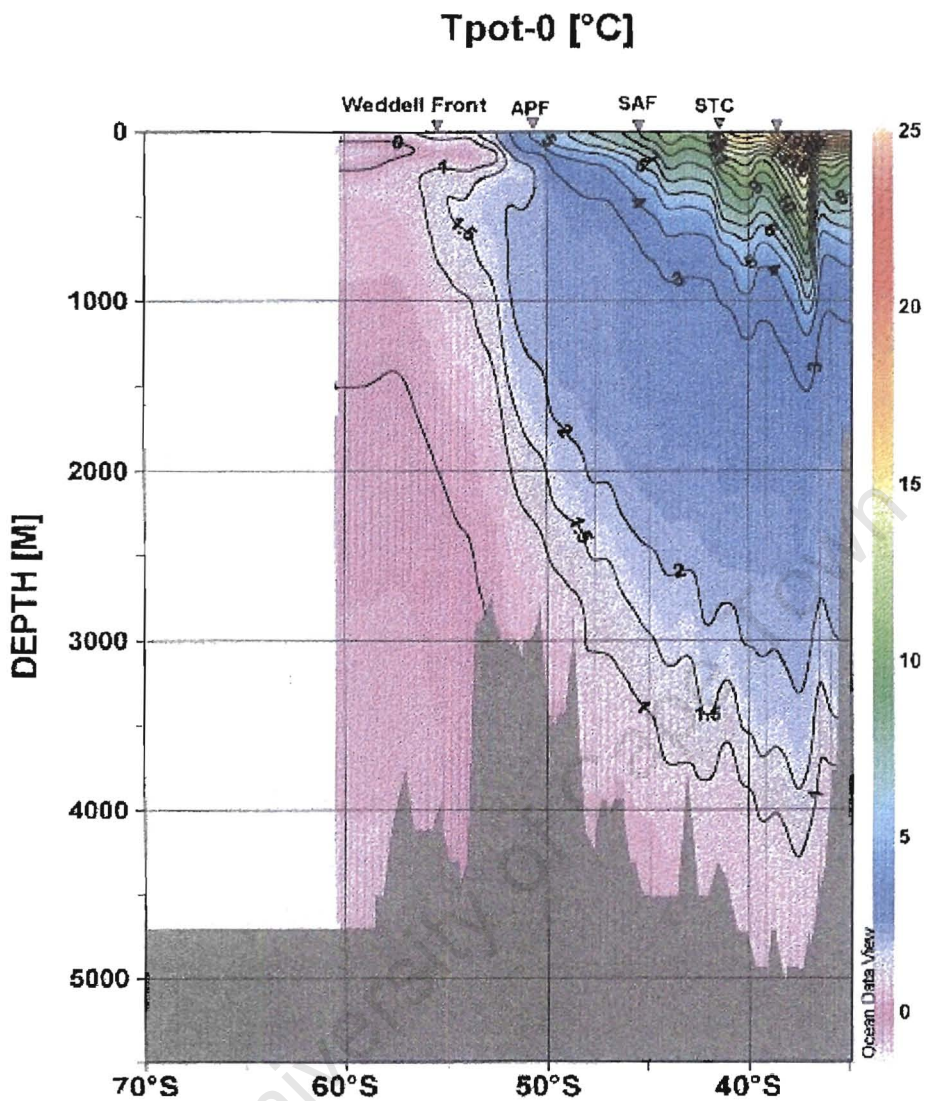

Fig 5.1c: Vertical Potential Temperature section of the SR02b section

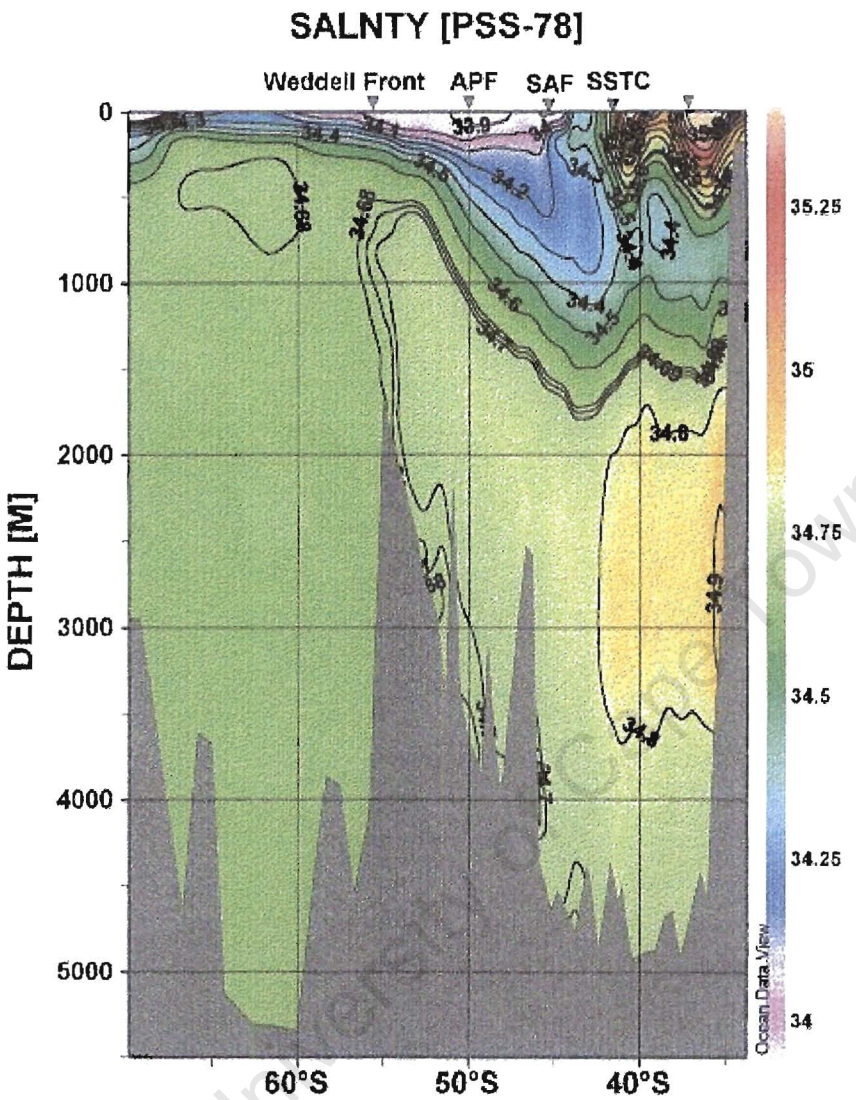

Fig 5.2a: Vertical Salinity section of the SR02a section

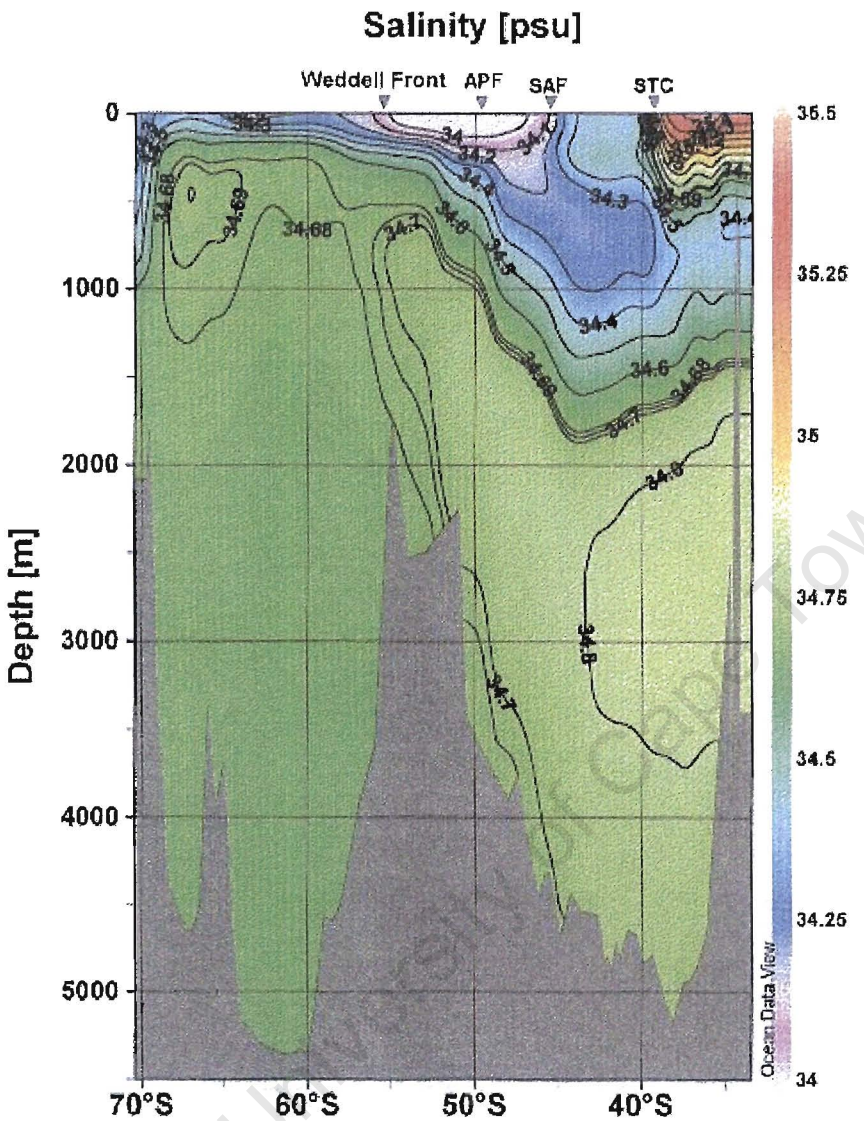

Fig 5.2b: Vertical Salinity section of the A12 section

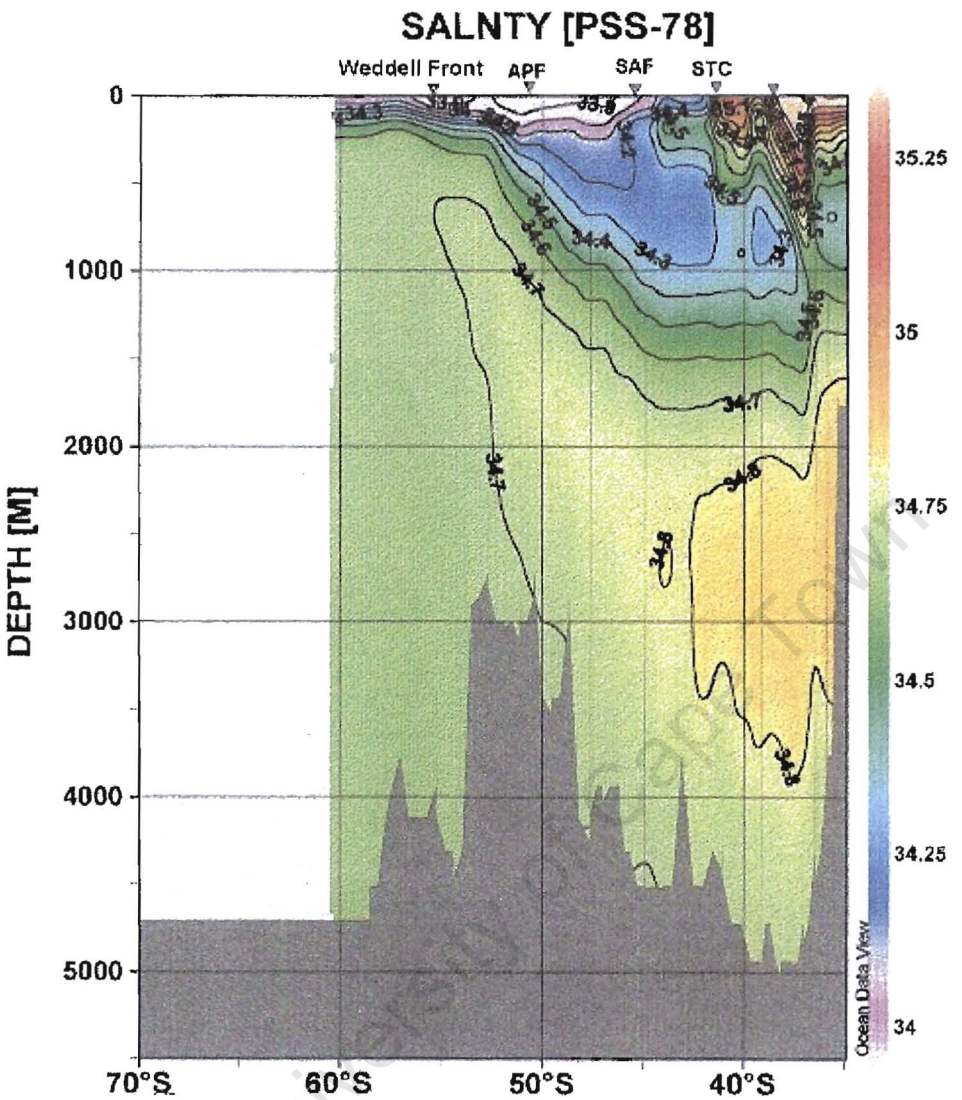

Fig 5.2c: Vertical Salinity section of the SR02b section

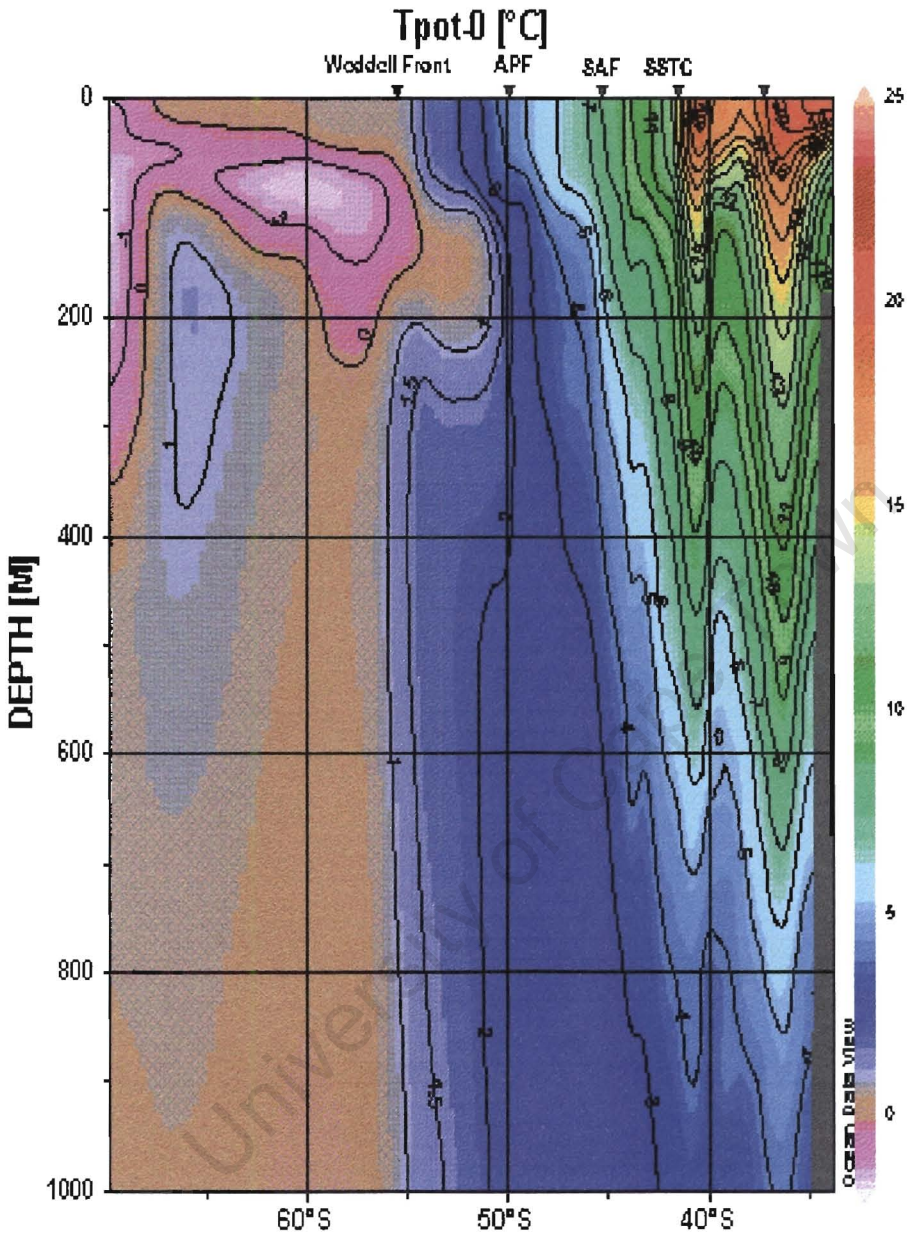

Fig 5.3a: Vertical Potential Temperature section of the SR02a section (upper 1000m)

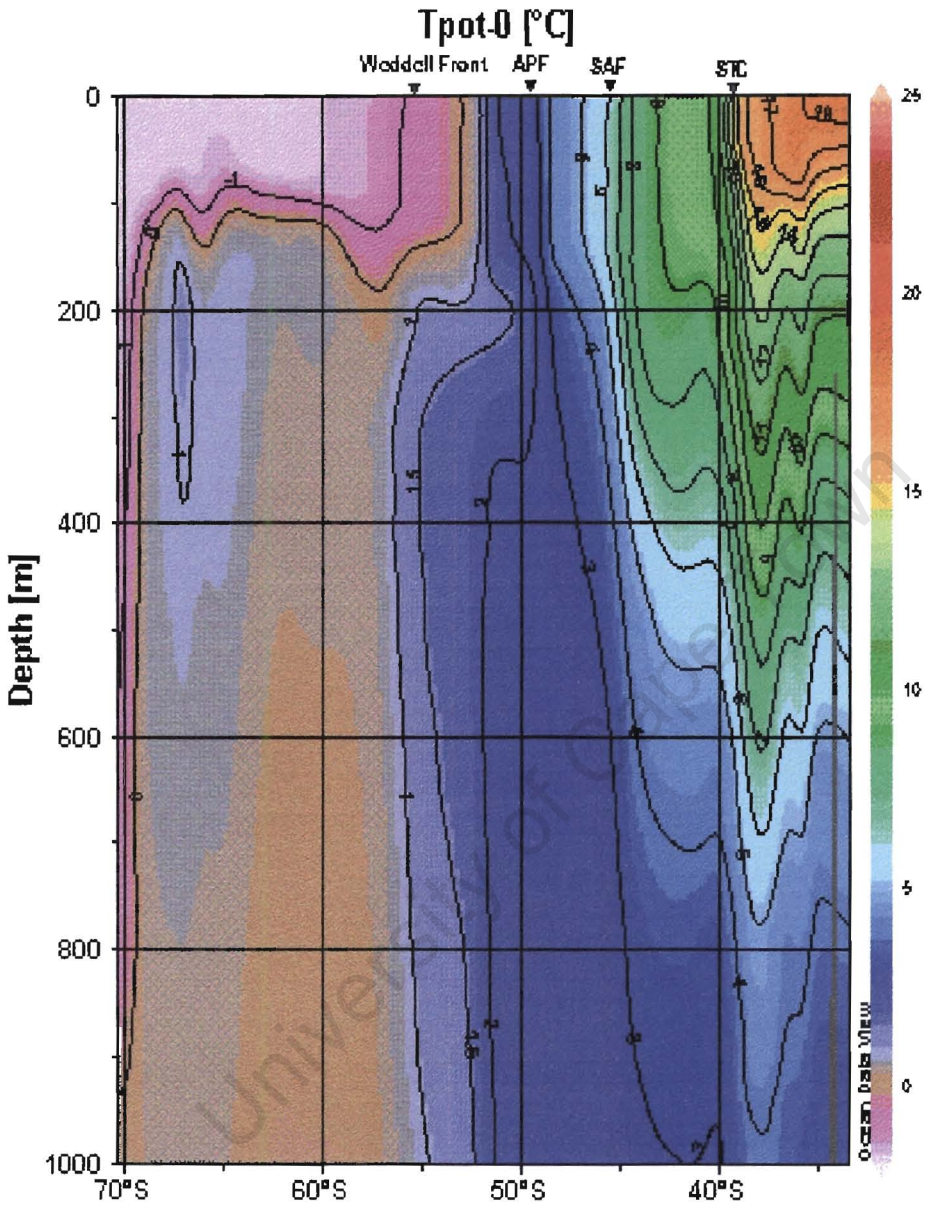

Fig 5.3b: Vertical Potential Temperature section of the A12 section (Upper 1000m)

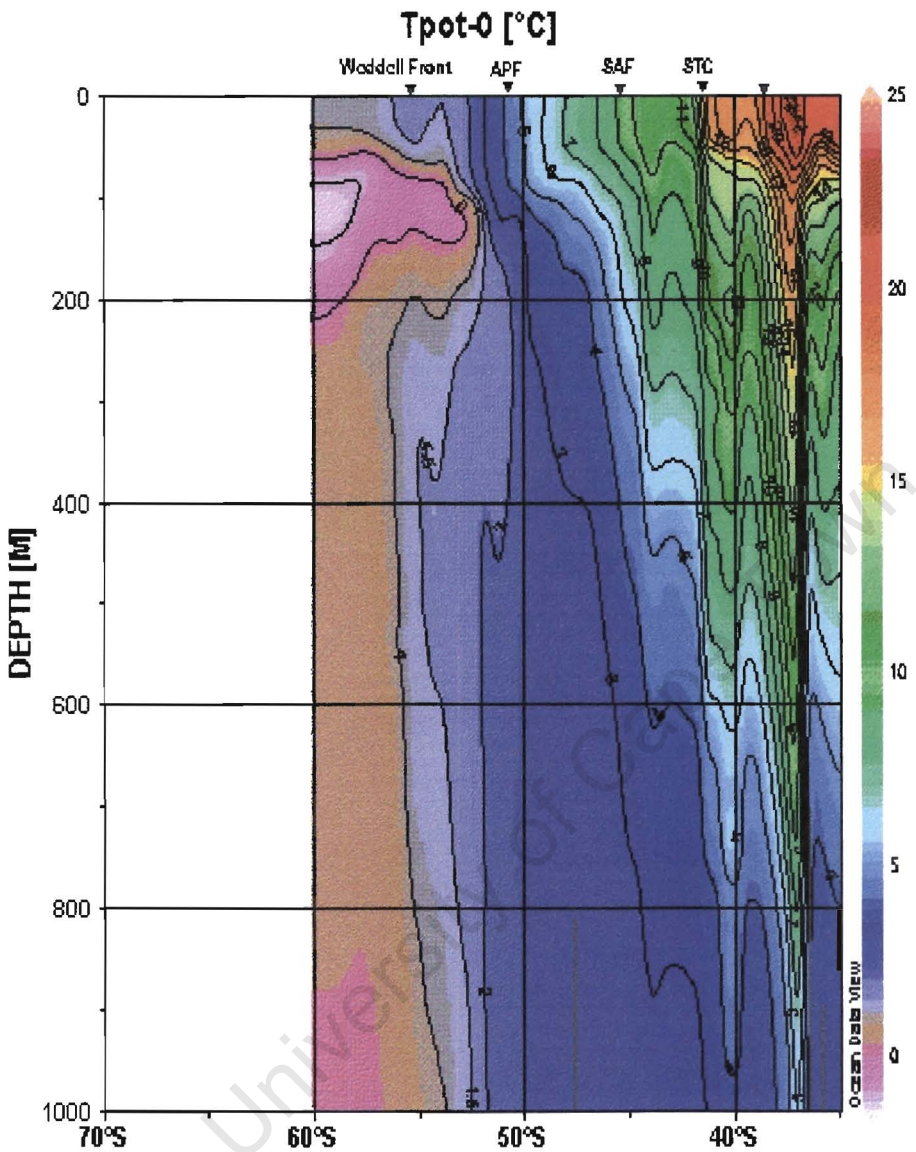

Fig 5.3c: Vertical Potential Temperature section of the SR02b section (Upper 1000m)

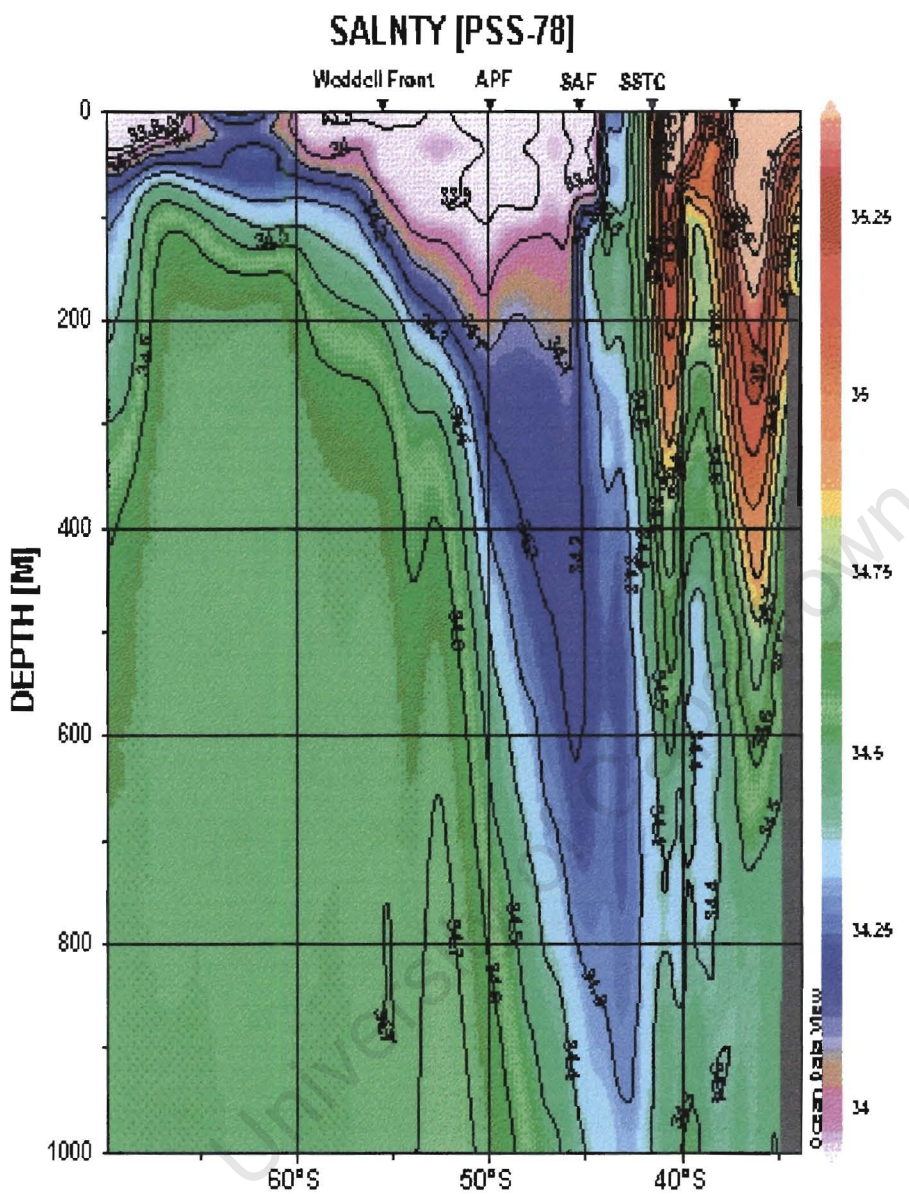

Fig 5.4a: Vertical Salinity section of the SR02a section (Upper 1000m)

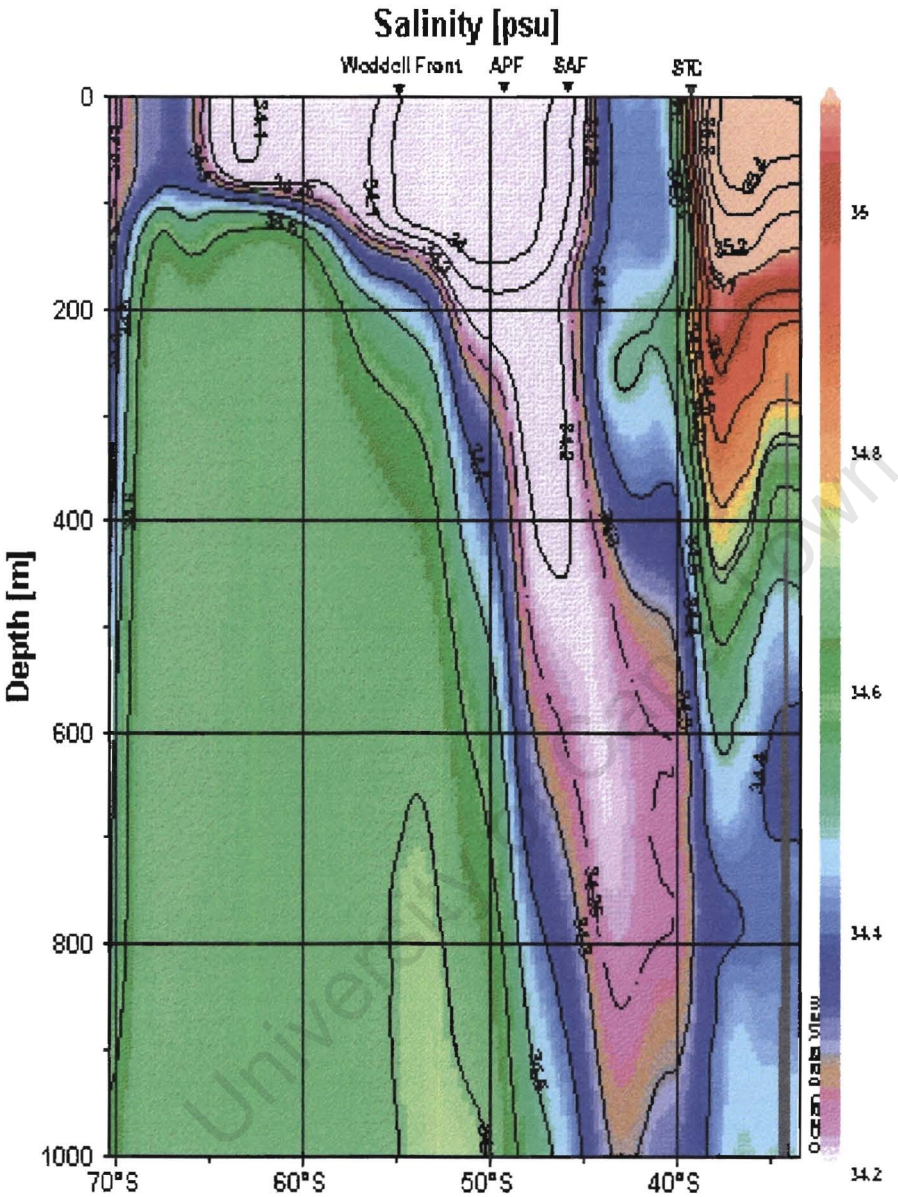

Fig 5.4b: Vertical Salinity section of the A12 section (Upper 1000 m)

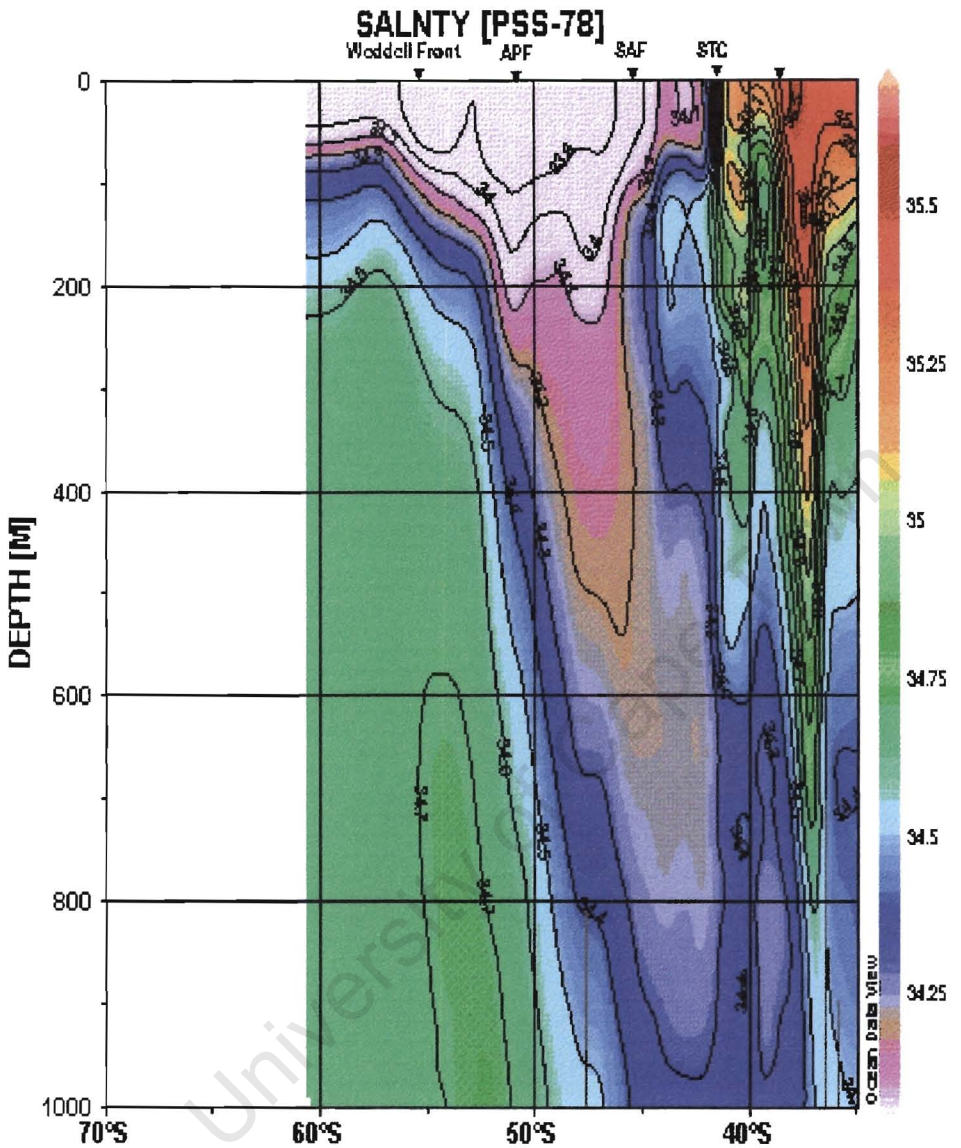

Fig 5.4c: Vertical Salinity section for the SR02b section (Upper 1000 m)

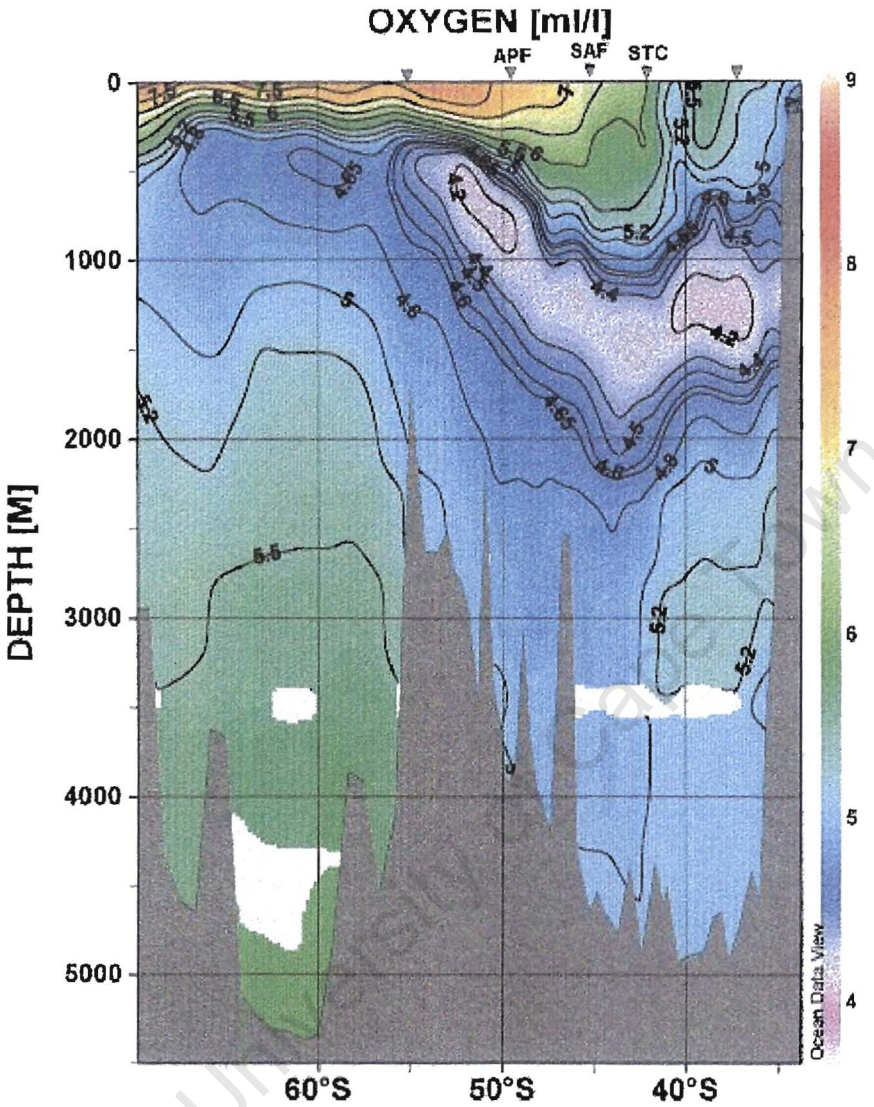

Fig 5.5a: Dissolved Oxygen section of the SR02a section

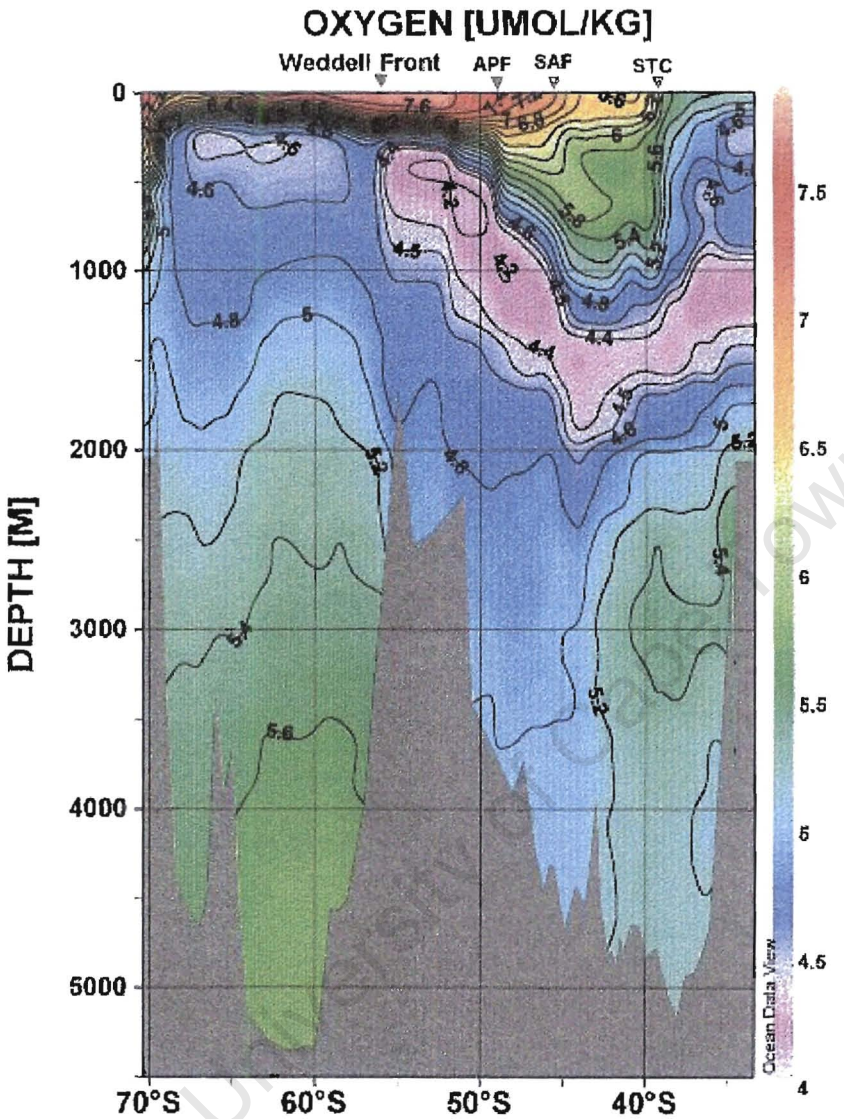

Fig 5.5b: Vertical Oxygen section of the A12 WOCE section

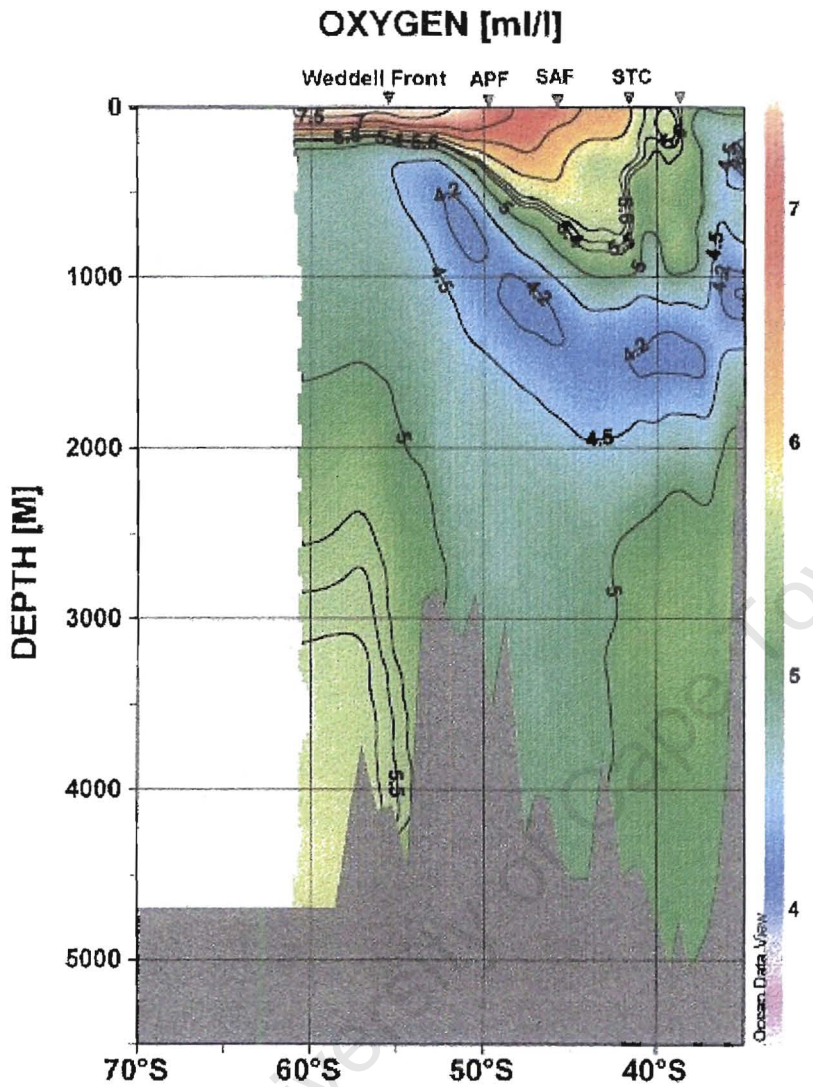

Fig 5.5c: Vertical Oxygen section of the SR02b WOCE section

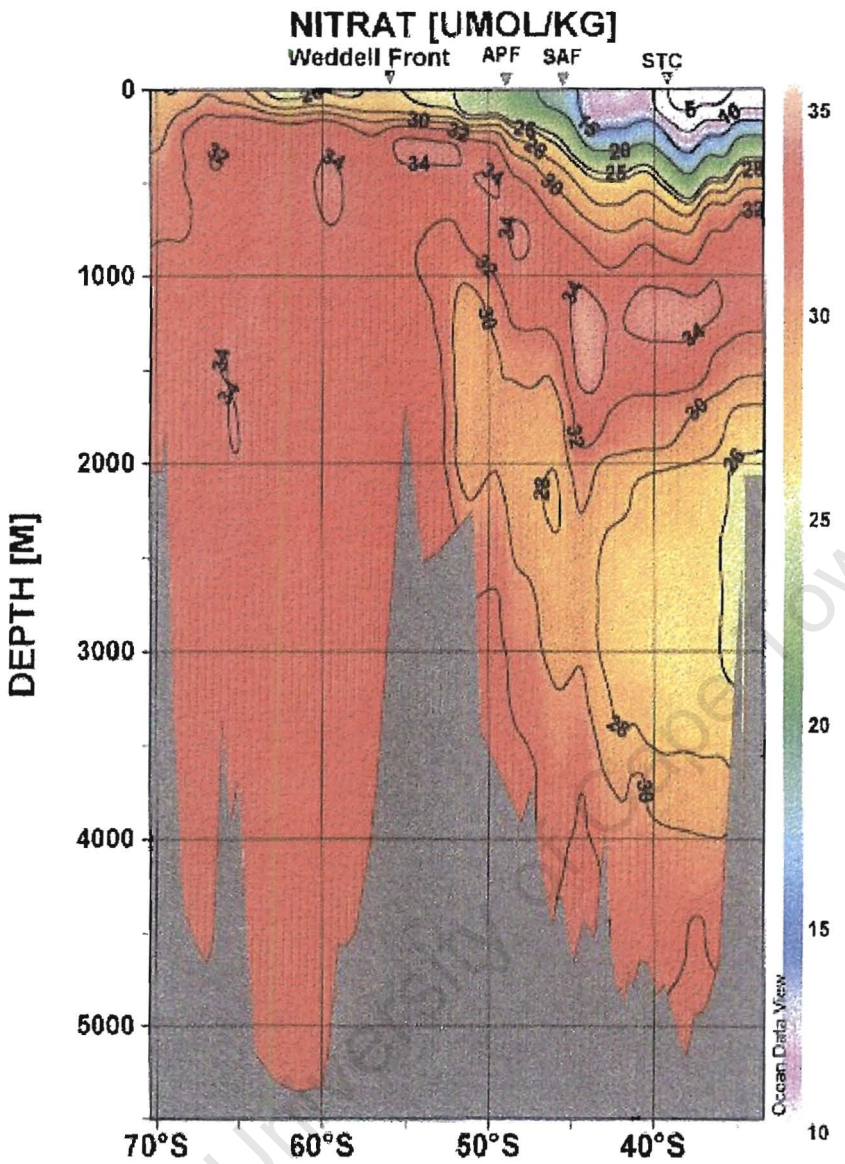

Fig 5.6a: Vertical Nitrate section of the A12 WOCE section

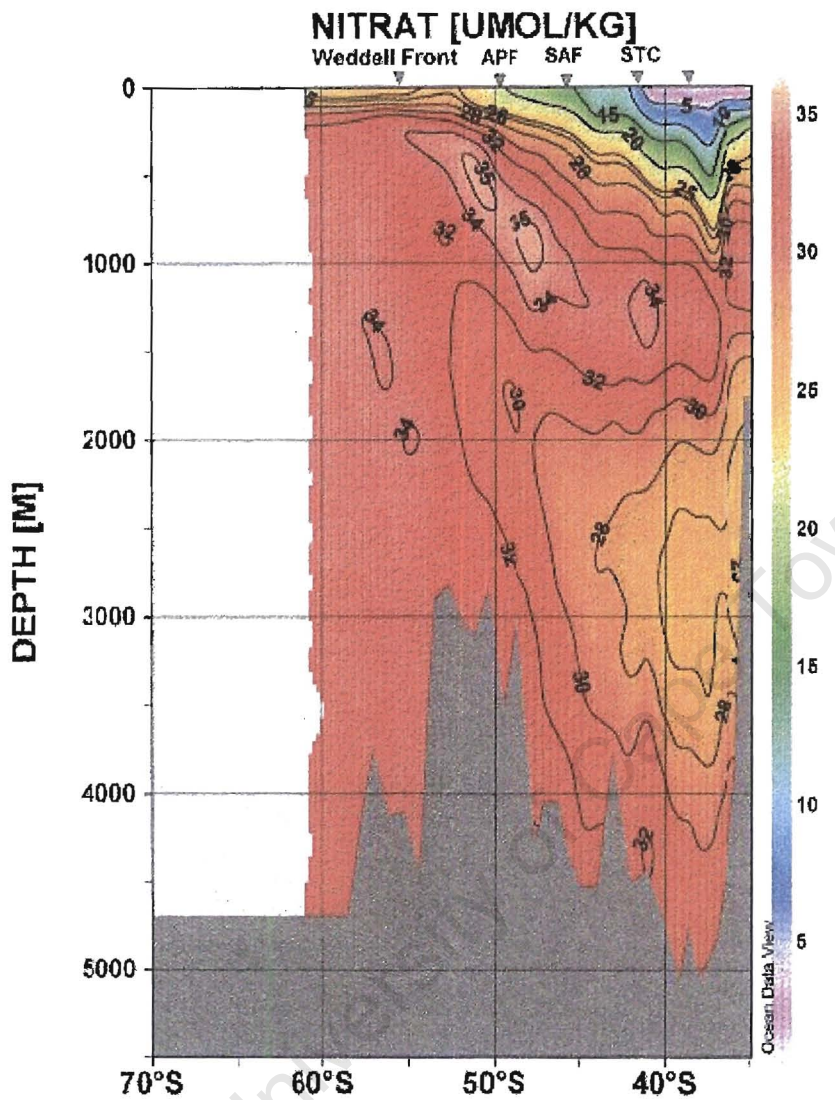

Fig 5.6b: Vertical Nitrate section of the SR02b WOCE section

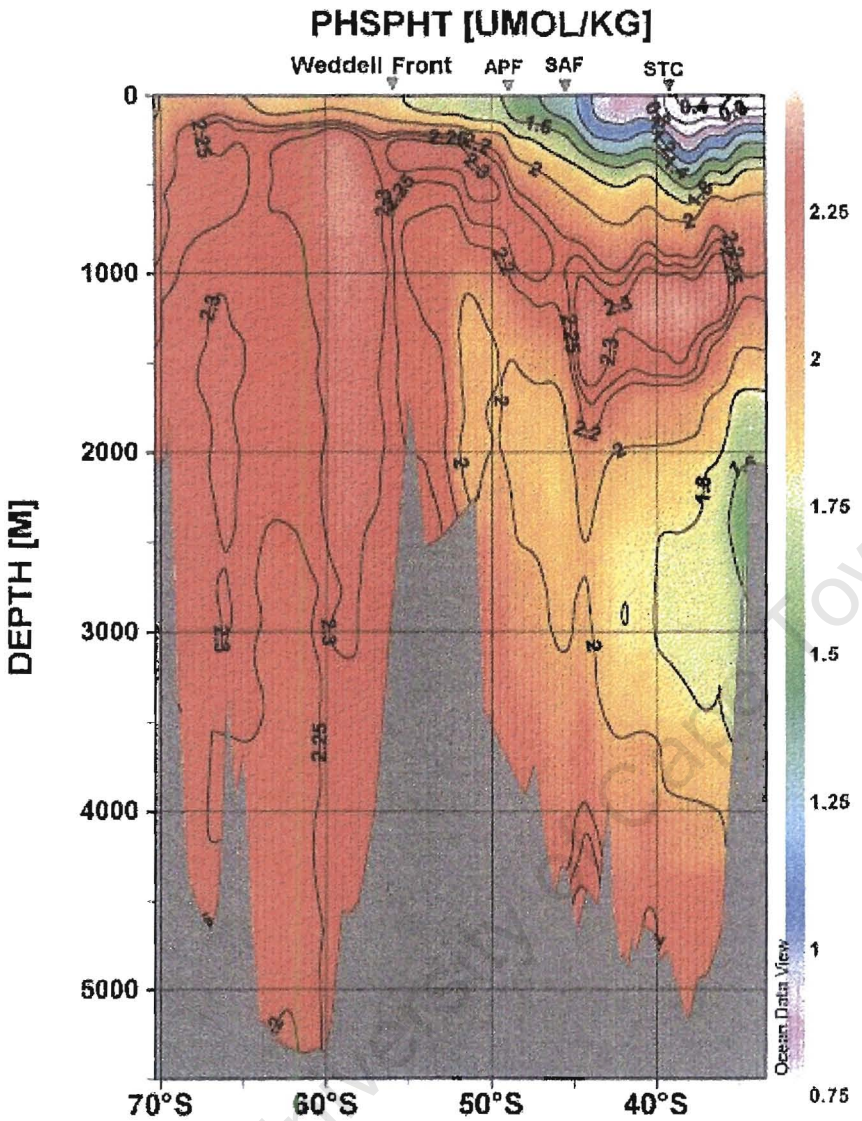

Fig 5.7a: Vertical Phosphate section of the A12 WOCE section

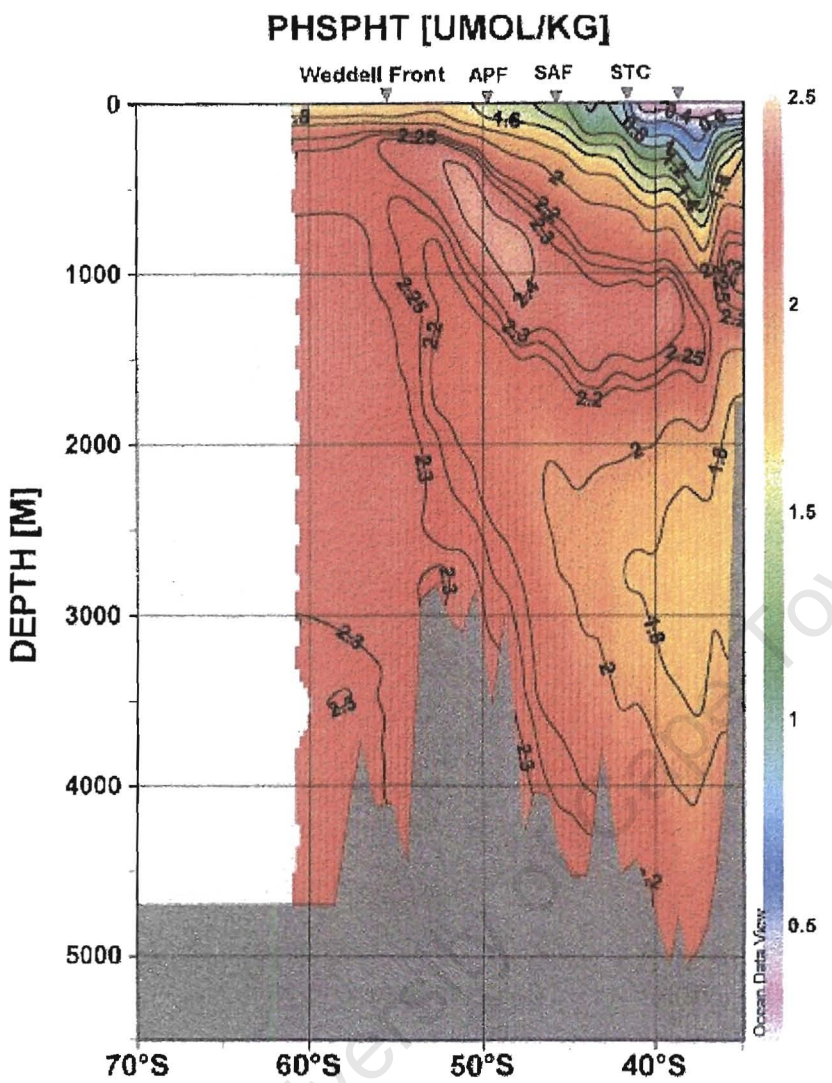

Fig 5.7b: Vertical Phosphate section of the SR02b WOCE section

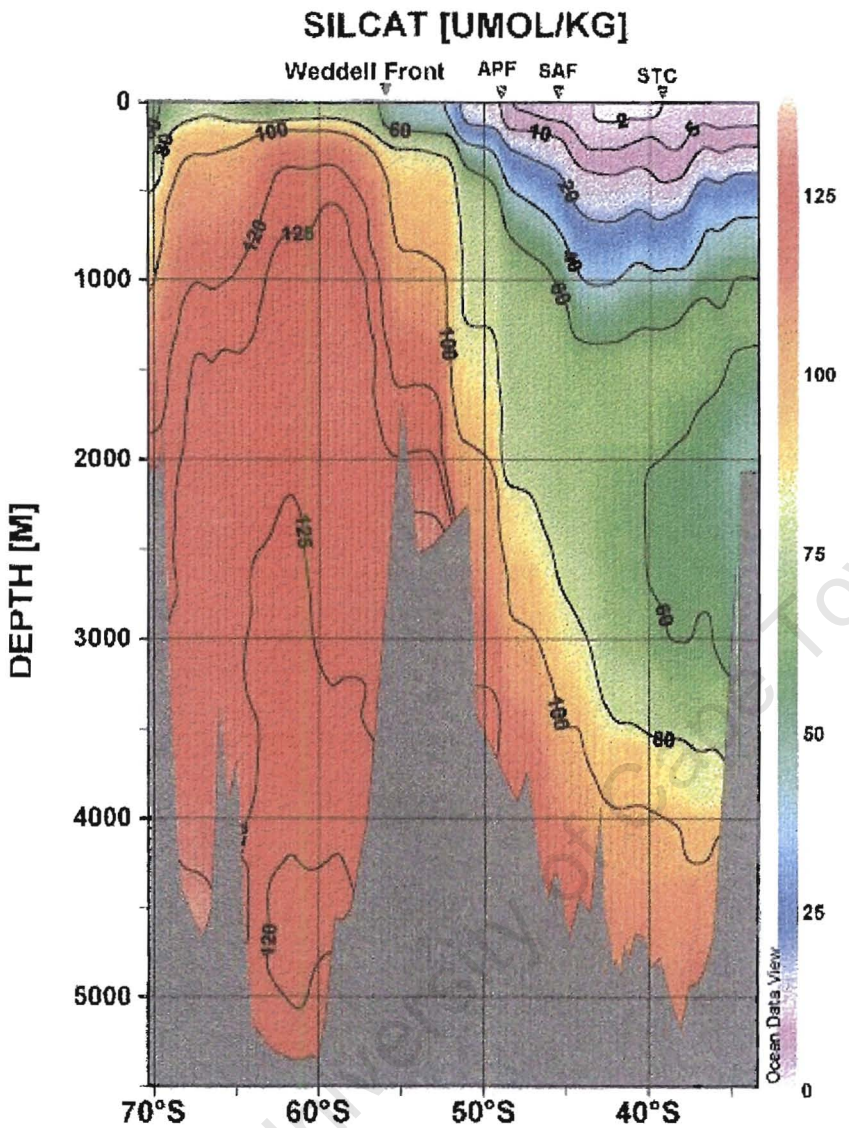

Fig 5.8a: Vertical Silicate section of the A12 WOCE section

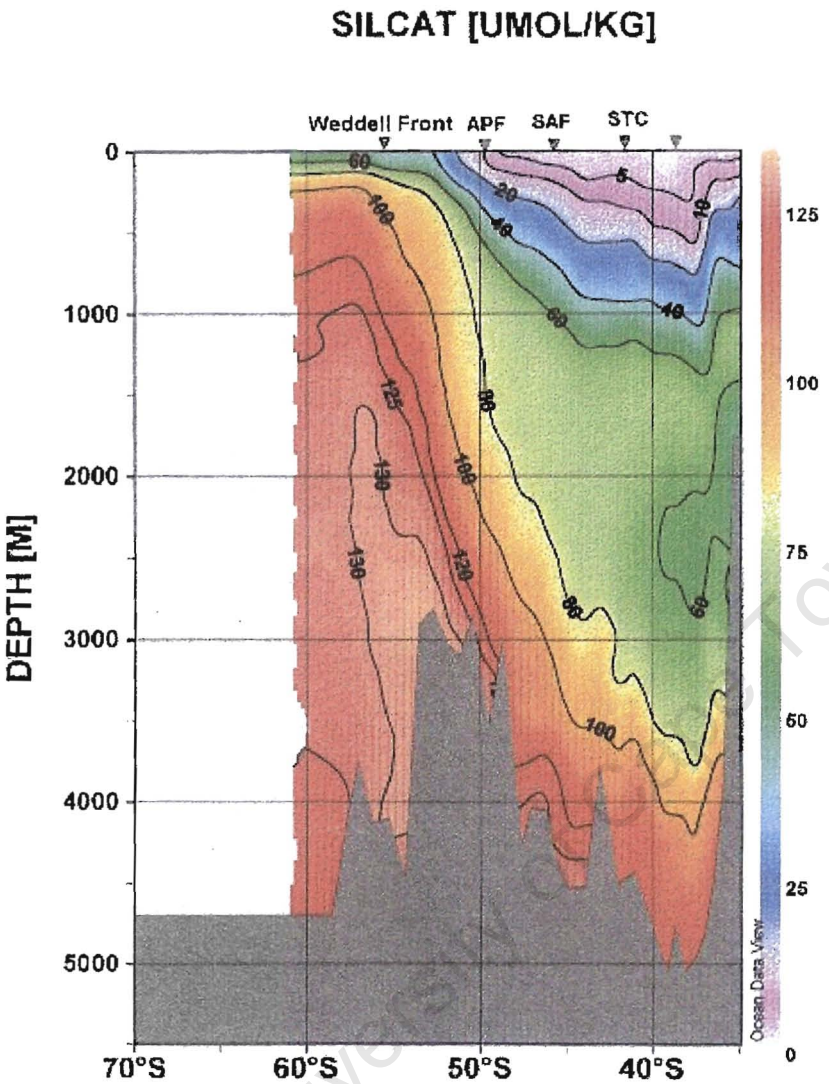

Fig 5.8b: Vertical Silicate section of the SR02b WOCE section

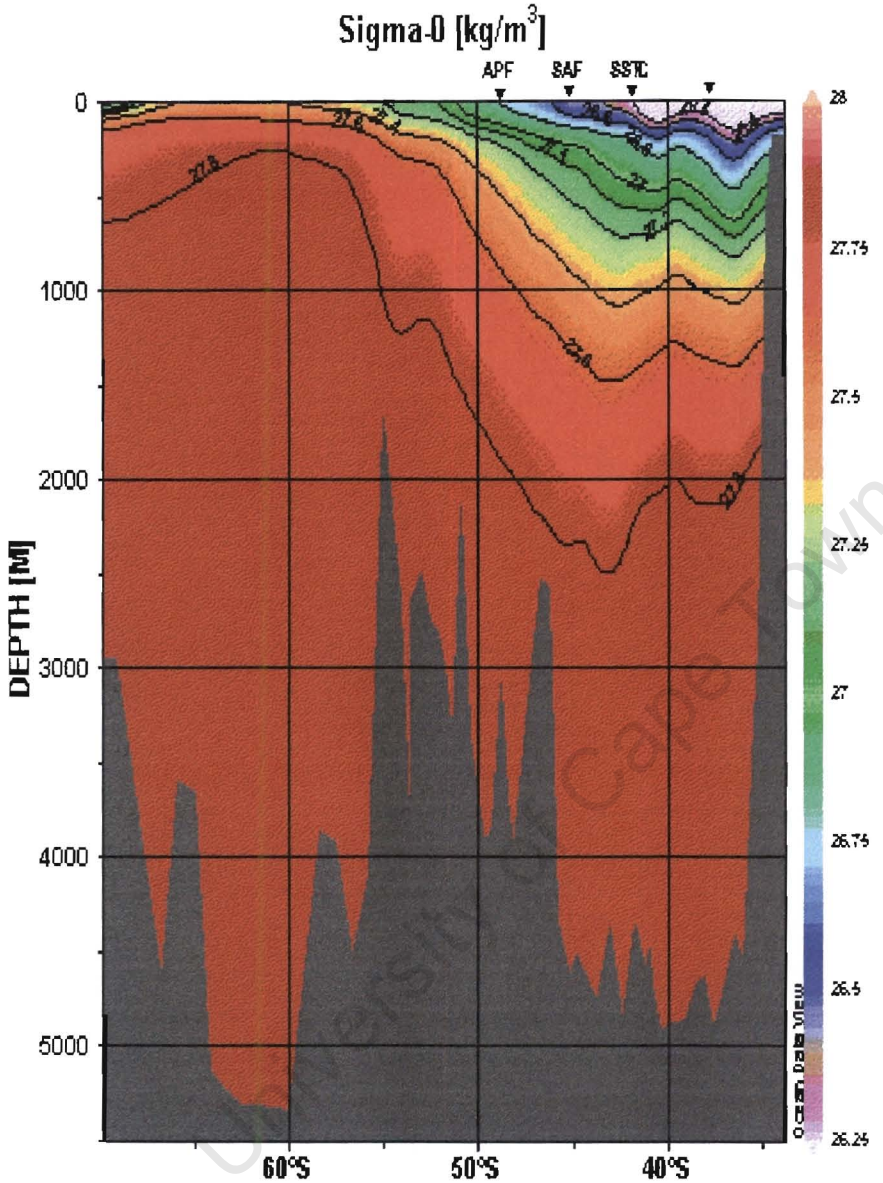

Fig 5.9a (i): Potential density section of the SR02a section

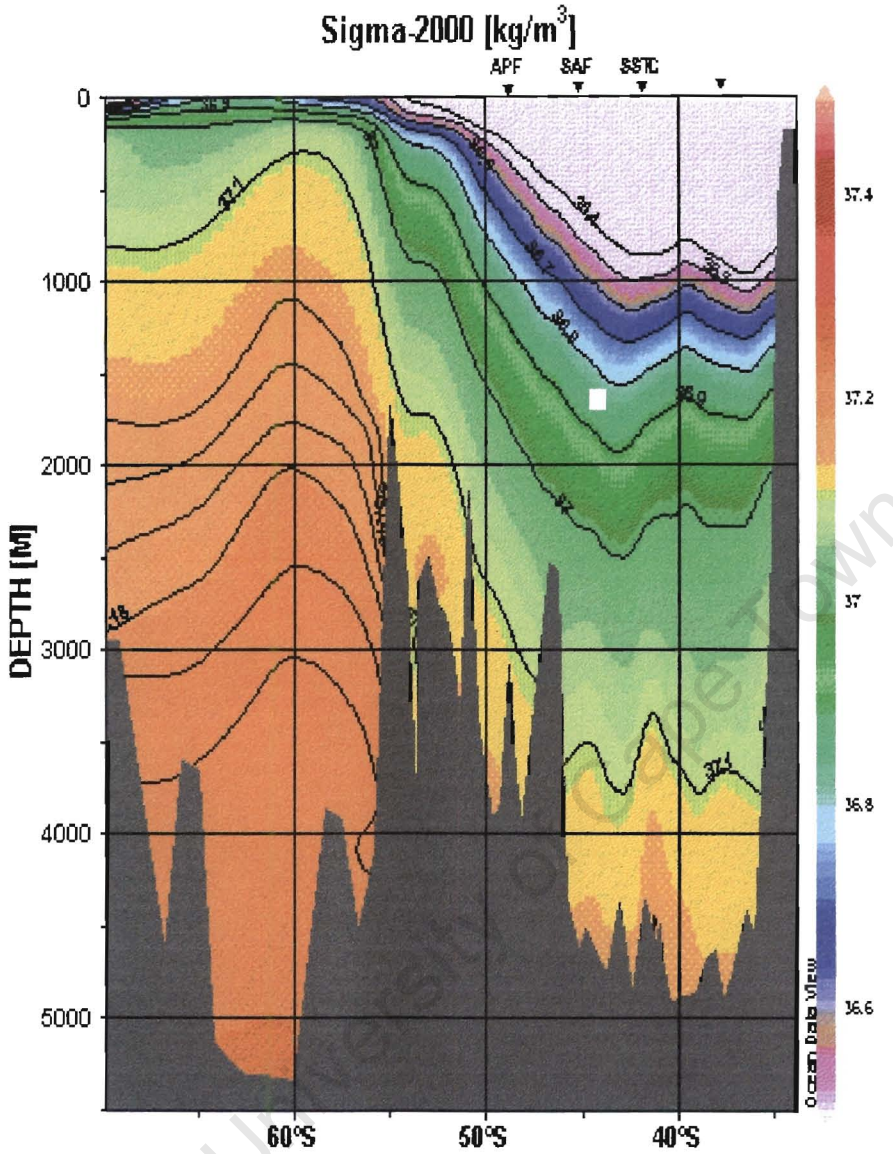

Fig 5.9a (ii): Potential density section of the SR02a section (Sigma-2000 m)

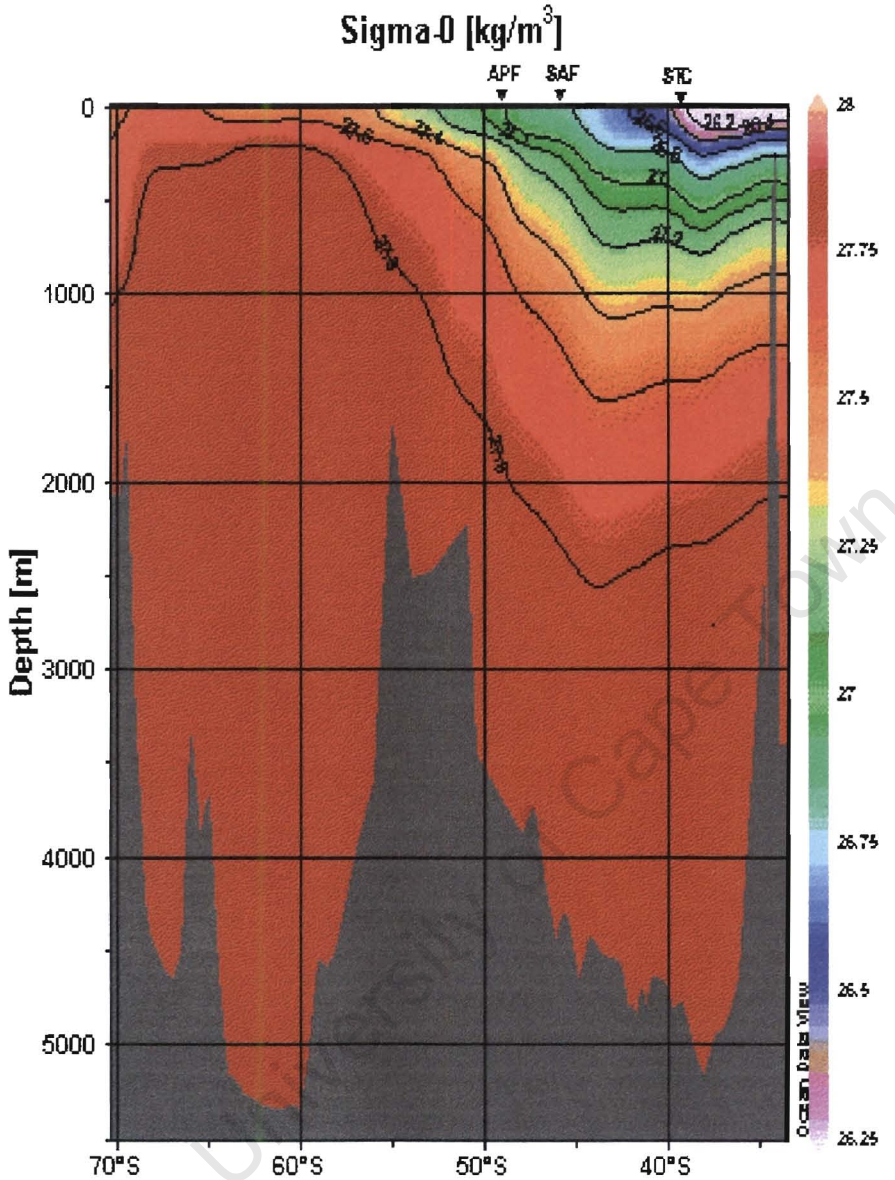

Fig 5.9b (i): Vertical Potential Density section of the A12 section

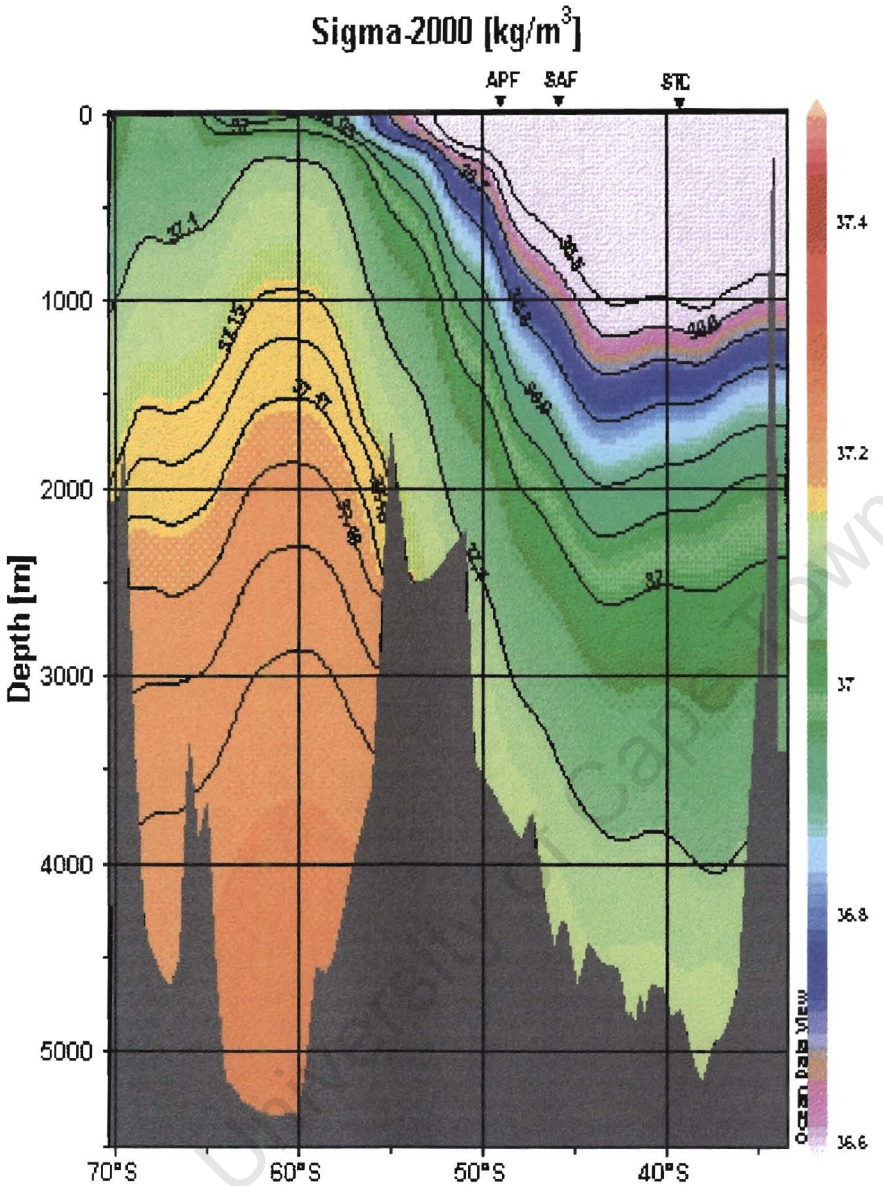

Fig 5.9b (ii): Vertical Potential Density section of the A12 section (Sigma-2000 m)

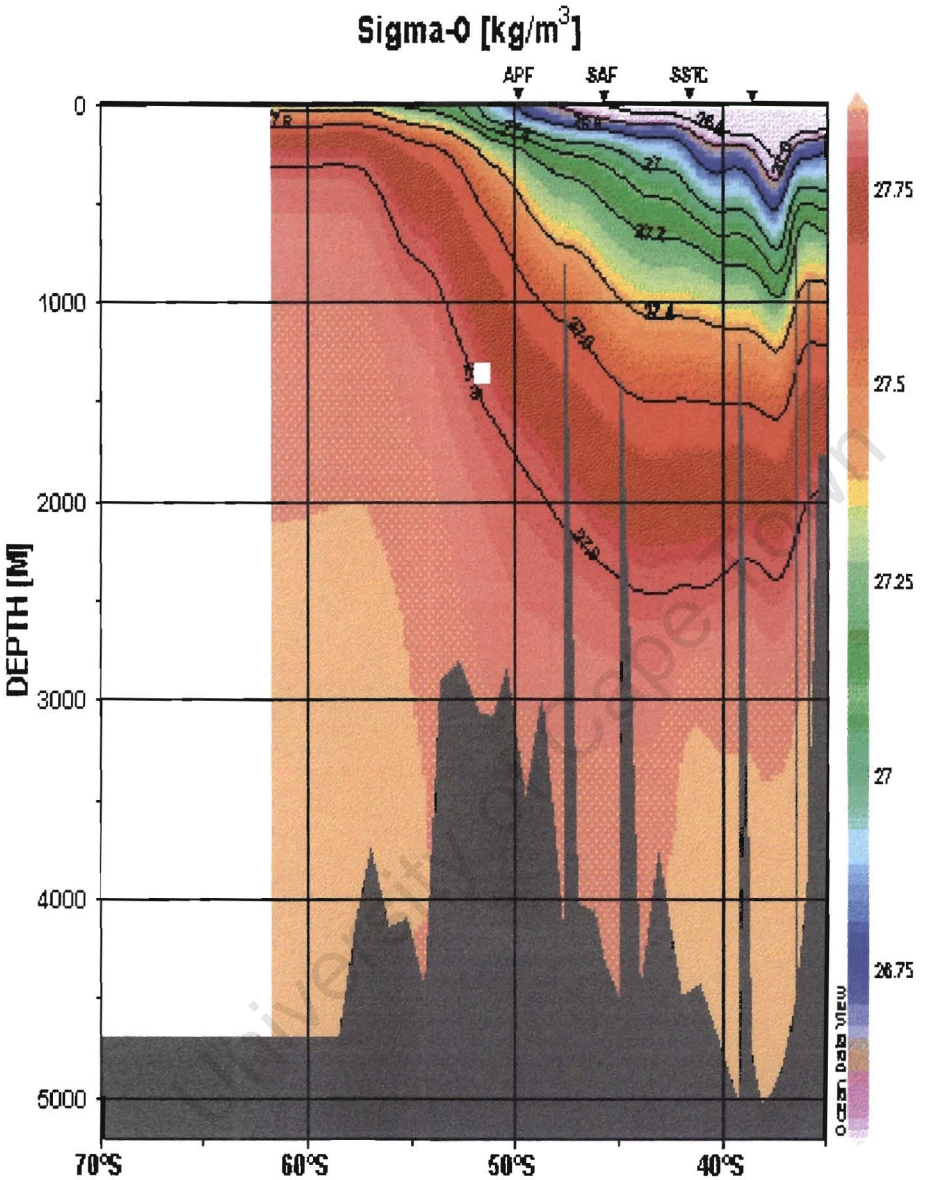

Fig 5.9c (i): Vertical Potential density section of the SR02b section

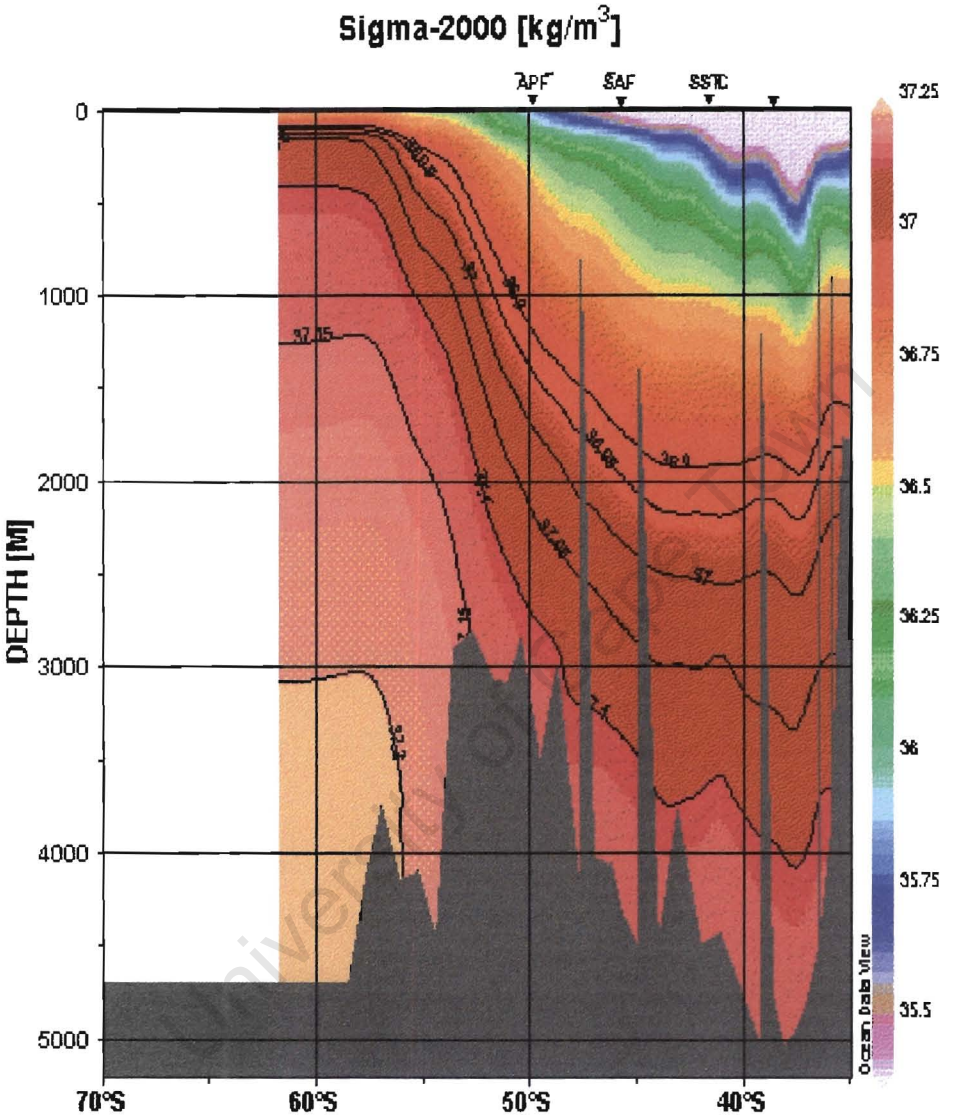

Fig 5.9c (ii): Vertical Potential density section of the SR02b section (Sigma-2000 m)

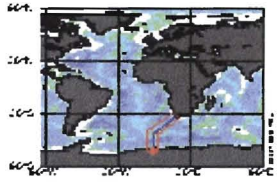

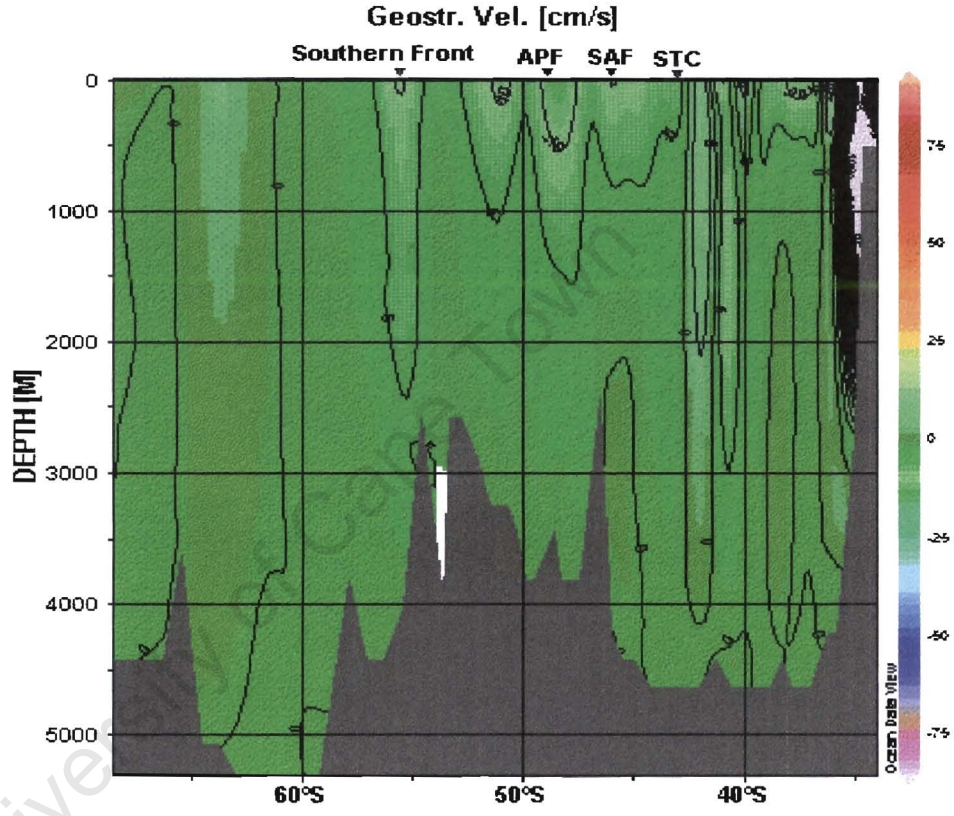

Fig 5.10a: Sectional display of geostrophic velocities along the SR02a section

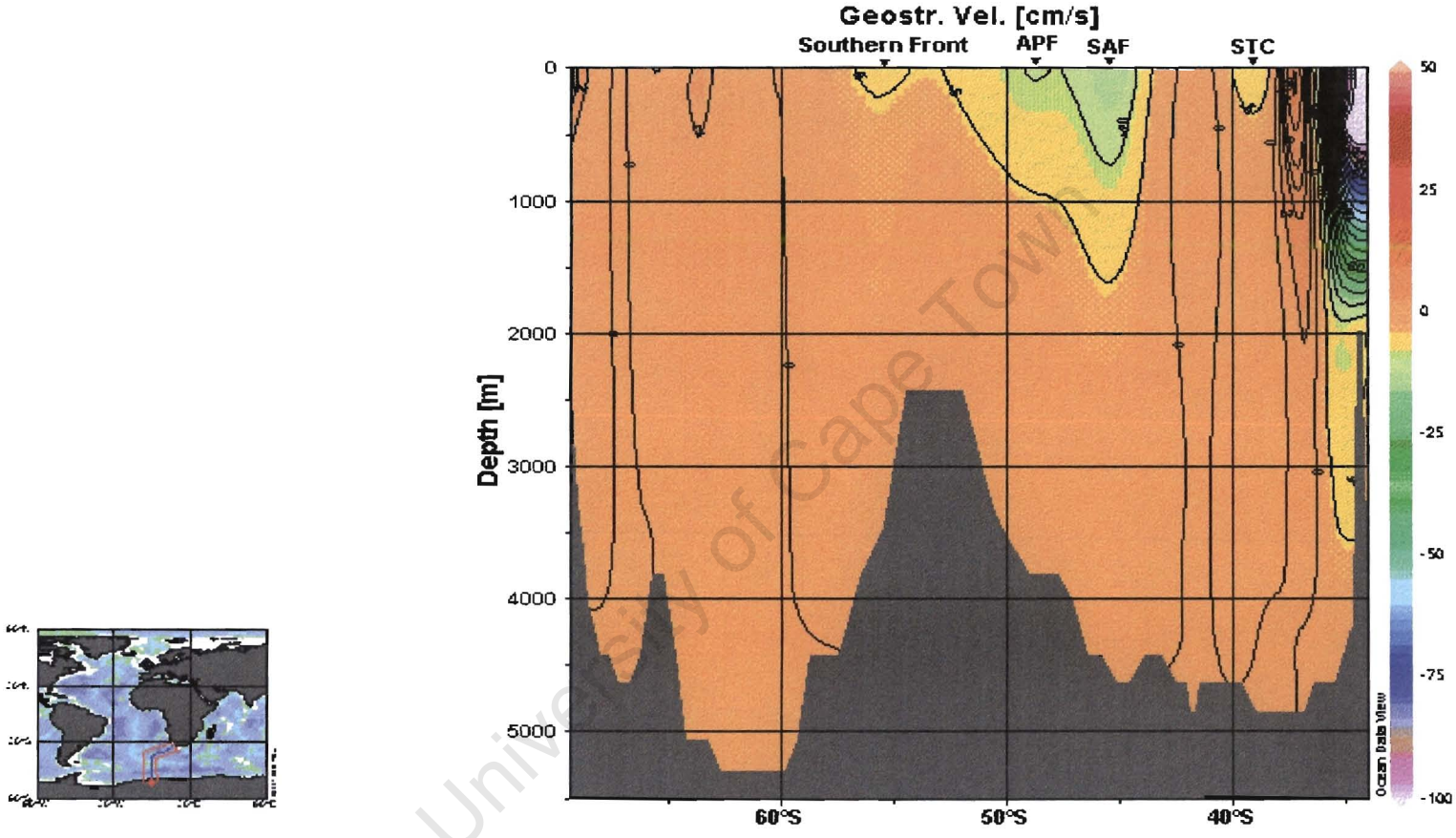

Fig 5.10b: Sectional display of geostrophic velocities along the A12 section.

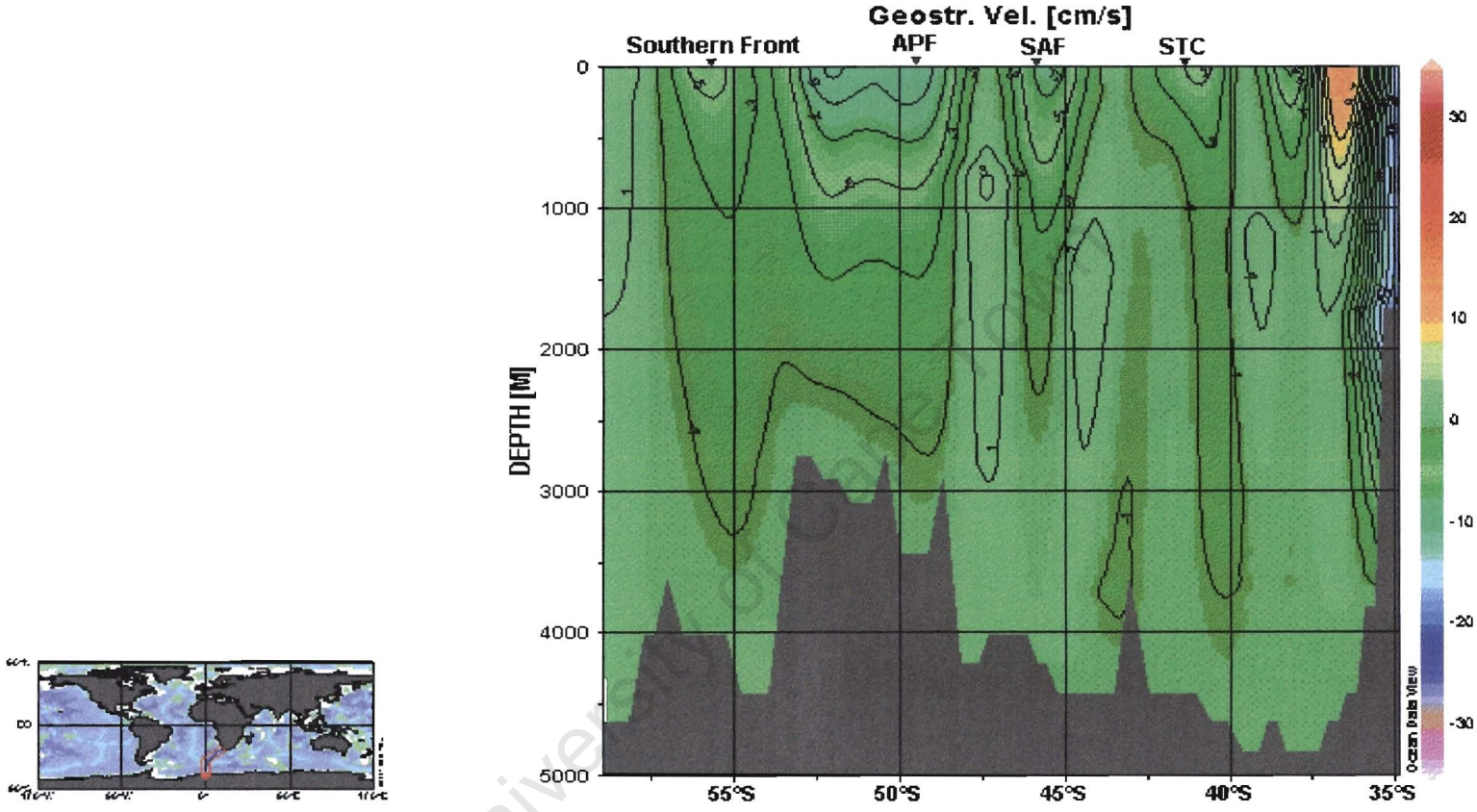

Fig 5.10c: Sectional display of geostrophic velocities along the SR02b section.

5.5 Fluxes

Described as the highway of global circulation the Southern Ocean play major role in the inter basin exchanges between the Atlantic and Indian Oceans (Ganachaud 1999). The geographical position of the SR02a section provides us with the opportunity to provide estimates for these transfers. In this section we will look at variability with respect to the above mentioned section by comparing it to the A12 section as calculated by myself and the A12 section with respect to results given by Ganachaud (1999) as well as Ganachaud and Wunsch (2000).

No nutrient fluxes across the SR02a were calculated due to the loss of the samples. Section SR02b does not reach the Antarctic continent and was not considered for this analysis. Ganachaud (1999) in his discussion indicated only $0.923 \pm 2.8 \times 10^{9} kg\ s^{-1}$ is transported across the A11 section to the north. Considering this as negligible the enclosed box consisted only of the A21 (Drake Passage) section and the SR02a or A12 WOCE sections (figure 5.5.1).

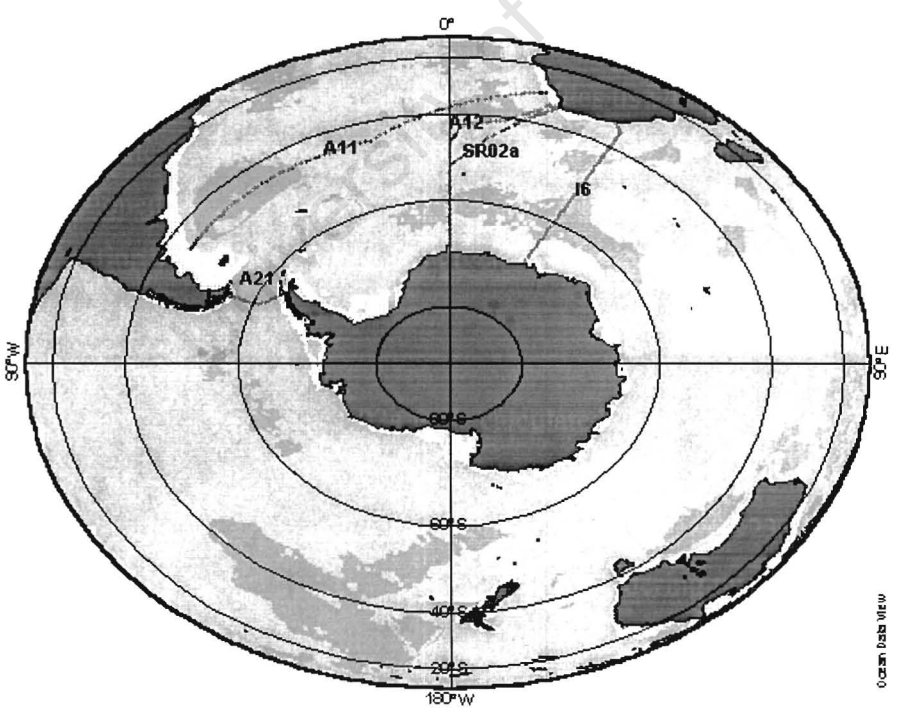

Figure 5.5.1: A21, A12, SR02a and I6 sections and topography

Using the method outlined in Chapter 4, transport of mass across the SR02a section (figure 5.5.1) was calculated as being139± 2x10^9 kg s^{-1} (figure 5.5b). This value was found to be consistent with the transport across the A12 section, which amounted to 139±3.1x10^9 kg s^{-1} (figure 5.5c). Ganachaud (1999) in his investigation of the A12 section found the transport to be 139± 7.9x10^9 kg s^{-1}. No variability is thus observed in terms of transport along the Greenwich meridian between South Africa and Antarctica. Taking the geographical positions of the two sections into account this was to be expected.

The heat flux for the SR02a section was 0.815 ± 0.15 PW (figure 5.5e) whilst along the A12 section it was only 0.675± 0.15PW (figure 5.5f). Although the value of the A12 section is lower it does however fall within the range of uncertainty of the SR02a section. The value for the A12 section compares well with the 0.7 PW calculated by Ganachaud and Wunsch (1999) for the same section. The heat flux for the SR02a section however is about midway between that of the A12 section and the I6 WOCE section transporting 0.9 PW (Ganachaud and Wunsch, 1999). Although the difference between the SR02a and A12 sections are not significant as they fall within each others range of uncertainty the following reasons could be given for the difference. When comparing the three sections the following differences can be noted: 1) time difference in the undertaking of these sections (A12 in 1990, the SR02a in 1993) and 2) the SR02a and I6 sections have an added hydrographic features namely Agulhas rings in the case of the SR02a section and the Agulhas Current and Agulhas Return Current in case of the I6 section. Time difference would play a role when considering the Antarctic Circumpolar Wave as discussed by White and Peterson (1996). The wave propagates eastward around the Southern Ocean with an 8-10 year period resulting in either and increase or decrease in SST at a certain position over time. Results from White and Peterson (1996) indicate a decrease in SST at 0°E over the period 1990 to 1993. Heat transport across 0°E can thus be expected to decrease over this time period since our calculation of the heat flux included the Ekman layer. The Antarctic Circumpolar Wave can thus not be considered as a reason for this increase. Also in terms of time it needs to be noted that the A12 section was done in winter and the SR02a section in summer. Along the SR02a section

surface waters across the Weddell Gyre is slightly warmer. This would result in a slight increase in the amount heat transported across the section. The two Agulhas rings in the SR02a section could also be considered as a possible reason for the increase in heat transport. This possibility is highly unlikely since previous measurements of the heat transport of Agulhas rings were only 0.045 PW for a total of six rings (van Ballegooyen et al., 1994). In addition this heat is transported into the South Atlantic.

The salt flux (figures 5.5g and 5.5h) across the SR02a and A12 sections are nearly similar. There is however a slight difference in the amount of oxygen (figures 5.5i and 5.5j) that is transported across the two sections. The quality of the data of the SR02a section could be the reason for this discrepancy.

a) A21 (Drake Passage)

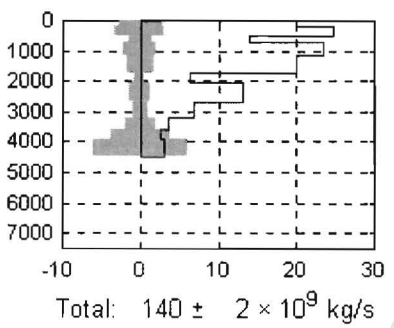

b) SR02a (0°E)

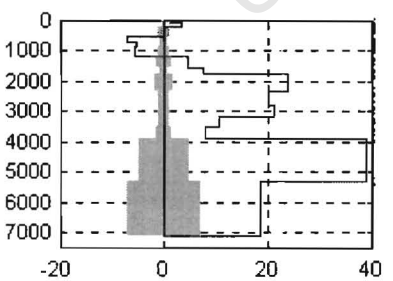

c) A12 (0°E)

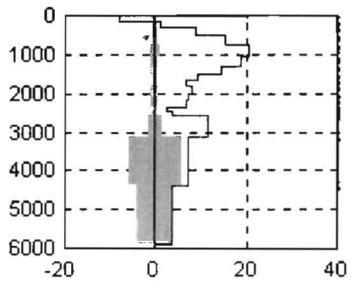

Total: 139± 3.1 x10^9kg/s

Figures 5.5 a, b and c: Mass transport (*10^9kg/s) across each section, integrated to the bottom. The shaded area corresponds to the uncertainty.

d) A21 (Drake Passage)

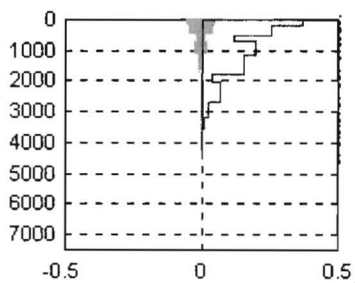

Total: 1.31 ± 0.14 PW

e) SR02a (0°E)

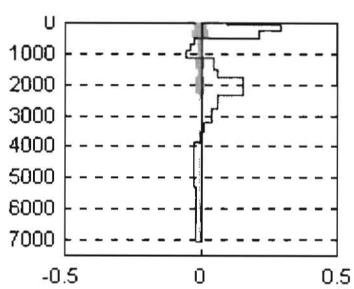

Total: 0.815 ± 0.15 PW

f) A12 (0°E)

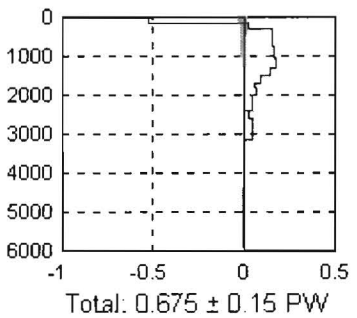

Figures 5.5 d, e and f: Heat transport (PW) across each section, integrated to the bottom The shaded area corresponds to the uncertainty.

g) SR02a (0°E)

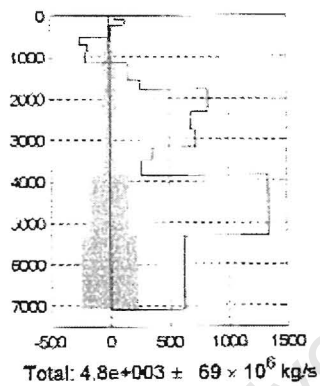

h) A12 (0°E)

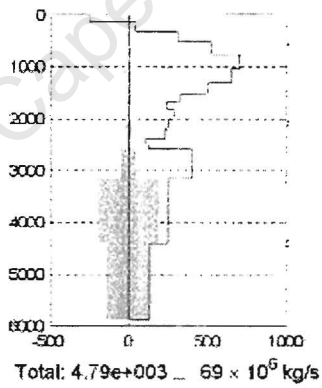

Figures 5.5 g and h: Salt fluxes (kg/s) across the SR02a and A12 sections

i) SR02a (0°E)

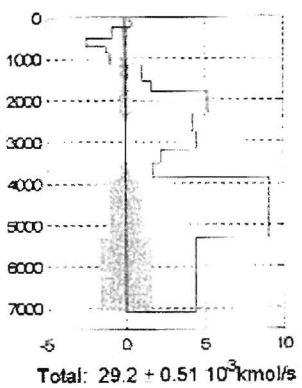

j) A12 (0°E)

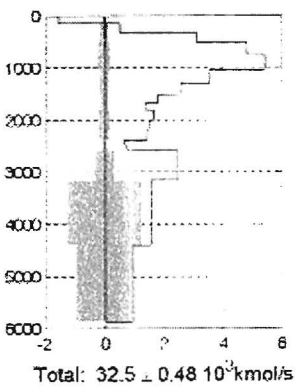

Figures 5.5 i and j: Oxygen fluxes (kmol/s) across the SR02a and A12 sections

Chapter 6

In this chapter conclusions are drawn in relation to the objectives set out in Chapter 3. These conclusions unless otherwise specified are drawn only with respect to the SR02a, SR02b and A12 sections

Conclusions

What is the flux of mass, heat and nutrients across the SR02a line?

In answering this key question I also compare the values calculated for the SR02a section with that of the A12 section. The freshwater flux across the SR02a sections was 139 ± 2×10^{9}kg s^{-1}. This value was consistent with the 139 ± 3.1 x 10^{9}kg s^{-1} found along the A12 section and previous findings. The heat flux across the SR02a section was 0.815±0.15 PW. This was slightly higher than the 0.675±0.15 PW calculated for the A12 section. This increase in the heat transport of the SR02a section can possibly be attributed to seasonal temperature variation. The calculation of the salt flux across the SR02a section yielded 4800 ± 69x10^{6} kg s^{-1}. This value deviated only slightly to the 4790± 69x10^{6} kg s^{-1} calculated for the A12 section. The oxygen flux for the SR02a section was 29.2 ± 0.51 x 10^{3} kmol s^{-1}. Conversely to the salt flux this was lower to the 32.5 ± 0.48x10^{3} kmol s^{-1} calculated for the A12 section. This slight difference could be ascribed to the quality and density of the samples in the SR02a section. The calculation of the other nutrients was not possible due to the loss of nutrient samples. This question could thus not be fully answered in its entirety.

What variability can be observed along the different sections?

Fronts

South of Africa between 0 and 20° E four fronts are clearly distinguishable namely the STC, SAF, APF and the Weddell Front. In the absence of the AF the STC was found to be the most prominent front with a thermal expression of 0.02 °C km^{-1}. It needs to be noted however that in terms of transport the SAF was found to be the most prominent front along the Greenwich meridian. The SAF was found to transport the most of the water for at least two of the sections. For these two sections the geostrophic velocities were greater than that found by Whitworth and Nowlin (1987) along the Greenwich

meridian but more inline with that found in the Drake Passage. The SAF does however show the largest degree of variability compared with the other fronts in terms of geostrophic velocities. Mean geostrophic velocities and positions for the respective fronts associated with the ACC were 50° 24'S and 19.7 cm s^{-1} for the APF, 45° 34'S and 27.3 cm s^{-1} for the SAF, 41° 06'S and 19 cm s^{-1} for the STC and 55° 10'S and 7.45 cm s^{-1} for the Weddell Front. These surface geostrophic speeds are smaller than at the Drake Passage. Along the Greenwich meridian geostrophic velocities were greater than along the AJAX section except for the APF and Weddell Front. This discrepancy could however be the artifact of station spacing. Variability in terms of the latitudinal positions the APF and SAF fell within previous calculated ranges. In terms of the STC this was only the case in sections within the Agulhas Retroflection region. East of this region the front is slightly northward of the range.

Water masses

Subtropical Surface Water

The extend to which typical Subtropical Surface Water covers the area north of the STC differs depending on whether the section cuts the Agulhas Retroflection region. Along sections that do not cross this region, Subtropical Surface Water covers the whole region north of the STC and is described as having a salinity (>34.8) and temperature (>12°C) maximum. These characteristics compared well with previous findings along the Greenwich meridian. However along sections that do cross the Agulhas Retroflection region typical Subtropical Surface Water are seen only as a patch at 38°S surrounded by surface water of the Agulhas Current and Agulhas Return Current in the form of two rings. In these sections Subtropical Surface Water display an added characteristic namely, a induced oxygen maximum (>5.4 ml/l) compared to the surface water of the Agulhas Current and Return Current.

SASW

This water mass is exhibits a salinity minimum and a oxygen (>7 ml/l) and temperature (>7C) maximum. The salinity minimum freshens dramatically as you move southward towards the APF. In the Subantarctic zone the salinity of SASW is 0.2-0.3 more saline than in the Drake Passage. Just south of the SAF values are more comparable to that in the Drake Passage. This water mass lies typically within the first 100 m in the SAZ but its depth increases as one move southward. Along the Greenwich meridian Whitworth and Nowlin (1987) described what would be called SAMW in the Drake Passage as SASW so comparison with a previous study was not possible.

SAMW

Termed with SASW by Whitworth and Nowlin (1987) this water mass lies just below the SASW in the SAZ. It has a characteristic salinity maximum (>34.5) and oxygen minimum associated with it, consistent with studies in the Drake Passage. As in the Drake Passage this water mass has a second minimum just above the level of AAIW. This minimum ranged between 5.4 ml/l and 5.5 ml/l.

AASW

Lying south of the APF this water mass has a salinity (<33.9) and temperature minimum (<1°C) and oxygen maximum. In the summer sections AASW has an intense subsurface temperature minimum (Winter Water) lying between 100 m to 120 m. This intense temperature minimum layer is not continuous but is seen as patches of cold water surrounded by relatively warm water. In contrast to the summer sections no Winter Water are seen along the winter section. This difference is explained in full by the process of formation of these patches, which occurs only in summer. The winter section does however still display the characteristic temperature and salinity minimum associated with AASW. However it needs to be noted that in the winter section there is an slight increases in the salinity minimum of the AASW due to the release of salt during the freezing process. The above characteristics were consistent with previous studies along the Greenwich meridian and elsewhere.

AAIW

AAIW has a salinity minimum and oxygen maximum due to the overlying SAMW and underlying UCDW. The salinity minimum associated with this water mass, surfaces at the SAF and does reach across to the APF, as is the case in the Drake Passage. AAIW sinks toward the north along the 27.1 and 27.2 isopycnals. These characteristics were consistent with that found along the AJAX section as described by Whitworth and Nowlin (1987). However along the sections that cross the Agulhas Retroflection AAIW is influenced by Red Sea water carried in the Agulhas Current, Return Current and Agulhas Rings at the same density level as AAIW. Within the two Agulhas Rings mixing of the two water masses result in an increase in salinities.

UCDW

This water mass has a salinity maximum compared to AAIW and an oxygen minimum. UCDW also has a nitrate and phosphate maximum. The oxygen trend indicates a decrease in the oxygen minimum from the SAZ (4.2 ml/l) to the PFZ (4.1 ml/l). In the SAZ the nitrate maximum north of the SAF was lower than that of the Drake Passage. The nitrate maximum was found to lie just slightly above the oxygen minimum. These observations were consistent with that along the AJAX section. However it needs to be noted that the highest nitrate values were between 1-2 μmols lower than in the AJAX section.

LCDW

LCDW has a salinity maximum and a nutrient minimum. Salinity values at the APF along the Greenwich Meridian, is greater than that at the Drake Passage whereas nutrient values shows a reduction. These changes can be attributed to extensive influence by NADW. North of the mid ocean ridge LCDW found near the bottom whereas south of the ridge in the Weddell Gyre it is found at intermediate depths. These characteristics were similar to that observed along the Greenwich meridian by Whitworth and Nowlin (1987).

Weddell Gyre

Water masses

Upper surface water of the Weddell Gyre consists of AASW discussed above. The intermediate water of the Weddell Gyre are unmodified LCDW. Within this water mass water warmer than 0.8°C just north of the APF is saltier than at the Drake Passage. LCDW with a water temperature less than 0.8°C was less salty displaying the influence of the fresher Weddell Gyre. LCDW in the southern limb of the Weddell Gyre rounds the Maude Rise between 300 to 600 m. The warmest most saline LCDW in the southern limb lies at depth above 600 m and is shallow enough to participate in the shelf-slope process that lead to the formation of Weddell Sea Bottom Water. Also found in the southern limb is a oxygen minimum layer at 200 m, a remnant of somewhat less dense LCDW. Central Intermediate Water is basically biochemecally altered LCDW in the central part of the Weddell Gyre. This water mass has a silicate maximum and a oxygen minimum. The silicate maximum is found to lie just below the oxygen minimum. Although the above mentioned characteristics are consistent with that along the AJAX section, the value of the silicate maximum does however differ between sections. Compared to the AJAX section (140 μmol/l) the silicate maximum was much less in the A12 (127 μmol/l) and SR02b (130 μmol/l) sections. Deep water lies between -0.7 and 0°C and are essentially featureless. This water escapes the confines of the Weddell Gyre to become AABW. Weddell Sea Bottom water has a relative temperature, salinity and nutrient minima and maxima in oxygen. Along all the sections the extrema characteristics of deep and bottom waters are seen as skewed to the north. These characteristics compares well with previous descriptions of Deep and Bottom water.

Fluxes

Freshwater flux across both the A12 and SR02a sections was 139 kg s^{-1}. This value was consistent with previous findings. Heat fluxes across the Greenwich meridian between South Africa and Antarctica does however show some differences. The heat transport for the A12 section was 0.675±0.15 PW which was more or less consistent with previous findings across this section. Transport across the SR02a was 0.815±0.15 PW, slightly greater than across the A12 section. Possible reason for this is the seasonal variation in

temperature between the winter A12 section and the summer SR02a section. The salt flux across the SR02a and A12 sections showed little deviation from each other and were $4.8e+003\pm69x10^{6}$ kg s^{-1} and $4.79e+003\pm69x10^{6}$ kg s^{-1} respectively. Unlike the salt flux, the oxygen flux differed slightly for the A12 and SR02a sections. Across the A12 section 32.5 ±51 10^{3} kmol s^{-1} was transported whilst only 29.2 ±51 10^{3} kmol s^{-1} was transported across the SR02a section. This slight difference could be ascribed to the quality and density of the samples in the SR02a section.

Chapter 7
Bibliography

Allanson, B. R., R. C. Hart and J. R. E. Lutjeharms (1981), Observations on the nutrients, chlorophyll and primary production of the Southern Ocean south of Africa, South African Journal of Antarctic Research, 10/11, 3-14.

Baker, D. J. (1991) World Ocean Circulation and Climate Change: Research Programs and a Global Observing System. In: Climate Change: Science, Impacts and Policy. Proceedings of the Second World Climate Conference. Edited by J. Jäger and H. L. Ferguson, University Press, Cambridge.

Belkin, I. M. and A. L. Gordon (1996) Southern Ocean fronts from the Greenwich meridian to Tasmania, J. Geophysical Research. 101, 3675-3696.

Boddem, J. and R. Schlitzer (1995) Interocean exchange and meridional mass and heat fluxes in the South Atlantic, J. Geophysical Research, 100, 15,821-15,834.

Botnikov, V. N. (1963) Geographical position of the Antarctic convergence in the Southern Ocean, Sov. Antarct. Exped. Inf. Bull., Engl. Transl., 4(41), 324-327.

Bryan, K. (1962) Measurements of meridional heat transport by ocean currents. J. Geophysical. Research, 67, 3403-3414.

Bryden, H. L. (1979) Poleward heat flux and conversion of available potential energy in Drake Passage, J. of Marine Research, 37, 1-22.

Bryden, H. L. and M. M. Hall (1980) Heat transport by currents across 25°N latitude in the Atlantic Ocean, Science, 207, 884-886.

Callahan, J. E. (1972) The structure and circulation of Deep Water in the Antarctic, Deep Sea Research, 19, 563-575.

Carmack, E. C. and T. D. Foster (1975) On the flow of water out of the Weddell Sea, Deep Sea Research, 22, 711-724.

Carpenter, J. H. (1965) The Chesapeake Bay Institute technique for the Winkler dissolved oxygen titration, Limnology and Oceanography, 10, 141-143.

de Soeke, R.A. and M.D. Levine (1981) The advective flux of heat by mean geostrophic motions in the Southern Ocean. Deep Sea Research, 28A, 1057-1085.

Deacon, G. E. R. (1933) A general account of the hydrology of the South Atlantic Ocean, Discovery Reports, 7, 171-238.

Deacon, G. E. R. (1937) The hydrology of the Southern Ocean. Discovery Rep., 15, 1-124.

Dickson, R.R., J. Meincke, S-.A. Malmberg and A.J. Lee (1988) The "Great salinity anomoly" in the Northern North Atlantic 1968-1982. Prog. Oceanogr., 20,103-151.

Eid, E. M. and C. H. Hulsbergen (1991) Sea Level Rise and Coastal Zone Management. In: Climate Change: Science, Impacts and Policy. Proceedings of the Second World Climate Conference. Edited by J. Jäger and H. L. Ferguson, University Press, Cambridge.

Emery, W. J. (1977) Antartic Polar frontal zone from Australia to the Drake Passage, J. Physical Oceanography, 7(6), 811-822.

Fahrbach, E., R. G. Peterson, G. Rohardt, P. Schlosser and R. Bayer (1994) Suppression of bottom water formation in the southeastern Weddell Sea, Deep Sea Research, 41, 389-411.

Foster, T. D. and E. C. Carmack (1976) Frontal Zone mixing and Antarctic Bottom Water formation in the southern Weddell Sea, Deep Sea Research, 23, 301-317.

Ganachaud, A. (1999). Large Scale Oceanic Circulation and Fluxes of Freshwater, Heat, Nutrients and Oxygen. Ph.D Thesis, Mass. Inst. of Technol./Woods Hole Oceanogr. Inst. Jt. Program, Cambridge.

Ganachaud, A. and Wunsch C. (2000) Improved estimates of global ocean circulation, heat transport and mixing from hydrographic data, Nature, vol. 408, 453-457.

Georgi, D. T. (1979) Modal properties of Antarctic Intermediate Water in the southeast Pacific and South Atlantic, J. Physical. Oceanography, 9, 456-468.

Georgi, D. T. and J. M. Toole (1982) The Antarctic Circumpolar Current and the oceanic heat and freshwater budgets, J. Marine Research, 40, suppl., 183-197.

Gill, A. E. (1973) Circulation and bottom water production in the Weddell Sea, Deep Sea Research, 20, 111-140.

Gordon, A. L. (1967) Structure of Antarctic waters between 20W and 170W, Antarct. Map Folio. Ser., folio 6, edited by V. C Bushnell, 10pp., 14 plates, Am. Geogr. Soc., New York.

Gordon, A. L. (1971a) Antarctic Polar Front zone, in Antarctic Oceanology 1, Antarct. Res. Ser., 15, 205-221, AGU, Washington, D.C.

Gordon, A. L. (1971b) Oceanography of Antarctic waters, in Antarctic Oceanology 1, Antarct. Res. Ser., 15, 169-203, AGU, Washington, D.C.

Gordon, A. L. (1973) Physical oceanography, Antarct. J. U. S., 8(3), 61-69.

Gordon, A. L. (1986) Interocean exchange of thermocline water, J Geophysical Research, 91, 5037-5046.

Gordon, A. L. (2001) Interocean Exchange, In: Ocean Circulation and Climate: Observing and modeling the Global Ocean, edited by G. Siedler, J. Church and J. Gould, Academic Press, London, 303-314.

Gordon, A. L. and B. A. Huber (1984) Thermohaline stratification below the Southern Ocean sea ice, J. Geophysical Research, 89, 641-648.

Gordon, A. L., C. T. A. Chen and W. G. Metcalf (1984) Winter mixed layer entrainment of Weddell Deep Water, J. Geophysical Research, 89, 637-640.

Gordon, A. L., D. T. Georgi and H. W. Taylor (1977a) Antarctic Polar Front zone in the western Scotia Sea-Summer 1975, J. Physical Oceanography, 7(3), 309-328.

Gordon, A. L., J. R. E. Lutjeharms and M. L. Gründlingh (1987) Stratification and circulation at the Agulhas Retroflection, Deep Sea Research, 34, 565-599.

Gordon, A. L., D. G. Martinson and H. W. Taylor (1981) The wind-driven circulation in the Weddell-Enderby Basin, Deep Sea Research, 28A, 151-163.

Gordon, A. L., E. Molinelli and T. Baker (1978) Large-scale relative dynamic topography of the Southern Ocean, J. Geophysical Research, 83, 3023-3032.

Gordon, A. L., H. W. Taylor and D. T. Georgi (1977b) Antarctic oceanographic zonation, in Polar Oceans, edited by M. J. Dunbar, Polar oceans. Proc. Polar Oceans Conf., Arct. Inst. of North Am., Calgary, Alberta, 45-76.

Gordon, A. L., R. F. Weiss, W. M. Smethie, and M. J. Warner (1992) Thermocline and intermediate water communication between the South Atlantic and Indian Oceans, J. Geophysical Research, 97, 7223-7240.

Gordon, A. L., B. Barnier, K. Speer and L. Stramma (1999) World Ocean Circulation Experiment: South Atlantic results, J. Geophysical Research, 104, 20,859-20861.

Gründlingh, M. L. (1983) On the course of the Agulhas Current, South African Geographical Journal, 65, 49-57.

Hall, M. M. and H. L. Bryden (1982) Direct estimates and mechanisms of ocean heat transport, Deep Sea Research, 29, 339-359.

Hofmann, E. E. (1985) The large-scale horizontal structure of the Antarctic Circumpolar Current from FGGE drifters, J. Geophysical Research, 90, 7087-7097.

Hofmann, E. E. and T. Whitworth III (1985) A synoptic description of the flow at the Drake Passage from year-long measurements, J. Geophysical Research, 90, 7177-7187.

Hanawa, K. and L. D. Talley (2001) Mode Waters, In: Ocean Circulation and Climate: Observing and modeling the Global Ocean, edited by G. Siedler, J. Church and J. Gould, Academic Press, London, 373-386.

Jacobs, S. S. and D. T. Georgi (1977) Observations on the southwest Indian/Antarctic Ocean, Deep Sea Research, 24, supplementary, 43-84.

Joyce, T. M. and S. L. Patterson (1977) Cyclonic ring formation of the Polar front in the Drake Passage, Nature, 265(5590), 131-133.

Joyce, T. M., S. L. Patterson and R. C. Millard (1981) Anatomy of a cyclonic ring in the Drake Passage, Deep Sea Research, 28A(11), 1265-1287.

Joyce, T. M., W. Zenk and J. M. Toole (1978) The anatomy of the Antarctic Polar Front in the Drake Passage, J. Geophysical Research, 83, 6093-6114.

Kawasaki, K. (1991) Effects of Climate Change on Marine Ecosystems and Fisheries. In: Climate Change: Science, Impacts and Policy. Proceedings of the Second World Climate Conference. Edited by J. Jäger and H. L. Ferguson, University Press, Cambridge.

Legeckis, R. (1977) Oceanic Polar in the Drake Passage-Satellite observations during 1976. Deep Sea Research, 24, 701-704.

Lutjeharms, J. R. E. (1985) Location of frontal systems between Africa and Antarctica: some preliminary results. Deep Sea Research, 32(12), 1499-1509.

Lutjeharms, J. R. E. and I. J. Ansorge (2001) The structure and transport of the Agulhas Return Current between South Africa and 70°E, J. Marine Systems, 30, 115-138.

Lutjeharms, J. R. E. and H. R. Valentine (1984) Southern Ocean fronts south of Africa, Deep Sea Research, 31,1461-1475.

McCartney, M. S. (1977) Subantarctic mode water, Deep Sea Research, 24, suppl., 103 – 119.

McCartney, M. S. (1982) The tropical recirculation of mode waters, J. Marine Research, 40, suppl., 427-464.

McDougall, T. J. (1987) Neutral Surfaces, J. Physical Oceanography, vol. 17, 1950-1964.

Molinelli, E. (1981) The Antarctic influence on Antarctic Intermediate Water, J. Marine Research, 39, 267-293.

Nagata, Y., Y. Michida and Y. Umimura (1988) Variations of the positions and structures of the oceanic fronts in the Indian ocean sector of the Southern Ocean in the period from 1965 to 1987. In: Antarctic Ocean and Resource Variability, edited by D. Sahrhage, Springer-verlag, Heidelberg, 92-98.

Nowlin, W. D. Jr. and M. Clifford (1982) The kinemetic and thermohaline zonation of the Antarctic Circumpolar Current at the Drake Passage, J. Marine Research, 40, suppl., 481-507.

Nowlin, W. D. Jr. and J. M. Klink (1986) The physics of the Antarctic Circumpolar Current, Rev. Geophys. Space Phys., 24, 469-491.

Nowlin, W.D. Jr. and W. Zenk (1988) Currents along the margin of the South Shetland Arc, Deep Sea Research, 40, 169-203.

Orsi, A. H., T. Whitworth III and W. D. Nowlin Jr (1995) On the meridional extent and fronts of the Antarctic Circumpolar Current, Deep Sea Research, 42, 641-673.

Ostapoff, F. (1962) The salinity distribution at 200 meters and the Antarctic frontal zones. Deutsche Hydrographische Zeitschrift, 15, 133-141.

Park Y.L., E. Charriaud and P. Craneguy (2001) Fronts, transport, and Weddell Gyre at 30°E between Africa and Antarctica, J. Geophysical Research, 106, 2857-2879.

Park, Y., L. Gamberoni and E. Charriaud (1993) Frontal Structure, Water Masses, and Circulation in the Crozet Basin, J. Geophysical Research, 98, 12,361-12,385.

Peterson, R. G., W. D. Nowlin and T. Whitworth III (1982) Generation and evolution of a cyclonic ring in the Drake Passage, J. Physical Oceanography, 12(7), 712-719.

Piola, A. R. and D. T. Georgi (1982) Circumpolar properties of Antarctic Intermediate Water and Subantarctic Mode Water, Deep Sea Research, 29, 687-711.

Piola, A. R. and A. L. Gordon (1989) Intermediate waters in the southwest South Atlantic, Deep Sea Research, 36, 1-16.

Read, J. F. and R. T. Pollard (1993) Structure and Transport of the Antarctic Circumpolar Current and the Agulhas Return Current at 40°E, J. Geophysical Research, 98, 12,281-12,295.

Read, J. L., R. T. Pollard, and U. Bathmann (2002) Physical and biological patchiness of an upper ocean transect from South Africa to the ice edge near the Greenwich Meridian, Deep Sea Research, pt II, 49 (18), 3713-3733.

Reid, J. L., W. D. Nowlin Jr., and W. C. Patzert (1977) On the characteristics and circulation in the southwestern Atlantic Ocean, J. Physical Oceanography, 7, 62-91.

Roemmich, D. (1980) Estimation of meridional heat flux in the North Atlantic Ocean by inverse methods. J. Physical Oceanography, 10:1972-1983.

Rintoul, S. R. (1991) South Atlantic interbasin exchange, J. Geophysical Research, 96, 2675-2692.

Rintoul, S. R. (1998) On the origin and influence of Adélie Land Bottom Water. In: Ocean, Ice and Atmosphere: Interactions at Antarctic Continental Margin, Vol. 75 of Antarctic Research Series, edited by S. S. Jacobs and R. Weiss, American Geophysical Union, Washington, DC, 151-171.

Schröder, M. and E. Fahrbach (1999) On the structure and transport of the eastern Weddell Gyre, Deep Sea Research, Part II, 46, 501-527.

Sciremammano, F. Jr., R. D. Pillsbury, W. D. Nowlin, Jr., and T. Whitworth III (1980) Spatial scales of temperature and flow in the Drake Passage, J. Geophysical Research, 85, 4015-4028.

Sievers, H. A. and W. J. Emery (1978) Variability of the Antarctic Polar Frontal Zone in the Drake Passage-Summer 1976-1977, J. Geophysical Research, 83, 3010-3022.

Sievers, H. A. and W. D. Nowlin, Jr. (1984) The Stratification and Water Masses at Drake Passage, J. Geophysical Research, 89, 10,489-10,514.

Sievers, H. A. and W. D. Nowlin, Jr. (1988) Upper ocean characteristics in the Drake Passage and adjoining areas of the Southern Ocean, 39°W-95°W, In Antarctic Ocean and Resources Variability, D. Sahrhage (ed.), Springer-Verlag, Berlin Heidelberg, 57-80.

Sinha, S. K. (1991) Impact of Climate Change on Agriculture, A Critical Assessment. In: Climate Change: Science, Impacts and Policy. Proceedings of the Second World Climate Conference. Edited by J. Jäger and H. L. Ferguson, University Press, Cambridge.

Smith S. G. (1989) On the Weddell-Scotia Confluence and the Scotia Front. Unpublished M. Sc., Texas A&M University, College Station.

Sverdrup, H. U. (1940) Hydrology, 2, Discussion, B.A.N.F. Antarct. Res. Exped., 1921-1931, Ser. A, 3, Oceanography, 89-125, 1940.

Sverdrup, H. U., M. W. Johnson and R. H. Fleming (1942) The Oceans: Their Physics, Chemistry, and General Biology. Prentice-Hall, Englewood Cliffs, New Jersey.

UNESCO (1983) Algorithms for the computation of fundamental properties of seawater, UNESCO Technical Papers in Marine Science, 44, 53.

Van Ballegooyen, R., M. Gründlingh and J. R. E. Lutjeharms (1994) Eddy fluxes of heat and salt from the southwest Indian Ocean into the southeast Atlantic Ocean: A case study, J. Geophysical Research, 99, 14053-14070.

White, W. B. and R. G. Peterson (1996) An Antarctic circumpolar wave in the surface pressure, wind, temperature and sea-ice extent, Nature, 380 (6576), 699-702.

Whitworth, T., III and W. D. Nowlin Jr. (1987) Water Masses and Currents of the Southern Ocean at the Greenwich Meridian, J. Geophysical Research, 92, 6462-6476.

Wigley, T. M. L. and S. C. B. Raper (1991) Detection of the Enhanced Greenhouse Effect on Climate. In: Climate Change: Science, Impacts and Policy. Proceedings of the Second World Climate Conference. Edited by J. Jäger and H. L. Ferguson, University Press, Cambridge.

Winkler, L. W. (1888). Die Bestimmung des in Wasser gelösten Sauerstoffes. ber.dtsch. chem. Ges, 21, 2843-2855.

Woods, J. D. (1985) The World Ocean Circulation Experiment, Nature, 314, 501-511.

Wunsch, C. (1984) An eclectic ATLANTIC ocean circulation model. Part 1: The meridional flux of heat. J. Physical Oceanography, 14,1712-1733.

Wunch, C (1996) The Ocean Circulation Inverse Problem. Cambridge Univ. Press, New York.

Wüst, G. (1935) The stratosphere of the Atlantic Ocean, English translation, W. Emery, editor, Amerind Publishing, New Delhi, 1980, 112.

Wyrtki, K. (1971) Oceanogrophic Atlas of the International Ocean Expedition. National Science Foundation, Washington, D.C. i-ix, 1-531.

Zillman, J. W. (1970) Sea surface temperature gradients south of Australia, Aust. Meteorol. Mag., 18, 22-30.